doi.org/10.26434/chemrxiv.7713632.v1

Regio- and Diastereoselective Intermolecular [2+2] Cycloadditions Photocatalyzed by Quantum Dots

Yishu Jiang, Chen Wang, Cameron Rogers, Mohamad S. Kodaimati, Emily Weiss

Submitted date: 13/02/2019 • Posted date: 14/02/2019

Citation information: Jiang, Yishu; Wang, Chen; Rogers, Cameron; Kodaimati, Mohamad S.; Weiss, Emily (2019): Regio- and Diastereoselective Intermolecular [2+2] Cycloadditions Photocatalyzed by Quantum Dots. ChemRxiv. Fileset.

Here we show that colloidal quantum dots serve as visible-light chromophores, photocatalysts, and resuable scaffolds for homo- and hetero-intermolecular [2+2] photocycloadditions of 4-vinylbenzoic acid derivatives, with >90% tunable regioselectivity and up to 98% diastereoselectivity for the previously minor syn-cyclobutane products, including the syn-heda-to-tail cyclobutane, which has never been produced as the major product of a photochemical reaction.

File list (2)

Jiang_MainText.pdf (2.17 MiB)	view on ChemRxiv • download file
Jiang_SI.pdf (13.94 MiB)	view on ChemRxiv • download file

Regio- and Diastereoselective Intermolecular [2+2] Cycloadditions Photocatalyzed by Quantum Dots

Yishu Jiang, Chen Wang, Cameron R. Rogers, Mohamad S. Kodaimati and Emily A. Weiss*

Department of Chemistry, Northwestern University, 2145 Sheridan Rd., Evanston, IL 60208-3113

*corresponding author. Email: e-weiss@northwestern.edu

Light-driven [2+2] cycloaddition is the most direct strategy to build tetrasubstituted cyclobutanes, which are core components of many important bioactive molecules[1,2], including lead compounds for drug development[3]. Significant advances in the chemoselectivity and enantioselectivity of [2+2] photocycloadditions have been made[4-8], but exceptional and tunable diastereoselectivity and regioselectivity (head-to-head vs. head-to-tail adducts), required for synthesis of bioactive molecules, have not yet been achieved. Here we show that colloidal quantum dots (QDs) serve as visible-light chromophores, photocatalysts, and reusable scaffolds for homo- and hetero-intermolecular [2+2] photocycloadditions of 4-vinylbenzoic acid derivatives, with >90% tunable regioselectivity and up to 98% diastereoselectivity for the previously minor *syn*-cyclobutane products, including the *syn*-head-to-tail cyclobutane, which has never before been accessed as the major product of a heterophotocycloaddition. Transient absorption spectroscopy confirms that our system is the first example of catalysis triggered by triplet-triplet energy transfer from a QD. The excellent diastereoselectivity and tunable regioselectivity is shown to occur through self-assembly of substrate molecules on the QD surface, the first example of either selectivity type using a QD, and the first examples of tunably regioselective hetero-intermolecular [2+2] photocycloadditions. The precisely controlled triplet energy levels of QD photocatalysts facilitate efficient and selective heterocoupling, overcoming a major challenge in direct cyclobutane synthesis.

Light-driven [2+2] photocycloadditions, simple routes to complex tetrasubstituted cyclobutanes, follow several possible excited-state routes, but those that proceed through the triplet excited state of the reagent olefin are advantageous because (i) their scope is not limited by the electrochemical potentials of the substrate, (ii) triplets have long enough lifetimes to mediate *inter*molecular cycloadditions, and (iii) triplets are accessible with visible light through excitation of a triplet sensitizer, such as a transition metal complex or organic chromophore[9], followed by triplet-triplet energy transfer (TT EnT). The TT EnT strategy minimizes deleterious side-reactions and has resulted in high-yield intra- and intermolecular [2+2] photocycloaddtions of quinolone[4], cinnamate[10,11] and acyclic enone[12,13] derivatives.

Pioneering work of Bach, Meggers, Yoon and others has demonstrated enantioselective intermolecular [2+2] photocycloadditions in the presence of hydrogen bonding templates[4,5], chiral secondary amines[6], chiral ligands of molecular catalysts[7] and Lewis-acid co-catalysts[8]. Outstanding challenges include achieving selectivities for a particular regioisomer or diastereoisomer of the coupled product, and for homo- vs. heterocoupling within a mixture of reactive olefins – the latter a priority because cyclobutane natural products and related compounds predominantly comprise two distinct olefins[14]. First, in untemplated reactions, the *anti* diastereomer of the cyclobutyl product is sterically favored but the preference is often not significant enough to achieve a efficient discrimination[15]. Second, the distribution of head-to-head (HH) vs. head-to-tail (HT) regioisomers is highly dependent on the relative stability of the corresponding intermediates and therefore difficult to control extrinsically. Third, selective heterocoupling is challenging to achieve even with a template[16-20], because it requires the template to selectively co-localize two different substrates. Consequently, prior to this work, *syn*-HT heterocoupled products, the class of tetrasubstituted cyclobutanes likely to serve as the scaffolds of bioactive molecules, had never been formed as major products of a [2+2] photocycloaddition. In fact, there were no examples of tunable regioselectivity for any hetero-intermolecular [2+2] photocycloadditions. A strategy for extrinsic control of the configuration of

the cyclobutane product is needed to counter the preferences driven by steric and electronic characteristics of the substrates.

Here, we use colloidal CdSe QDs as visible light absorbers, triplet exciton donors, and self-assembly scaffolds to drive homo- and hetero-intermolecular [2+2] photocycloadditions of 4-vinylbenzoic acid derivatives. CdSe QDs donate energy to triplet states of organic molecules from triplet-like excitonic "dark" states, which lie <20 meV below their optically active "bright states"[21-24]. A QD's triplet energy is tunable *via* size-dependent quantum confinement; here we adjust the size of the QD to selectively sensitize only one reagent olefin within a mixture, and thereby achieve efficient *hetero*-intermolecular couplings. The QD catalytic systems exhibit >90% tunable regioselectivity with up to 98% diastereoselectivity for the previously minor *syn*-HH or *syn*-HT configurations of the adducts (**Figs. 1A,B**). With one exception, highlighted below, the diasteromeric ratios (d.r.) we achieve are a factor of 5–10 higher than those reported with all other triplet sensitizers for similar systems[10,11].

The Supplementary Information (SI) contains all details of synthesis and chemical analysis. The QDs do not etch, aggregate, or otherwise degrade for at least three 48 h reaction cycles (**Fig. 1C**). We readily separate the QD catalysts from reaction mixtures through addition of MeOH and centrifugation, and reuse them with no detectable decline in catalytic activity, Table S1. No reactions occurred without QDs or without illumination, Table S2. Through transient absorption spectroscopy, we observe coincident decays of the photoexcited electron and hole of the QD when the substrate is present, **Fig. 1D**. This result indicates that they are extracted from the QD as an electron-hole pair, and that the reaction is EnT-initiated rather than redox-initiated (and specifically TT EnT-initiated, since the singlet excited states of all substates are too high-energy to access). The coupling yields of all reactions are ≥10x lower when we do not functionalize both substrates with carboxylate groups to reversibly bind to the QD (Scheme S1), indicating that the reaction occurs at the surface of the particle. Carboxylates are "medium-strength" ligands for the

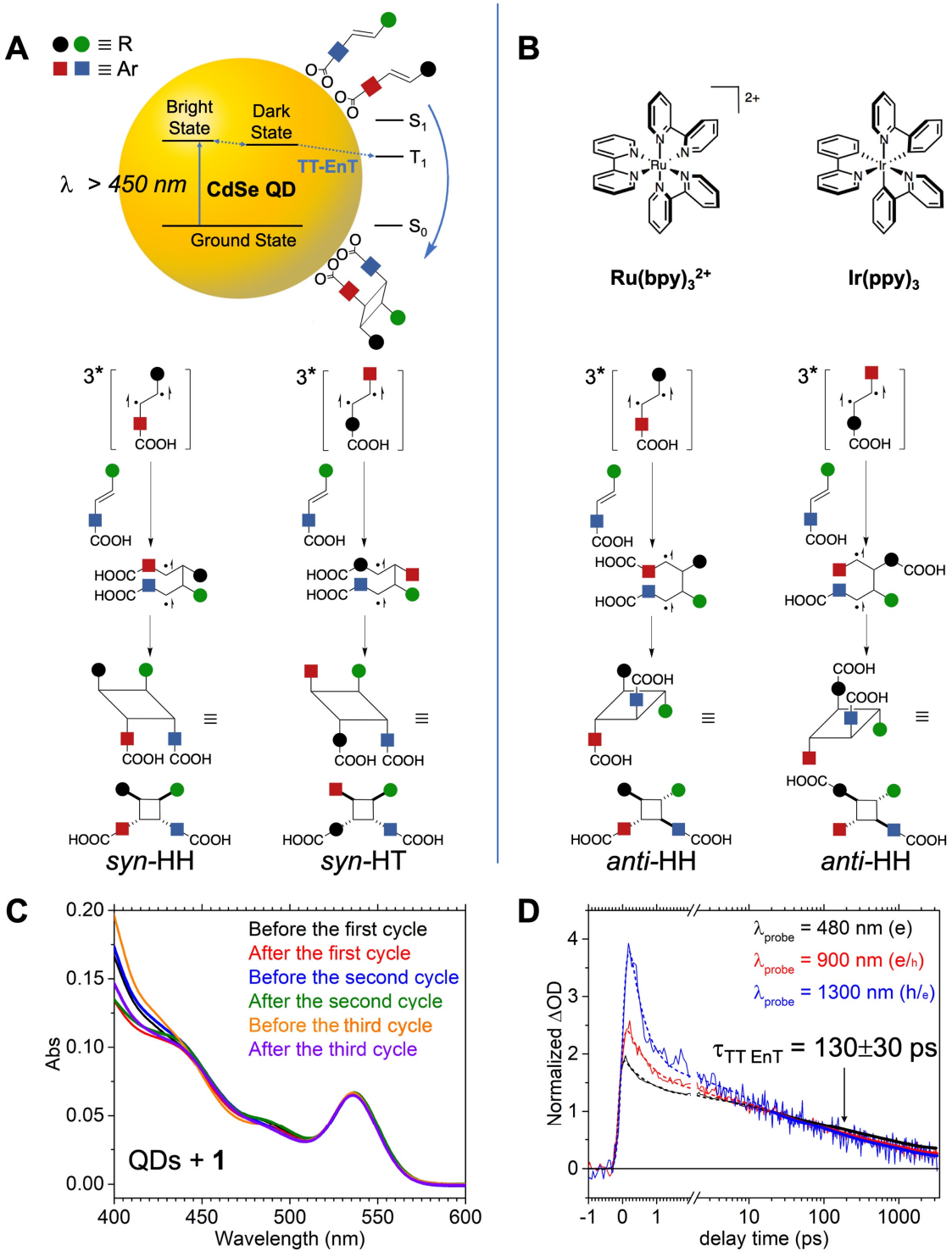

Fig. 1. **Sensitization *via* the QD Photocatalyst and Mechanisms of Selectivity. (A)** Sensitization of the triplet excited state of the substrate (T_1) through TT-EnT from CdSe QDs, and schematic representation of *syn*-HH or *syn*-HT selectivity of QDs. A proposed mechanism of the route to each diastereomer is shown in Scheme S2. **(B)** Chemical structures of the molecular

sensitizers compared to the QDs, and the mechanism of *anti*-HH preference of reactions driven by these molecules. **(C)** Ground state absorption spectra of a mixture of CdSe QDs (radius = 1.4 nm) and **1** in THF, before and after three 48 h illumination cycles. The differences between spectra at λ < 450 nm are due to consumption of **1**. **(D)** Decay dynamics of the exciton in CdSe QDs mixed with 250 eq of **1** in THF, upon photoexcitation at 470 nm, monitored at three wavelengths: 480 nm (pure electron dynamics), 900 nm (primarily electron dynamics), and 1300 nm (primarily hole dynamics). Electrons and holes decay with a time constant of 130±30 ps in the presence of **1**; this time constant is absent if **1** is not present, see Fig. S1, Table S3.

surfaces of CdSe ($k_{\text{self-exchange}}$ ~500 s^{-1})[25], so coupled products desorb from the QD surface to make room for new substrates.

Figure 2 shows a set of [2+2] photocycloadditions of 4-vinylbenzoic acid and derivatives that demonstrate the activity and diastereoselectivity of our QD photocatalyst when directly compared to tris(2,2'-bipyridine)ruthenium(II) ($Ru(bpy)_3^{2+}$) or tris(2-phenylpyridinato)iridium (III) ($Ir(ppy)_3$), which have been used to perform similar reactions[10,11]. The QD systems generate *syn* products with d.r. > 30:1, while the molecular complexes prefer *anti* products with much lower selectivity (d.r. < 3:1). The *syn* stereochemistry of the QD products is verified by X-ray crystallography of **4** (Fig. S4) and NOESY NMR spectroscopy of all products. For the heterocoupling of **3** and either **1** or **2**, the QDs produce *syn* products with d.r. > 40:1, while the molecular complexes prefer *anti* products with d.r. < 2:1.

The selective production of the kinetically disfavored *syn* configuration by the QDs, even in the case of two different coupling partners, is remarkable considering that the only templating chemistry is the reversible association of a carboxylate on the substrate with Cd^{2+} on the QD surface. The ability of intermolecular π-π interactions among rigid olefins to promote *syn* stereochemistry in solid-state reactions[26-28] suggests that these same non-covalent interactions are responsible for the *syn* selectivity in the QD system, **Fig. 1A**.

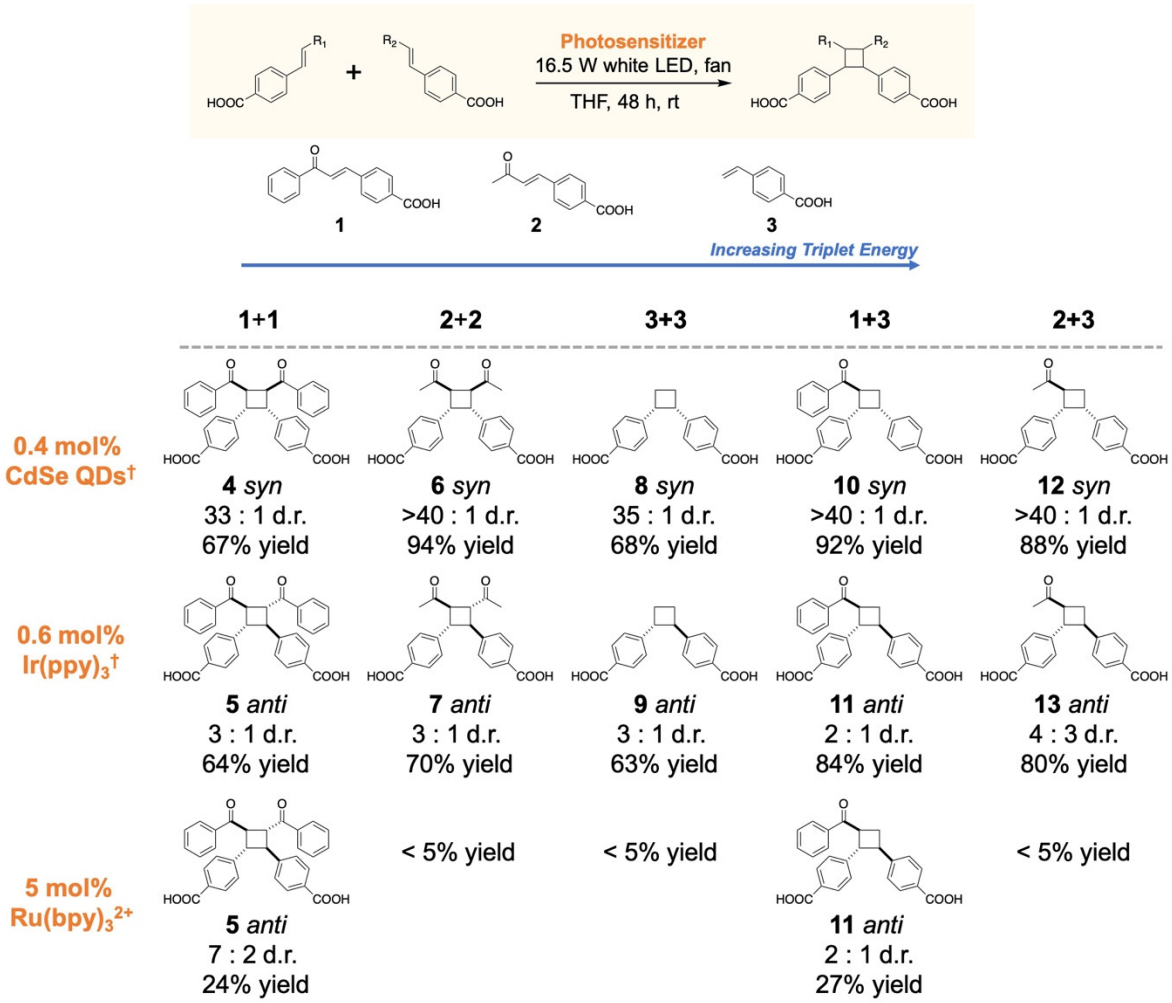

Fig. 2. Diastereoselectivity through Pre-organization on the QD Surface. Conditions and product distributions of the homo- and hetero- [2+2] photocycloadditions **1**, **2**, and **3** with QD and molecular photosensitizers, with triplet spectra shown in Figure S2. The yields listed are the isolated yields of the diastereomers drawn for QD systems (remaining mass ≡ starting material and its *cis*-isomer; zero HT product) and the NMR yields of the regioisomers drawn for $Ir(ppy)_3$ and $Ru(bpy)_3^{2+}$ systems (remaining mass ≡ starting material and its *cis*-isomer, minor unidentified side products), see the SI. Reactions of **1** were illuminated with >455 nm light so as not to excite the substrate directly. †Listed loadings are for homocycloadditions; catalyst loadings for heterocycloadditions are 1.2 mol% QDs and 1.9 mol% molecular sensitizers.

Figure 3 illustrates the role of tunable QD size in achieving heterocoupling (over homocoupling) through selective TT EnT. The difficulty in controlling competition between homo-

and heterocoupling has limited the scope of previous heterocouplings to substrates with large triplet energy differences. In this case, the triplet energies of **1** and **3** (2.25 eV and 2.51 eV respectively) are close enough such that $Ir(ppy)_3$ indiscriminantly sensitizes both substrates (**Fig. 3B**), resulting in 23% of the substrate **3** producing the undesired homocoupled product **9**. In contrast, 1.4 nm CdSe QDs perform selective TT EnT to **1** without sensitizing **3**, yielding highly efficient heterocoupling (92% yield of **10**) with <5% of **3** participating in homocoupling. The comparatively unselective performance of the higher-energy 1.0 nm CdSe QDs illustrates that selective energetic overlap with a specific substrate is the key to efficient heterocoupling.

Figure 4 demonstrates the >90% tunable regioselectivity achievable for hetero-[2+2] photocycloadditions using our QD system. Most notably this system produces the disfavored heterocoupled HT regioisomer **18**. For untemplated reactions, i.e., those photosensitized by $Ir(ppy)_3$ or by QDs but where one substrate does not have a carboxylic acid substituent (gray shaded area), formation of the HH regioisomer is strongly favored through benzylic stabilization of the corresponding 1,4-diradical intermediate. In order to access the *syn*-HT heterocoupled product **18**, which has never been formed as a major product of [2+2] photocycloaddition, we tuned the regioselectivity of the QD-catalyzed reactions through the position of the carboxylate on each substrate (**Fig. 4A**). For coupling of **1** and **2**, we achieve perfect HH regioselectivity with no HT products detected. When the carboxylate moiety is relocated to the opposite side of the substrate (**14** *vs*. **1**), the observed regioselectivity of the QD catalyst switches entirely, providing the HT product for the heterocoupling of **14** and **2** with r.r. >10:1. The *syn* diastereoselectivity is preserved in these regioselective reactions. In contrast, the $Ir(ppy)_3$ sensitizer produces the HH configuration as the major product regardless of whether **2** is coupled with **14** or **1**. The loss of regioselectivity upon removing the carboxylate from one of the substrates (**15**) shows that the QD system achieves regioselective heterocoupling through pre-arrangement of substrates at the QD surface, a manner entirely independent of electronics of the reactive olefin.

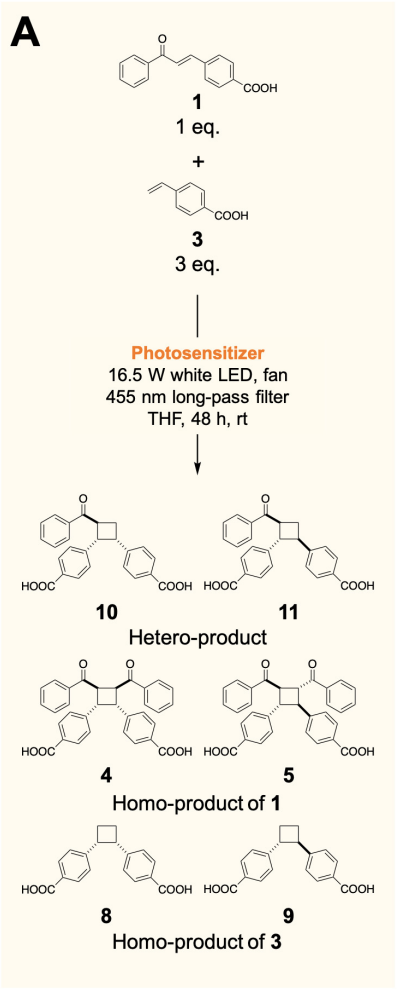

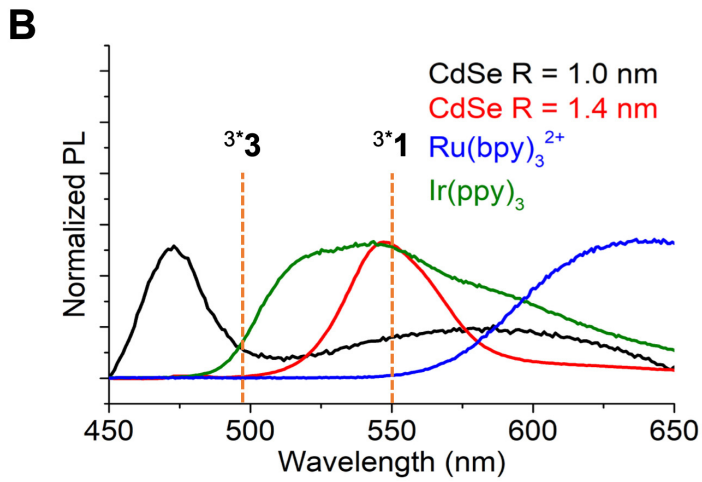

C

	Yield of Hetero-product	Yield of Homo-product of **1**	Percent **1** Unreacted	Percent **3** Homocoupled
1.2 mol% 1.4 nm CdSe QDs (536 nm)	92% **10** *syn* d.r. >40 : 1	< 5% **4** *syn* d.r. 34 : 1	< 5%	< 5% **8** *syn* d.r. 35 : 1
1.2 mol% 1.0 nm CdSe QDs (456 nm)	87% **10** *syn* d.r. >40 : 1	8% **4** *syn* d.r 35 : 1	5%	31% **8** *syn* d.r. 33 : 1
1.9 mol% $Ir(ppy)_3$	84% **11** *anti* d.r. 2 : 1	6% **5** *anti* d.r. 2 : 1	< 5%	23% **9** *anti* d.r. 3 : 1
5 mol% $Ru(bpy)_3^{2+}$	27% **11** *anti* d.r. 2 : 1	6% **5** *anti* d.r. 5 : 2	64%	< 5%

Fig. 3. **Control of Homo- *vs*. Hetereocycloaddition with QD Size. (A)** Conditions for and possible products of [2+2] photocyloadditions of **1** and **3**. **(B)** Emission spectra of four photosensitizers, compared with the triplet energies of substrates **1** and **3**, determined from phosphorescence spectra and calculations, see the SI. **(C)** Product distributions from reaction mixtures with the four photosensitizers. The yields listed are for the regioisomers indicated (drawn in **A**); the remaining mass is exclusively starting materials and the *cis*-isomer of **1** for the QD systems, and the same plus minor unidentified side products for the molecule-catalyzed reactions, see the SI.

The low overall yield of the QD-catalyzed reaction is not due to side products (72% of the remaining yield can be accounted for by starting material), but, we believe, is limited by the location of triplet acceptor orbitals of the substrate (**Fig. 4B**). For **1**, the triplet excited state

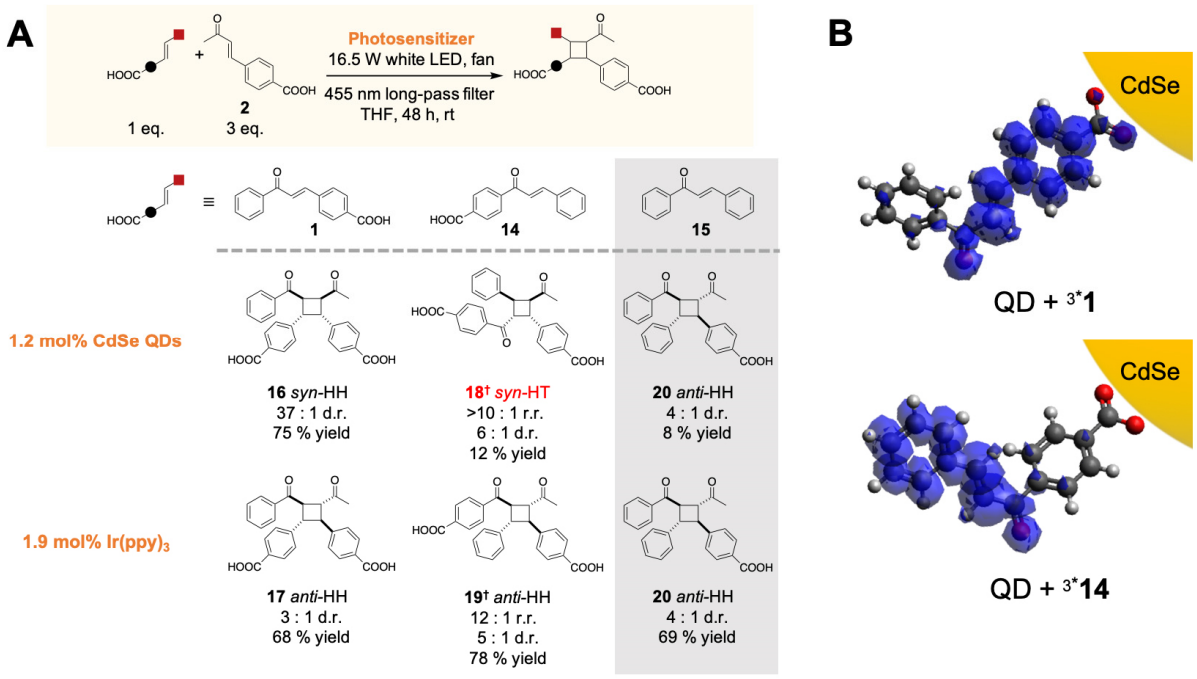

Fig. 4. **Regioselectivity through Substrate Affinity for the QD Surface. (A)** Conditions and product distributions for the [2+2] photocycloadditions of **2** and **1**, **14**, or **15**. When **2** is coupled with **15**, with no carboxylic acid, the distribution of regioisomer products matches that of $Ir(ppy)_3$.The yields listed are NMR yields for the regioisomers drawn (the major product) except **16**. The remaining mass of the coupling with **2** and **14** is starting materials and their *cis*-isomers (>72%), the HH regioisomer, and the homocycloaddition products of both substrates for the QD system, and is the same plus minor unidentified side products for the $Ir(ppy)_3$ system, see the SI. †The reaction was illuminated with a blue LED for 4 days. **B.** Transition densities for the first triplet excited states for **1** and **14** calculated using TD-DFT.

transition ($S_0 \rightarrow T_1$) has good spatial overlap with the binding group of the substrate, and therefore good electronic coupling with the QD. For **14**, there is a spatial gap between the QD surface and the triplet density; this gap makes TT EnT inefficient.

In summary, we have described a new and powerful approach to selective [2+2] photocycloadditions, and simultaneously presented the first example of catalysis triggered by triplet-triplet energy transfer from a quantum dot. By inducing self-assembly of substrate molecules through reversible association with the QD surface, we have accessed excellent

diastereoselectivity and tunable regioselectivity – including previously inaccessible *syn*-HT photo-adducts – the first example of either selectivity type using the QD ligand shell, and the first examples of tunably regioselective hetero-intermolecular [2+2] photocycloadditions. The precisely controlled triplet energy levels of QD photocatalysts facilitate efficient and selective heterocoupling. Overall, QDs present a strategy for extrinsic control of the configuration of the cyclobutane product that counters the stereo-electronic preferences of the substrates.

References

1 Dembitsky, V. M. Bioactive cyclobutane-containing alkaloids. *J. Nat. Med.* **62**, 1-33 (2008).

2 Lee-Ruff, E. & Mladenova, G. Enantiomerically Pure Cyclobutane Derivatives and Their Use in Organic Synthesis. *Chem. Rev.* **103**, 1449-1484, doi:10.1021/cr010013a (2003).

3 Tsai, I.-L. *et al.* New cytotoxic cyclobutanoid amides, a new furanoid lignan and anti-platelet aggregation constituents from Piper arborescens. *Planta Med.* **71**, 535-542 (2005).

4 Alonso, R. & Bach, T. A Chiral Thioxanthone as an Organocatalyst for Enantioselective [2+2] Photocycloaddition Reactions Induced by Visible Light. *Angew. Chem.* **126**, 4457-4460, doi:10.1002/ange.201310997 (2014).

5 Maturi, M. M. & Bach, T. Enantioselective Catalysis of the Intermolecular [2+2] Photocycloaddition between 2‐Pyridones and Acetylenedicarboxylates. *Angew. Chem. Int. Ed.* **53**, 7661-7664, doi:10.1002/anie.201403885 (2014).

6 Hörmann, F. M., Chung, T. S., Rodriguez, E., Jakob, M. & Bach, T. Evidence for Triplet Sensitization in the Visible‐Light‐Induced [2+2] Photocycloaddition of Eniminium Ions. *Angew. Chem. Int. Ed.* **57**, 827-831, doi:10.1002/anie.201710441 (2018).

7 Hu, N. *et al.* Catalytic Asymmetric Dearomatization by Visible‐Light‐Activated [2+2] Photocycloaddition. *Angew. Chem. Int. Ed.* **57**, 6242-6246, doi:10.1002/anie.201802891 (2018).

8 Blum, T. R., Miller, Z. D., Bates, D. M., Guzei, I. A. & Yoon, T. P. Enantioselective photochemistry through Lewis acid–catalyzed triplet energy transfer. *Science* **354**, 1391-1395 (2016).

9 Prier, C. K., Rankic, D. A. & MacMillan, D. W. C. Visible Light Photoredox Catalysis with Transition Metal Complexes: applications in Organic Synthesis. *Chem. Rev.* **113**, 5322-5363, doi:10.1021/cr300503r (2013).

10 Lei, T. *et al.* General and Efficient Intermolecular [2+ 2] Photodimerization of Chalcones and Cinnamic Acid Derivatives in Solution through Visible‐Light Catalysis. *Angew. Chem. Int. Ed.* **56**, 15407-15410 (2017).

11 Pagire, S. K., Hossain, A., Traub, L., Kerres, S. & Reiser, O. Photosensitised regioselective [2+ 2]-cycloaddition of cinnamates and related alkenes. *Chem. Commun.* **53**, 12072-12075 (2017).

12 Ischay, M. A., Anzovino, M. E., Du, J. & Yoon, T. P. Efficient Visible Light Photocatalysis of [2+2] Enone Cycloadditions. *JACS* **130**, 12886-12887, doi:10.1021/ja805387f (2008).

13 Du, J. & Yoon, T. P. Crossed intermolecular [2+ 2] cycloadditions of acyclic enones via visible light photocatalysis. *JACS* **131**, 14604-14605 (2009).
14 Gutekunst, W. R. & Baran, P. S. Applications of C–H Functionalization Logic to Cyclobutane Synthesis. *J. Org. Chem.* **79**, 2430-2452 (2014).
15 Poplata, S., Tröster, A., Zou, Y.-Q. & Bach, T. Recent Advances in the Synthesis of Cyclobutanes by Olefin [2 + 2] Photocycloaddition Reactions. *Chem. Rev.* **116**, 9748-9815, doi:10.1021/acs.chemrev.5b00723 (2016).
16 Hopf, H. *et al.* One‐Pot Preparation of [n] Ladderanes by [2 π + 2 π] Photocycloaddition. *Eur. J. Org. Chem.* **2005**, 567-581 (2005).
17 Bassani, D. M., Darcos, V., Mahony, S. & Desvergne, J.-P. Supramolecular Catalysis of Olefin [2 + 2] Photodimerization. *JACS* **122**, 8795-8796, doi:10.1021/ja002089e (2000).
18 Nakamura, A. & Inoue, Y. Electrostatic Manipulation of Enantiodifferentiating Photocyclodimerization of 2-Anthracenecarboxylate within γ-Cyclodextrin Cavity through Chemical Modification. Inverted Product Distribution and Enhanced Enantioselectivity. *JACS* **127**, 5338-5339, doi:10.1021/ja050704e (2005).
19 Jon, S. Y., Ko, Y. H., Park, S. H., Kim, H.-J. & Kim, K. A facile, stereoselective [2+ 2] photoreaction mediated by cucurbit [8] uril. *Chem. Commun.*, 1938-1939 (2001).
20 Karthikeyan, S. & Ramamurthy, V. Self-assembled coordination cage as a reaction vessel: triplet sensitized [2+ 2] photodimerization of acenaphthylene, and [4+ 4] photodimerization of 9-anthraldehyde. *Tetrahedron Lett.* **46**, 4495-4498 (2005).
21 Mongin, C., Garakyaraghi, S., Razgoniaeva, N., Zamkov, M. & Castellano, F. N. Direct observation of triplet energy transfer from semiconductor nanocrystals. *Science* **351**, 369-372 (2016).
22 Huang, Z., Simpson, D. E., Mahboub, M., Li, X. & Tang, M. L. Ligand enhanced upconversion of near-infrared photons with nanocrystal light absorbers. *Chem. Sci.* **7**, 4101-4104 (2016).
23 Efros, A. L. *et al.* Band-edge exciton in quantum dots of semiconductors with a degenerate valence band: Dark and bright exciton states. *Phys. Rev. B* **54**, 4843 (1996).
24 Nirmal, M. *et al.* Observation of the" dark exciton" in CdSe quantum dots. *Phys. Rev. Lett.* **75**, 3728 (1995).
25 Fritzinger, B., Capek, R. K., Lambert, K., Martins, J. C. & Hens, Z. Utilizing self-exchange to address the binding of carboxylic acid ligands to CdSe quantum dots. *JACS* **132**, 10195-10201 (2010).
26 MacGillivray, L. R. *et al.* Supramolecular Control of Reactivity in the Solid State: From Templates to Ladderanes to Metal−Organic Frameworks. *Acc. Chem. Res.* **41**, 280-291, doi:10.1021/ar700145r (2008).
27 Ito, Y. *Solid-state organic photochemistry of mixed molecular crystals*. Vol. 3 (Dekker: New York, 1999).
28 Natarajan, A. B., B. R. in *Supramolecular Photochemistry. Controlling Photochemical Processes* (ed V. Ramamurthy, Y. Inoue) 175-228 (Wiley, 2011).

Supplementary Information is linked to the online version of the paper at www.nature.com/nature.

Acknowledgements The authors thank Profs. Regan Thomson and Andrew Lee for helpful discussions. Research primarily supported by through the Air Force Office of Scientific Research (grant 9550-17-1-0271) (synthesis, photocatalysis, analytical chemistry), and by the Center for Bio-Inspired Energy Science, an Energy Frontier Research Center funded by the U.S. Department of Energy (DOE), Office of Science, Basic Energy Sciences (BES), under Award # DE-SC0000989 (calculations). C.R.R. thanks the International Institute for Nanotechnology at Northwestern University for a fellowship. This work made use of the IMSERC at Northwestern University, which has received support from the NIH (1S10OD012016-01 / 1S10RR019071-01A1); Soft and Hybrid Nanotechnology Experimental (SHyNE) Resource (NSF ECCS-1542205); the State of Illinois and International Institute for Nanotechnology (IIN).

Author Contributions: Y.J., C.W., C.R.R., and E.A.W. conceived the project and contributed to experimental design and analysis. Y.J. and C.W. conducted the optimization and control studies described in the supplementary materials. C.R.R. synthesized the substrates and analyzed the 2D NMR data. M.S.K. performed the computational studies. All authors contributed to the writing and editing of the manuscript. All data is available in the manuscript or Supplementary materials. The authors have no competing interests.

Competing interests The authors declare no competing interests.

Correspondence and requests for materials should be addressed to E.A.W.

Supplementary Information for

Regio- and Diastereoselective Intermolecular [2+2] Cycloadditions Photocatalyzed by Quantum Dots

Yishu Jiang, Chen Wang, Cameron R. Rogers, Mohamad S. Kodaimati and Emily A. Weiss*

*Corresponding author. Email: e-weiss@northwestern.edu

Table of Contents:

A. General Information

THF was purified by elution through alumina as described by Grubbs[29]. A 16.5-W (2050 lumens) Green Creative 58240 high output LED light bulb or a 34W Kessil KSPR160-467 blue LED (emission centered at 467 nm) was used for all photochemical reactions, unless otherwise noted. Reverse-phase flash column chromatography was performed with Fluka 40–63Å C_{18}-reverse phase silica (230–240 mesh). HPLC grade methanol, water and MeCN were purchased from Sigma Aldrich and used as received. $Ir(ppy)_3$, $Ru(bpy)_3(PF_6)_2$, methyl-THF and all other compounds were purchased from Sigma Aldrich and were used without further purification unless otherwise noted.

Characterization Methods. The yields listed in the main text are isolated yields for all the QDs systems except molecule **18,** and are NMR yields for all the molecular catalyst systems, as determined by ^{1}H NMR analysis of the crude reaction mixtures compared with NMR spectra of the purified products in section **M**. 3,4,5-trichloropyridine was used as an internal integration standard. Diastereomeric ratios for all compounds were determined by comparing relative intensities of ^{1}H NMR signals of the products in unpurified reaction mixtures. ^{1}H NMR data were acquired using a Bruker Neo 600 MHz spectrometer with QCI-F cryoprobe and ^{13}C NMR data were acquired using a Bruker Avance III 500 MHz spectrometer with DCH cryoprobe, referenced to dimethyl sulfoxide-d_6 (2.5 ppm and 39.52 ppm, respectively). Preparative reverse phase HPLC was performed with C18 columns (Phenomenex Polar RP 150 × 21.20 mm; 4 μm and Agilent C18 250 × 21.20 mm; 10 μm). UV-vis ground state absorption spectra were acquired using a Varian Cary 5000 spectrophotometer. Analytical LC-MS were performed on Bruker AmaZon X mass spectrometer connected to a LC using a C18 column (Thermo Hypersil BDS 50 × 3 mm; 5 μm). Steady-state emission spectra were acquired using a HORIBA Nanolog spectrofluorimeter equipped with the time-correlated single photon counting (TCSPC) module for measuring the phosphorescence lifetime.

B. QD Catalyst Recycling Experiment

A 4 mL vial was charged with (*E*)-4-(3-oxo-3-phenylprop-1-en-1-yl)benzoic acid **1** (8.4 mg, 0.033 mmol, 1.0 equiv.) and 1.4 nm oleate-capped CdSe QDs (0.27 mL of 501 μM solution in hexanes, 0.132 μmol, 0.004 equiv.); the solvent was removed *in vacuo.* The vial was then transferred to a N_2 glove box, a magnetic stir bar was added, and the contents were dissolved in 1

mL of anhydrous THF. (*Note*: exposure of QDs to peroxide-contaminated THF causes QD degradation, so THF used with QDs should be regularly tested and stored in a glovebox.) The vial was sealed with a Teflon-lined cap, removed from the glovebox, and stirred under 16.5 W white-light LED irradiation for 48 h with a 455 nm longpass filter to prevent excitation of the substrate. Axial fans were employed to keep the sample at room temperature. After illumination, 14 mL of MeOH was added to the reaction mixture and the resulting QD precipitate was collected by centrifugation. The QD pellet was then transferred back to a N_2 glove box and redispersed in THF for use in another catalytic cycle. The yields reported in **Table S1** were obtained by ^{1}H NMR spectroscopic analysis of the crude reaction mixture relative to 3,4,5-trichloropyridine internal standard. The reported NMR yields represent the total yield of both the major and minor diastereomeric cycloadducts. A 10-μL aliquot of each reaction mixture was taken before and after each cycle and diluted by 50-fold to measure the ground state absorption spectra within a 1-cm quartz cuvette.

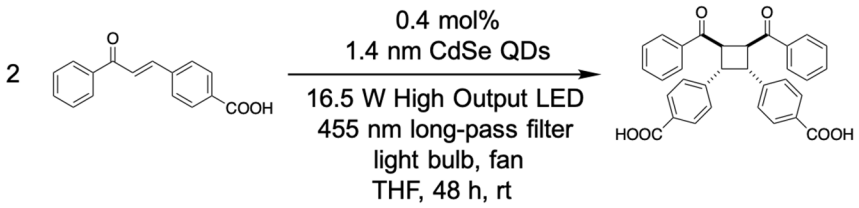

Cycle	Yield of Homo-coupling	Starting Material and its cis-isomer	d.r. (*syn* : *anti*)
1	67%	32%	34 : 1
2	69%	30%	40 : 1
3	65%	35%	37 : 1

Table S1. QD catalyst recyclability. QD catalysts exhibit no significant change in reactivity or selectivity for [2+2] homo-photocycloadditions of **1** across three successive experiments reusing the same catalyst. The yields and d.r. values were determined by ^{1}H NMR analysis of the unpurified reaction mixtures, and comparison with NMR spectra of **4** and **5** in section **M**. 3,4,5-trichloropyridine was used as an internal integration standard.

C. Control Studies in Table S2 and Scheme S1

Control studies were conducted with the following representative procedure. A 4 mL vial was charged with (*E*)-4-(3-oxo-3-phenylprop-1-en-1-yl)benzoic acid **1** (8.4 mg, 0.033 mmol, 1.0 equiv.) and 0.27 mL of 501 μM (0.132 μmol, 0.004 equiv.) 1.4 nm oleate-capped CdSe QDs in hexanes. The solvent was removed *in vacuo.* The vial was transferred to a N_2 glove box, a magnetic stir bar was added, and the contents were dissolved in 1 mL of anhydrous THF. (*Note:* the exposure of QDs to peroxide-contaminated THF causes QD degradation, so THF used with QDs should be regularly tested and stored in a glovebox.) The vial was sealed with a Teflon-lined cap and stirred under 16.5 W of white-light LED irradiation for 48 h with a 455 nm longpass filter to prevent excitation of the substrate. Axial fans were employed to keep the sample at room temperature. After illumination, 14 mL of MeOH was added to the reaction mixture and the resulting QD precipitate was collected by centrifugation. The supernatant was removed by pipette and dried under reduced pressure. The yields reported in **Table S2** and **Scheme S1** were obtained by ^{1}H NMR spectroscopic analysis of the crude reaction mixture relative to 3,4,5-trichloropyridine internal standard. The NMR yields represent the total yield of both the major and minor diastereomeric cycloadducts.

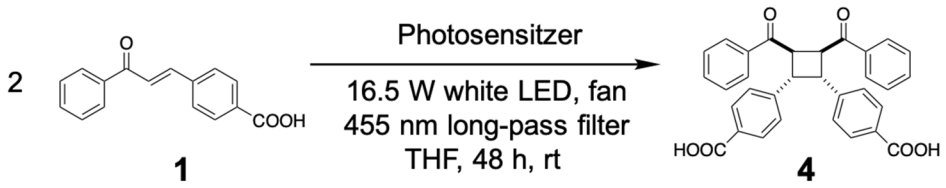

Entry	Photosensitizer	Note	Yield
1	None	--	< 5% yield
2	CdSe QDs (0.4 mol%)	No light	< 5% yield
3	CdSe QDs (0.4 mol%)	--	67%

Table S2. Control Studies for QD–catalyzed [2+2] photocycloadditions of (*E*)-4-(3-oxo-3-phenylprop-1-en-1-yl)benzoic acid 1. The yields were determined by ^{1}H NMR analysis of the unpurified reaction mixtures, and comparison with NMR spectra of **4** in section **M**. 3,4,5-trichloropyridine was used as an internal integration standard.

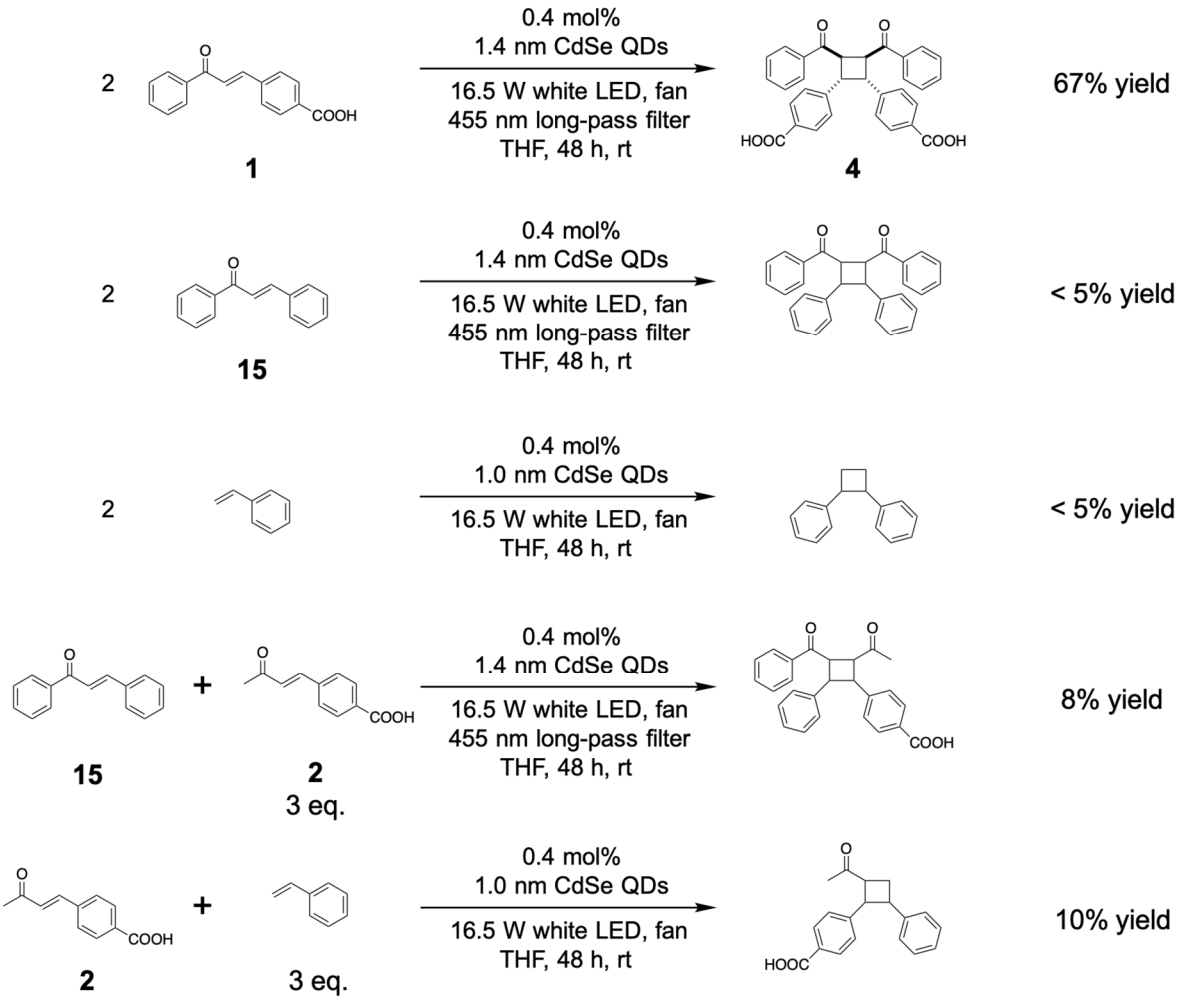

Scheme S1. Control Studies for QD–catalyzed [2+2] Photocycloadditions of Substrates with and without a Carboxylate Group. The yields were determined by ^{1}H NMR analysis of the unpurified reaction mixtures, and comparison with NMR spectra of the purified products in section **M** or reported results. 3,4,5-trichloropyridine was used as an internal integration standard.

D. Transient Absorption Spectroscopy Studies of the Exciton Decay Dynamics in CdSe QDs

More details of the femtosecond-transient absorption (TA) setup can be found elsewhere[30]. Briefly, TA experiments were conducted with a commercial system (Ultrafast Systems LLC, Helios) powered by a Ti:sapphire amplifier (Spectra-Physics, Solstice). The amplifier generated an 800 nm, 2.5 mJ, 100 fs pulse which was then split as pump and probe beams. The pump beam was directed through an optical parametric amplifier (Light Conversion, TOPAS-C), The outcoming signal line at 1140 nm was combined with the 800 nm pump residue with sum-frequency generation to produce pump pulses at wavelengths of 470 nm. For the visible probe experiment, the probe beam was directed through a 5-mm pathlength cuvette filled with 50% H_2O/D_2O (v/v) to generate a white light continuum probe spanning from 390 nm to 700 nm. For the NIR experiment, the broadband probe was generated with a 1.2-cm thick sapphire window. The pump and the probe were focused and overlapped at the sample contained in a 2-mm quartz cuvette. The sample consisted of 20 μM 490 nm CdSe QDs and 5 mM substrate **1**. The oleate-capped CdSe QDs were mixed with the substrate in an N_2-filled glove box and stirred for 12 h before use. As the control experiment, a sample with 20 μM 490 nm CdSe QDs and 5 mM benzoic acid was prepared under the same conditions to mimic the effect of the substrate binding on the QD surface. Samples were stirred vigorously during the experiments.

The triplet-triplet energy transfer (TT-EnT) process between CdSe QDs and substrate **1** is confirmed by the kinetics of TA spectral features of QDs that correspond to the electrons in the conduction band and the holes in the valence band. In the visible spectral region, the recovery kinetics of the ground state bleach (GSB) primarily reflect the evolution of the excitonic electrons. In the NIR spectral window, it has been shown that photo-induced absorption (PIA) greater than 1300 nm is primarily due to the intraband hole transitions, while the absorption feature that centers on 900 nm is primarily due to intraband electron transitions[31]. Kinetic traces of these spectral features are plotted in **Figure S1** for both the CdSe-**1** sample and a control sample containing identical QDs but without compound **1**.

The kinetics of the control sample can be fitted with a sum of three exponential decay components, convoluted with the instrument response function, with time constants listed in **Table S3**. The initial fast decay with time constants $\tau 1 = 0.77 \pm 1.2$ ps can be attributed to the fast surface trapping, whereas the slower kinetic components are related to other non-radiative recombination pathways[30-31]. We notice that these three kinetic traces do not overlap, possibly due to benzoic acid

induced defects on QDs' surface which complicate the decay of the electrons and holes. Treating QDs with substrate **1** drastically enhances the initial fast decay for all three spectral features, likely because the bulky substrate molecules provide poorer passivation than the benzoate groups.

For the CdSe-**1** sample, we observe that, after the initial ~15 ps, the kinetic traces at 480 nm, 900 nm, and 1300 nm have similar rates of decay. We fit the kinetic traces of CdSe-**1** with a sum of four exponential terms. In the fit, we allow the initial fast kinetics to vary freely, while fixing the time constants of the two slower components to their values obtained from the control sample. The fit yields kinetic components with time constants of 130 ps for 480 nm (all electron) and 900 nm (mostly electron), and 120 ps for 1300 nm (mostly hole). These results suggest that the electrons and holes of the excitons of QDs transfer from the QD together at the same rate. This observation implies energy transfer in our catalytic system rather than charge transfer, in which the electron and the hole should migrate successively.

Since the $S_0 \rightarrow S_1$ transition of substrate **1** (4 eV) is significantly higher than the bandgap emission of the 490 nm CdSe QDs (2.4 eV), the energy transfer process must happen between the QD excited states and the triplet excited state of **1**, which has an energy level of ~2.3 eV. The 130 ps energy transfer time constant is consistent with the previously reported rates for TT-EnT from CdSe QDs to polyacene acceptors[32].

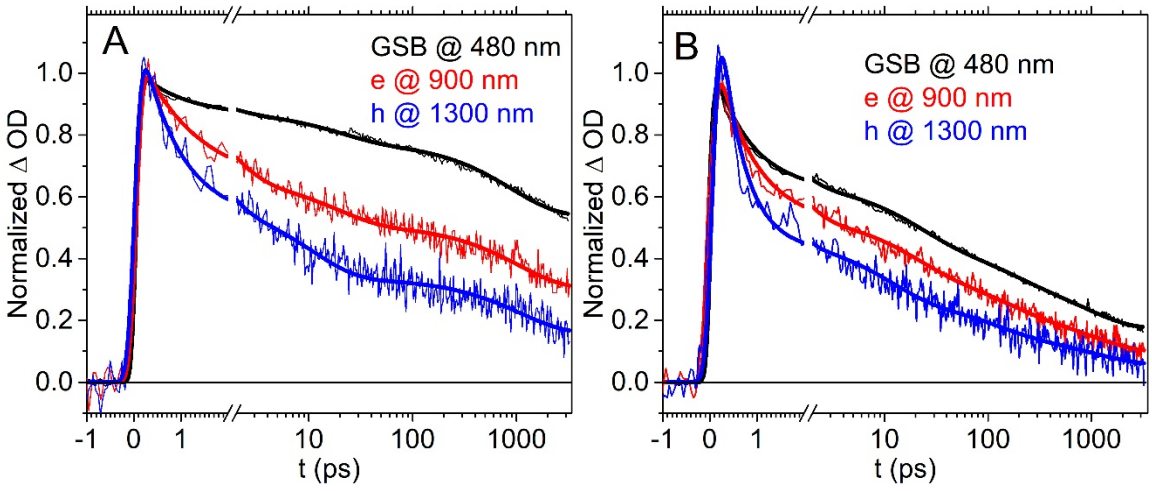

Figure S1. Normalized Kinetic Traces of Transient Absorption Spectral Features of (A) the CdSe Control Sample (QDs without Compound 1) and (B) the Mixture of CdSe and Compound 1 ("CdSe-1"). The kinetic traces for **A** are fit with the convolution of three exponential decays and a Gaussian-shape instrument response function. The fit of the kinetics traces in **B** is described in the text. Time constants resulting from these fits are listed in **Table S3**.

Table S3. Time Constants and Amplitudes of Components Extracted from Fitting the Kinetic Traces shown in Figure S1.

Spectral features	τ1 /ps (%)	τ2 /ps (%)	τ3 /ps (%)	**τ4 /ps (%)**	τ5 (%) [1]
CdSe 480 nm	0.92 ± 0.09 (13.4 ± 0.6)	19 ± 1 (10.1 ± 0.3)	890 ± 30 (23.6 ± 0.3)		>3 ns (54.0 ± 0.3)
CdSe 900 nm	1.2 ± 0.1 (39 ± 2)	18 ± 2 (15 ± 1)	1000 ± 100 (18.9 ± 0.9)		>3 ns (33.1 ± 0.04)
CdSe 1300 nm	0.77 ± 0.08 (51 ± 3)	11 ± 2 (21 ± 2)	1100 ± 200 (15 ± 1)		>3 ns (13 ± 1)
CdSe-**1** 480 nm	0.77 ± 0.03 (38.5 ± 0.7)	0.77 [2] (17.2 ± 0.8)	-- (16.7 ± 0.7)	**130 ± 20 (11.1 ± 0.06)**	>3 ns (16.6 ± 0.2)
CdSe-**1** 900 nm	0.80 ± 0.05 (52 ± 2)	0.80 [2] (15 ± 2)	-- (12 ± 2)	**130 ± 40 (12 ± 1)**	>3 ns (9.0 ± 0.6)
CdSe-**1** 1300 nm	0.48 ± 0.04 (67 ± 4)	0.48 [2] (14 ± 2)	-- (6 ± 1)	**120 ± 40 (9 ± 1)**	>3 ns (3.9 ± 0.8)

[1] These time constants are longer than the time window of our experiment.

[2] The values of these time constants were fixed to their values from the control experiment when fitting the kinetics of CdSe-**1**.

E. Kinetic Model for the Competing Formation of *syn* and *anti* Photocycloadditions Products

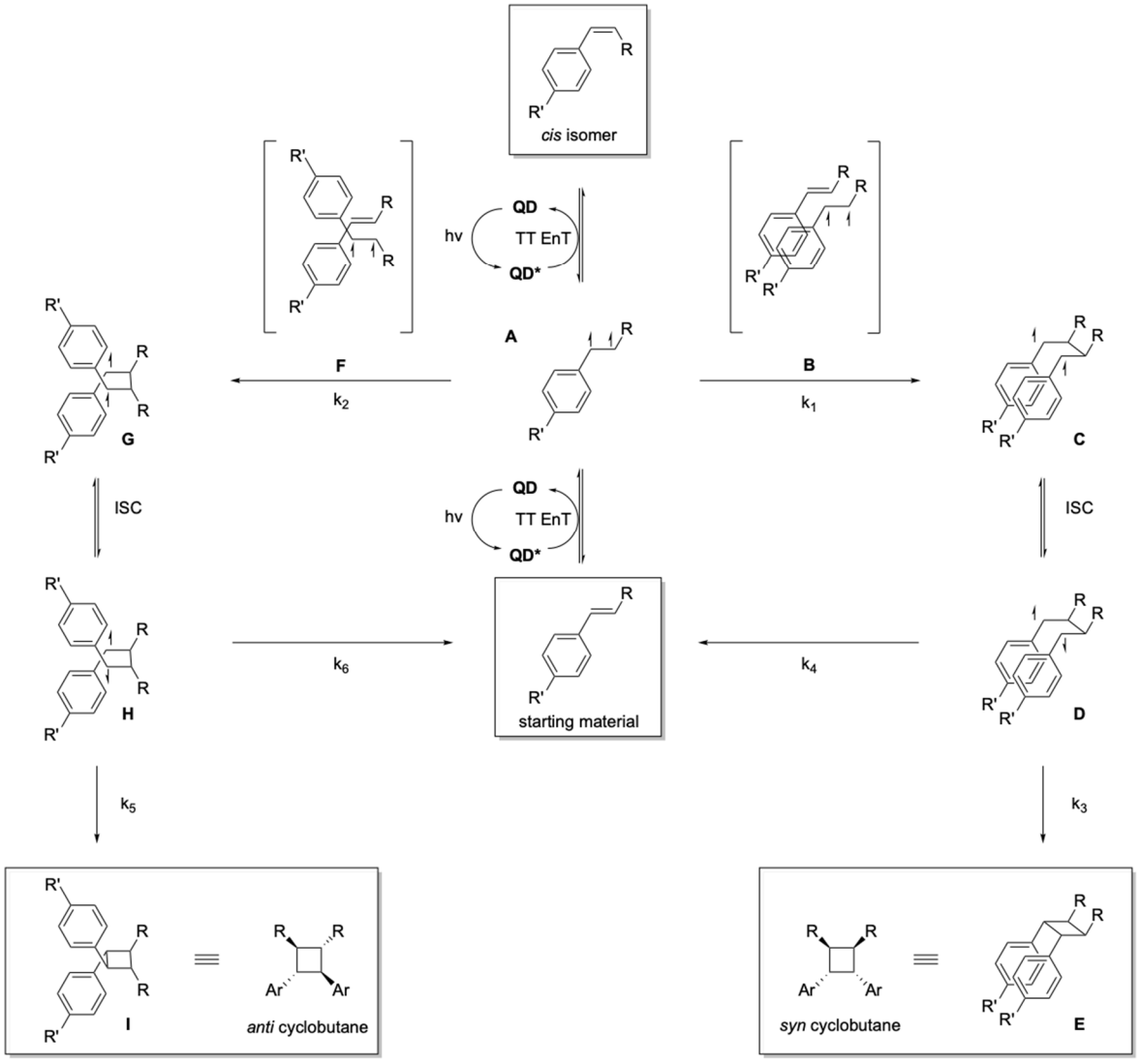

Scheme S2. Kinetic model for the formation of *syn* and *anti* cyclobutane stereoisomers following formation of A by TT EnT from a photoexcited QD. Isolable species are shown in boxes. Structures in brackets suggest the relative orientations of chalcones leading to the observed cyclobutane stereoisomers**.**

In this section, we present a kinetic model for the competing formation of *syn* and *anti* cyclobutane products, to better understand the contrary selectivities observed when using quantum dot or molecular photocatalysts. In this analysis, we make comparisons only between reactions using the same substrates but different photocatalysts, to isolate the role of QDs in determining *syn*/*anti* selectivity. Through this model, we find support for the perhaps intuitive conclusion that

selectivity depends linearly on the availability of addition partners in a given reactive conformation; this result provides an estimate of the degree of self-assembled substrate preorganization on the QD surface.

As shown in **Figure 1** of the main text, [2+2] photocycloaddition of a triplet-sensitized chalcone proceeds through a 1,4-diradical intermediate following formation of a carbon-carbon bond with a second chalcone molecule[33-34]. Importantly, formation of this bond sets the stereochemistry at those two centers; the resulting diradical intermediate can either revert to starting material or form a cyclobutane product, but cannot convert to the other stereoisomer except following reversion to the starting material. It is therefore appropriate to treat formation of the *syn* and *anti* cyclobutanes as separate pathways diverging upon initial bond formation, as shown in **Scheme S2**. No other stereoisomers are observed.

As **Scheme S2** illustrates, the *syn* cyclobutane product **E** is formed by unimolecular reaction of the singlet diradical **D**, so the rate of formation of **E** is trivially:

$$\frac{\mathrm{dE}}{\mathrm{dt}} = \mathrm{k_3[D]} \qquad (S1)$$

We can then treat the diradical with a steady-state approximation. The 1,4-diradical is a transient intermediate and undergoes rapid intersystem crossing between singlet and triplet states, and we observe no significant products from the diradical except formation of the cyclobutane and reformation of the starting chalcone. It therefore holds that:

$$\mathrm{k_1[A][B] = k_3[D] + k_4[D]} \qquad (S2)$$

where [**B**] is the concentration of chalcone coupling partners *in the correct conformation* to yield **C**, rather than yield **G**. The rate of formation of the *syn* cyclobutane can therefore be expressed as:

$$\frac{\mathrm{dE}}{\mathrm{dt}} = \frac{\mathrm{k_1 k_3[A][B]}}{\mathrm{k_3 + k_4}} \qquad (S3)$$

and the rate of formation of the *anti* product is analogously:

$$\frac{\mathrm{dI}}{\mathrm{dt}} = \frac{\mathrm{k_2 k_5[A][F]}}{\mathrm{k_5 + k_6}} \qquad (S4)$$

The ratio *S* of *syn* and *anti* products is the ratio of these rates of formation:

$$\mathrm{S} = \frac{\mathrm{syn}}{\mathrm{anti}} = \frac{\mathrm{k_1 k_3[B](k_5+k_6)}}{\mathrm{k_2 k_5[F](k_3+k_4)}} \qquad (S5)$$

Recall that [**B**] and [**F**] represent the availability of coupling partners in the appropriate conformation (relative to the sensitized species **A**) to produce *syn* or *anti* cyclobutanes,

respectively. While these terms are not particularly useful individually, their ratio represents a "preorganization factor" *P*, corresponding simply to the likelihood that a given chalcone coupling partner is oriented so as to yield a *syn* cyclobutane. Note that this preorganization factor is not the sole determinant of selectivity; the rates of forward and reverse reaction from the diradical determine an "innate" *syn*/*anti* preference for a given substrate.

$$S = \frac{syn}{anti} = \frac{k_1 k_3 (k_5 + k_6)}{k_2 k_5 (k_3 + k_{4)}} P \qquad (S6)$$

In the case of a molecular photocatalyst, like $Ir(ppy)_3$, catalyzing substrates freely diffusing in solution, the preorganization factor must be 1, as the species in solution have no preferred orientation relative to one another. The observed selectivity in the molecular case therefore equals the constant term in Equation S6, allowing us to estimate the preorganization factor for the QD catalyst by comparing diastereoselectivities obtained with QDs and with molecular catalysts:

$$P_{mol} = 1;\ S_{mol} = \frac{k_1 k_3 (k_5 + k_6)}{k_2 k_5 (k_3 + k_{4)}} \qquad (S7)$$

$$S_{QD} = S_{mol} P_{QD} \qquad (S8)$$

This final substitution relies on an assumption that the reaction rates of the diradical are unchanged in proximity to the QD surface. **Figure 4** of the main text suggests this is a reasonable approximation; when QDs catalyze the reaction between one bound substrate and one freely diffusing substrate, the observed diastereoselectivity matches exactly with that observed using a molecular catalyst. This reaction takes place at the QD surface but does not benefit from any preorganization, as one species is freely diffusing. We therefore conclude that the rate constants shown are not dramatically altered by proximity to the QD surface, Equation S8 is a reasonable estimate of the preorganization factor.

The value of the preorganization factor translates simply to a physical interpretation. For example, the calculated preorganization factor for the homocoupling of substrate **1** is about 100; we estimate therefore that a self-assembled monolayer of substrate **1** at the QD surface features approximately 99% of molecules aligned to each other, in an orientation corresponding to the *syn* product, and only about 1% of substrates misaligned within the monolayer.

F. Measured and Calculated Triplet Energies of Substrates 1, 2, 3 and 14

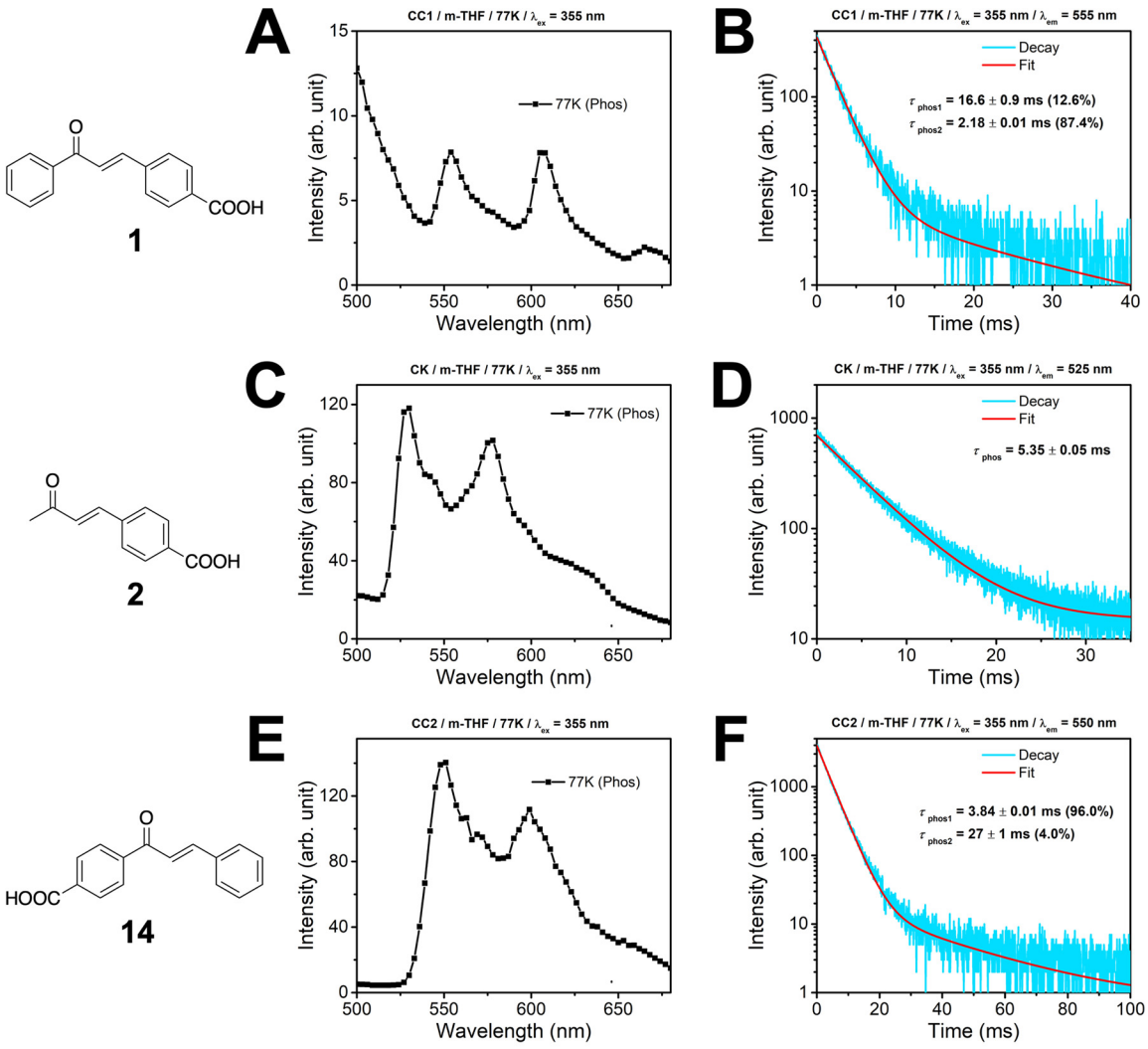

Figure S2. Phosphorescence Spectra and Lifetimes of Substrates. The phosphorescence spectra and lifetimes of (**A**, **B**) (*E*)-4-(3-oxo-3-phenylprop-1-en-1-yl)benzoic acid **1**, (**C**, **D**) (*E*)-4-(3-oxobut-1-en-1-yl)benzoic acid **2** and (**E**, **F**) (*E*)-4-(1-Oxo-3-phenyl-2-propen-1-yl)benzoic acid **14**. All measurements obtained at 77 K in 2-methyltetrahydrofuran. The average phosphorescence lifetimes of **1**, **2** and **14** are 4.0 ms, 5.4 ms and 4.6 ms, respectively.

Phosphorescence Measurements. Samples were first dissolved in methyl-THF and then transferred into 4mm-diameter quartz tubes (Wilmad-LabGlass). The optical density at the 355nm excitation wavelength was about 1. The sample in the quartz tube underwent at least three freeze-pump-thaw cycles, and the quartz tube was then flame-sealed.

Phosphorescence measurements were performed at 77K using a HORIBA Nanolog spectrofluorimeter equipped with time-correlated single-photon counting (TCSPC) module. The excitation wavelength is 355 nm. Time-resolved phosphorescence emission was collected from 380 to 680 nm, with a 3 nm increment. The final phosphorescence spectrum was generated by summing all the phosphorescence emission decays together.

Substrate **3** absorbs at higher energy than the excitation wavelength, 355 nm, so its phosphorescence spectrum cannot be accessed by the above procedure. In order to determine the triplet energy of **3**, we performed the density functional theory (DFT) calculations of the triplet energies of substrates **1**, **2** and **3**, determined the systematic error of these calculations by comparing them to the experimentally measured triplet energies of **1** and **2**, and then adjusted the calculated triplet energy of **3** by this systematic error (see below for details of calculations).

Density-Functional Theory Calculations. Quantum chemical calculations were performed at the DFT level using Nwchem 6.6 software[35]. All of the calculations were performed using the 6-311++G** basis set for all atoms along with the hybrid PBE0 functional. Calculations were performed using the Conductor-like Screening Model (COSMO) to account for solvent interactions where the solvent (THF) is approximated as a dielectric continuum[36]. We accounted for dispersion interactions by using the empirical Grimme DFT-D3 dispersion correction[37]. Additionally, all of the calculations were performed using an open-shell configuration where the spin was specified. We performed geometry optimizations for all of the molecules and intermediates using the above procedure.

In order to calculate the triplet energy of the molecules, we performed open-shell time-dependent DFT (TD-DFT) calculations of molecules in the triplet state and calculated the energy of the first 30 excitations. We selected the first excited state energy to represent the triplet energy of our molecule; the calculated triplet energies are listed in **Table S4** with the experimental results.

In order to understand the increased reactivity of substrate **1** (over substrate **14**), we visualized the transition densities of their first triplet excited states, **Figure S3** (also Figure 4 of the main text). We observed that, in the case of substrate **1**, the transition density is localized near the carboxylate binding group, while in the case of substrate **14**, the transition density is localized away from the carboxylate binding group. The difference between **1** and **14**'s transition densities make EnT from the QDs to **14** slower than EnT from the QDs to **1**, explaining the discrepancy in the yields of their respective triplet-initiated reactions.

Table S4. Triplet Energies of Substrates **1, 2, 3,** and **14** from TD-DFT Calculations and Phosphorescence Measurements.

Substrate	**1**	**2**	**3**	**14**
Calculated Triplet Energy	2.33 eV	2.33 eV	2.58 eV	2.38 eV
Measured Triplet Energy	2.25 eV	2.36 eV	-	2.28 eV
Calibrated Triplet Energy for **3**			2.51 eV	

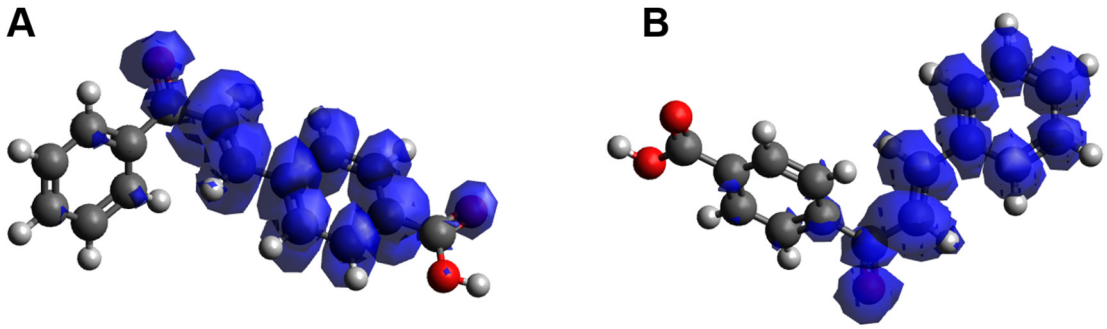

Figure S3. Visualization of the transition densities for the first triplet excited states for (*E*)-4-(3-oxo-3-phenylprop-1-en-1-yl)benzoic acid **1 (A)** and (*E*)-4-(1-Oxo-3-phenyl-2-propen-1-yl)benzoic acid **14 (B)**. Transition densities were calculated using TD-DFT. Blue surfaces indicate regions with high transition density.

G. Materials and Methods

G-1. Preparation of Substrates:

(*E*)-4-(3-oxo-3-phenylprop-1-en-1-yl)benzoic acid (Figure 2, **1**)

Compound **1** was prepared by modified literature procedure[38]. A 50 mL round-bottom flask was charged with acetophenone (500 mg, 4.16 mmol, 1.0 equiv.), 4-formylbenzoic acid (625 mg, 4.16 mmol, 1.0 equiv.), and EtOH (20 mL). KOH (700 mg, 12.48 mmol, 3.0 equiv.) was dissolved in 1.6 mL water and added to the reaction mixture, which was then stirred 12 h at room temperature. The pH value of the reaction mixture was then adjusted to 2 using 2 M HCl. The resulting precipitate was collected by vacuum filtration and recrystallized from ethanol to afford (*E*)-4-(3-

oxo-3-phenylprop-1-en-1-yl)benzoic acid **1** (514 mg, 49%) as a pale yellow powder. The ^{1}H and ^{13}C NMR spectra matched those reported in the literature[38].

(*E*)-4-(3-oxobut-1-en-1-yl)benzoic acid (Figure 2, **2**)

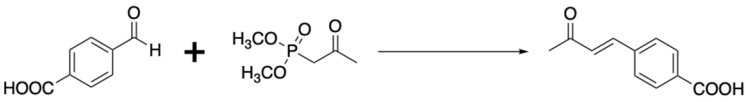

Compound **2** was prepared by modified literature procedure[39]. A 150 mL round-bottom flask was charged with 4-formylbenzoic acid (2.2 g, 14.67 mmol, 1.0 equiv), dimethyl 2-oxopropylphosphonate (2.4 g, 14.67 mmol, 1.0 equiv) and THF (65 mL). K_2CO_3 (4.05 g, 29.34 mmol, 2.0 equiv) was dissolved in water (16 mL) and added to the reaction mixture. The resulting solution was stirred 12 h at room temperature, after which 25 mL of water was added and the pH value of the resulting solution was adjusted to 2 with 2 M HCl. The resulting precipitate was collected by vacuum filtration and recrystallized from ethanol to afford (*E*)-4-(3-oxobut-1-en-1-yl)benzoic **2** (1.7 g, 61%) acid as a white solid. The ^{1}H and ^{13}C NMR spectra matched those reported in the literature[39].

(*E*)-4-(1-oxo-3-phenyl-2-propen-1-yl)benzoic acid (Figure 4, **14**)

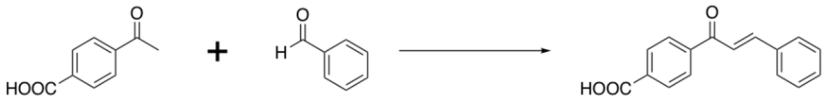

Compound **14** was prepared by modified literature procedure[40]. A 50 mL round-bottom flask was charged with 4-acetylbenzoic acid (500 mg, 3.05 mmol, 1.0 equiv.), benzaldehyde (324 mg, 3.05 mmol, 1.0 equiv.), and EtOH (20 mL). KOH (512 mg, 9.14 mmol, 3.0 equiv.) was dissolved in water (1.6 mL) and added to the reaction mixture, which was then stirred 12 h at room temperature. The pH value of the reaction mixture was then adjusted to 2 with 2 M HCl. The resulting precipitate was collected by vacuum filtration and recrystallized from ethanol to afford (*E*)-4-(1-oxo-3-phenyl-2-propen-1-yl)benzoic acid **14** (523 mg, 68%) as a pale yellow powder. The ^{1}H and ^{13}C NMR spectra matched those reported in the literature[40].

G-2. Preparation of QDs

QDs were prepared by a modified literature procedure[41]. A 25 mL three neck flask was charged with CdO (0.514 g, 4 mmol, 1.0 equiv.), oleic acid (3.02 mL, 3.338 g, 12 mmol, 3.0 equiv.) and 1 octadecene (ODE, 10 mL) under flow of nitrogen. The reaction mixture was heated to 270 °C to dissolve the red CdO in ODE, forming the cadmium carboxylate complex. The heterogeneous ODE-Se precursor was prepared by adding Se (680 mg, 20 mmol, 5.0 equiv.) powder to 10 mL of

ODE in a 20 mL vial at room temperature. The resulting dispersion was stirred for injection under nitrogen, during which time the Se did not dissolve. To initiate the reaction, 1 mL of the heterogeneous ODE-Se precursor dispersion was swiftly injected into the colorless reaction mixture containing the Cd precursor. Injection was performed at 270 °C, and growth took place for 0.5 min to 2 min at 260 °C to get CdSe QDs with a radius from 1.0 nm to 1.4 nm. The black color of the heterogeneous ODE-Se precursor disappeared upon injection, and the color of the mixture turned from yellow to orange to red depending on the size of the CdSe nanocrystals formed. The reaction mixture was then allowed to cool to room temperature and was purified by the addition of ethanol in a 3:1 ratio relative to the ODE. The resulting turbid solution was centrifuged to obtain a pellet of QDs that was redispersed in hexanes.

H. Procedure for Diastereoselective [2+2] Photocycloaddition (Figure 2)

H-1. Diastereoselective Homo [2+2] Photocycloaddition using CdSe QDs as Photocatalysts

***General Procedure for Homo [2+2] Photocycloaddition with 16.5 W High Output LED using CdSe QDs as Photocatalysts*:**

A 4 mL vial was charged with the appropriate 4-vinylbenzoic acid derivative (0.033 mmol, 1.0 equiv.) and oleate-capped CdSe QDs in hexanes (0.132 μmol, 0.004 equiv.), and the solvent was removed *in vacuo.* The vial was then transferred to a N_2 glove box, a magnetic stir bar was added, and the contents were dissolved in 1 mL dry THF. (*Note*: exposure to peroxide-contaminated THF causes QD degradation, so THF for use with QDs should be regularly tested and stored in a glovebox.) The vial was sealed with a Teflon-lined cap, removed from the glovebox, and stirred under 16.5 W white-light LED irradiation for 48 h with a 455 nm longpass filter to prevent excitation of the substrate. Axial fans were employed to maintain the room temperature. After illumination, 14 mL of MeOH was added to the reaction mixture and the resulting QD precipitate was collected by centrifugation. The supernatant was removed by pipette and concentrated under reduced pressure, and the products were purified by reverse-phase flash column chromatography (eluted with a gradient of 15% - 100% MeOH in water) unless otherwise noted. The yields reported in **Figure 2** represent the isolated yield of the major diastereomeric cycloadducts.

The QD system: syn-4,4'-(3,4-dibenzoylcyclobutane-1,2-diyl)dibenzoic acid (Figure 2, **4**)

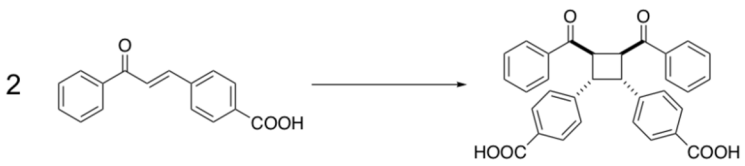

Prepared according to general procedure using 8.4 mg (0.033 mmol, 1.0 equiv.) (*E*)-4-(3-oxo-3-phenylprop-1-en-1-yl)benzoic acid **1** and 1.4 nm oleate-capped CdSe QDs (0.27 mL, 501 μM solution in hexanes, 0.132 μmol, 0.004 equiv.), yielding major product *syn*-4,4'-(3,4-dibenzoylcyclobutane-1,2-diyl)dibenzoic acid (5.6 mg, 67%) **4** as a white powder.

***syn* diastereomer** (**4**, *major product*):

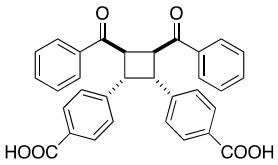

^{1}H NMR (600 MHz, DMSO-d_6): δ = 7.84 (d, *J* = 7.6 Hz, 4H), 7.69 (d, *J* = 8.2 Hz, 4H), 7.55 (t, *J* = 7.4 Hz, 2H), 7.43 (t, *J* = 7.8 Hz, 4H), 7.32 (d, *J* = 8.2 Hz, 4H), 5.21 – 5.18 (m, 2H), 4.40 – 4.37 (m, 2H).

^{13}C NMR (126 MHz, DMSO-d_6): δ = 198.0, 167.1, 144.1, 135.3, 133.1, 128.8, 128.7, 128.7, 128.3, 127.9, 47.1, 44.4.

HRMS (ESI$^-$) (*m/z*): [M-H]$^-$ calculated for $C_{32}H_{23}O_6$, 503.1495; found, 503.1493.

***The QD system: syn*-4,4'-(3,4-diacetylcyclobutane-1,2-diyl)dibenzoic acid** (Figure 2, **6**)

Prepared according to general procedure using 6.33 mg (0.033 mmol, 1.0 equiv.) (*E*)-4-(3-oxobut-1-en-1-yl)benzoic acid **2** and 1.2 nm oleate-capped CdSe QDs (0.67 mL, 200 μM solution in hexanes, 0.132 μmol, 0.004 equiv.), yielding major product *syn*-4,4'-(3,4-diacetylcyclobutane-1,2-diyl)dibenzoic acid (5.9 mg, 94%) **6** as a white powder.

***syn* Diastereomer** (**6**, *major product*):

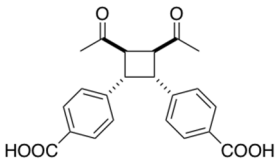

^{1}H NMR (600 MHz, DMSO-*d*$_6$): δ = 7.58 (d, *J* = 7.5 Hz, 4H), 6.98 (d, *J* = 7.6 Hz, 4H), 4.11 (d, *J* = 5.9 Hz, 2H), 4.05 (d, *J* = 5.7 Hz, 2H), 2.10 (s, 6H).

^{13}C NMR (126 MHz, DMSO-*d*$_6$): δ = 207.2, 168.7, 165.3, 141.0, 128.5, 127.1, 50.2, 43.6, 28.3.

HRMS (ESI$^-$) (*m/z*): [M-H]$^-$ calculated for $C_{22}H_{19}O_6$, 379.1182; found, 379.1189.

***The QD System: syn*-4,4'-(cyclobutane-1,2-diyl)dibenzoic acid** (Figure 2, **8**)

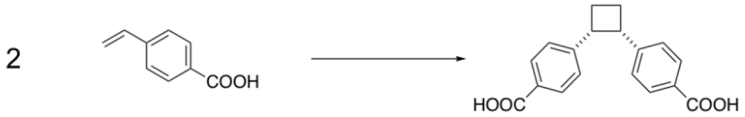

Prepared according to general procedure using 4.93 mg (0.033 mmol, 1.0 equiv.) 4-vinylbenzoic acid **3** and 1.1 nm oleate-capped CdSe QDs (0.63 mL, 213 μM solution in hexanes, 0.132 μmol, 0.004 equiv.), yielding major product *syn*-4,4'-(cyclobutane-1,2-diyl)dibenzoic acid (3.35 mg, 68%) **8** as a white powder.

***syn* Diastereomer** (**8**, *major product*):

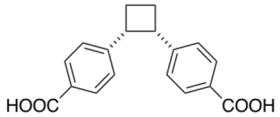

^{1}H NMR (600 MHz, DMSO-*d*$_6$): δ = 7.64 (d, *J* = 8.0 Hz, 4H), 7.09 (d, *J* = 7.9 Hz, 4H), 4.14 – 4.12 (m, 2H), 2.47 – 2.45 (m, 4H).

^{13}C NMR (126 MHz, DMSO-*d*$_6$): δ = 168.3, 165.4, 145.8, 129.1, 128.0, 45.0, 24.0.

HRMS (ESI$^-$) (*m/z*): [M-H]$^-$ calculated for $C_{18}H_{15}O_4$, 295.0970; found, 295.0963.

H-2. Diastereoselective Homo [2+2] Photocycloaddition using Ir(ppy)$_3$ or Ru(bpy)$_3$(PF$_6$)$_2$ as Photocatalysts

General Procedure for Homo [2+2] Photocycloaddition with 16.5 W LED using Ir(ppy)$_3$ or Ru(bpy)$_3$(PF$_6$)$_2$ as Photocatalysts:

For Ir(ppy)$_3$: A 4 mL vial was charged with the appropriate 4-vinylbenzoic acid derivative (0.033 mmol, 1.0 equiv.). The vial was then transferred to a N_2 glove box, a magnetic stir bar was added, and the contents were dissolved in 1 mL of a saturated THF solution of Ir(ppy)$_3$ (0.14 mg Ir(ppy)$_3$, 0.208 μmol, 0.0063 equiv.). The vial was sealed with a Teflon-lined cap, removed from the glovebox, and stirred under 16.5 W white-light LED irradiation for 48 h. Axial fans were employed

to maintain sample at room temperature. After illumination, the crude products were purified by reverse phase preparative HPLC (Phenomenex Polar RP 150 × 21.20 mm; 4 μm eluted with a gradient of 30-80 % MeCN:water with 0.1 % formic acid over 50 min, then 10 min at 100 % MeCN. The flow rate was 10 mL/min.) unless otherwise noted. The NMR yields reported in **Figure 2** represent the total yield of both the major and the minor diastereomeric cycloadducts.

For $Ru(bpy)_3(PF_6)_2$: A 4 mL vial was charged with the appropriate 4-vinylbenzoic acid derivative (0.033 mmol, 1.0 equiv.) and $Ru(bpy)_3(PF_6)_2$ (1.42 mg, 1.65 μmol, 0.05 equiv.) in MeCN, and the solvent was removed *in vacuo.* The vial was then transferred to a N_2 glove box, a magnetic stir bar was added, and the contents were dissolved in 1 mL 5:1 THF:MeCN solution. The vial was sealed with a Teflon-lined cap, removed from the glovebox, and stirred under 16.5 W white-light LED irradiation for 48 h. Axial fans were employed to maintain the room temperature. The NMR yields reported in **Figure 2** represent the total yield of both the major and the minor diastereomeric cycloadducts.

$Ir(ppy)_3$ and $Ru(bpy)_3(PF_6)_2$ systems: anti-4,4'-(3,4-dibenzoylcyclobutane-1,2-diyl)dibenzoic acid (Figure 2, **5**)

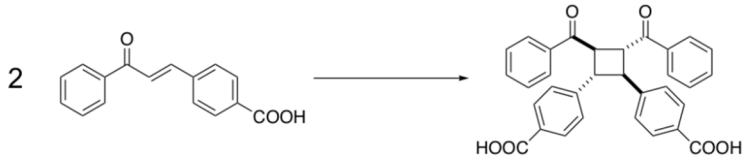

The $Ir(ppy)_3$ system: Prepared according to general procedure using 8.4 mg (0.033 mmol, 1.0 equiv.) (*E*)-4-(3-oxo-3-phenylprop-1-en-1-yl)benzoic acid **1** yielding major product *anti*-4,4'-(3,4-dibenzoylcyclobutane-1,2-diyl)dibenzoic acid (3.8 mg, 45%) **5** and minor product the *syn*-diastereomer (1.3 mg, 16%) **4**, both as white powders.

The $Ru(bpy)_3(PF_6)_2$ system: Prepared according to general procedure using 8.4 mg (0.033 mmol, 1.0 equiv.) (*E*)-4-(3-oxo-3-phenylprop-1-en-1-yl)benzoic acid **1**. The yields were obtained by ^1H NMR spectroscopic analysis of the crude reaction mixture relative to 3,4,5-trichloropyridine internal standard.

***anti* diastereomer** (**5**, *major product*):

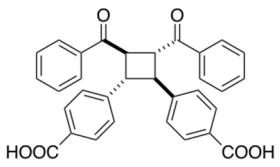

^{1}H NMR (600 MHz, DMSO-d_6): δ = 7.87 (d, *J* = 8.0 Hz, 4H), 7.78 (d, *J* = 7.7 Hz, 4H), 7.54 (t, *J* = 7.4 Hz, 2H), 7.42 (d, *J* = 8.0 Hz, 4H), 7.37 (t, *J* = 7.7 Hz, 4H), 4.72 – 4.62 (m, 2H), 4.01 – 3.92 (m, 2H).

^{13}C NMR (126 MHz, DMSO-d_6): δ = 198.4, 168.6, 165.2, 142.9, 135.2, 133.6, 129.4, 128.6, 128.4, 126.6, 47.2, 47.0.

HRMS (ESI$^-$) (*m/z*): [M-H]$^-$ calculated for $C_{32}H_{23}O_6$, 503.1495; found, 503.1485.

See section **H-1** for the characterization information of **4**.

Ir(ppy)$_3$ and Ru(bpy)$_3$(PF$_6$)$_2$ systems: anti-4,4'-(3,4-diacetylcyclobutane-1,2-diyl)dibenzoic acid (Figure 2, **7**)

The Ir(ppy)$_3$ system: Prepared according to general procedure using 6.33 mg (0.033 mmol, 1.0 equiv.) (*E*)-4-(3-oxobut-1-en-1-yl)benzoic acid **2** yielding major product *anti*-4,4'-(3,4-diacetylcyclobutane-1,2-diyl)dibenzoic acid (3.1 mg, 49%) **7** and minor product the *syn*-diastereomer (0.8 mg, 13%) **6**, both as white powders.

The Ru(bpy)$_3$(PF$_6$)$_2$ system: Prepared according to general procedure using 6.33 mg (0.033 mmol, 1.0 equiv.) (*E*)-4-(3-oxobut-1-en-1-yl)benzoic acid **2**. The yield of cycloadducts was too small to detect.

***anti* Diastereomer** (**7**, *major product*):

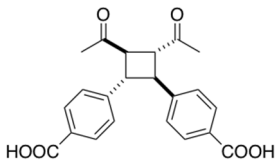

^{1}H NMR (600 MHz, DMSO-d_6): δ = 7.87 (d, *J* = 7.9 Hz, 4H), 7.36 (d, *J* = 7.9 Hz, 4H), 3.64 – 3.62 (m, 2H), 3.59 – 3.57 (m, 2H), 2.04 (s, 6H).

^{13}C NMR (126 MHz, DMSO-d_6): δ = 206.5, 167.9, 164.9, 144.7, 129.5, 126.9, 50.7, 45.9, 28.1.

HRMS (ESI$^-$) (*m/z*): [M-H]$^-$ calculated for $C_{22}H_{19}O_6$, 379.1182; found, 379.1187.

See section **H-1** for the characterization information of **6**.

Ir(ppy)$_3$ and Ru(bpy)$_3$(PF$_6$)$_2$ systems: anti-4,4'-(cyclobutane-1,2-diyl)dibenzoic acid (Figure 2, **9**)

The Ir(ppy)$_3$ system: Prepared according to general procedure using 4.93 mg (0.033 mmol, 1.0 equiv.) 4-vinylbenzoic acid **3** yielding a 4:1 mixture of the major product *syn*-4,4'-(cyclobutane-1,2-diyl)dibenzoic acid **9** and minor product the *syn*-diastereomer **8** as white powders (2.3 mg, 46%).

The Ru(bpy)$_3$(PF$_6$)$_2$ system: Prepared according to general procedure using 4.93 mg (0.033 mmol, 1.0 equiv.) 4-vinylbenzoic acid **3**. The yield of cycloadducts was too small to detect.

anti **Diastereomer** (**9**, *major product*) and ***syn*** **Diastereomer** (**8**, *minor product*) as a mixture:

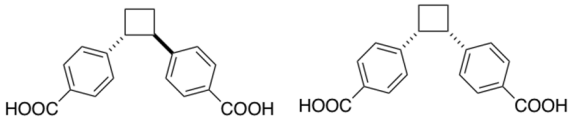

^{1}H NMR (600 MHz, DMSO-d_6): δ = 7.85 (d, *J* = 8.1 Hz, 4H), 7.63 (d, *J* = 8.0 Hz, 1H), 7.32 (d, *J* = 8.1 Hz, 4H), 7.06 (d, *J* = 8.0 Hz, 1H), 4.14 – 4.08 (m, 0.5H), 3.68 – 3.60 (m, 2H), 2.48 – 2.43 (m, 1H), 2.34 – 2.24 (m, 2H), 2.16 – 2.06 (m, 2H).

^{13}C NMR (126 MHz, DMSO-d_6): δ = 167.63, 167.53, 164.56 (2C), 148.13, 145.89, 129.40, 128.68, 127.65, 126.52, 47.17, 44.47, 25.60, 23.36.

HRMS (ESI$^-$) (*m/z*): [M-H]$^-$ calculated for $C_{18}H_{15}O_4$, 295.0970; found, 295.0972.

See section **H-1** for the characterization information of **8**.

H-3. Diastereoselective hetero [2+2] photocycloadditions using CdSe QDs as photocatalysts

General Procedure for Hetero [2+2] Photocycloaddition with a 16.5 W High Output LED using CdSe QDs as Photocatalysts:

A 4 mL vial was charged with the sensitized molecule (0.011 mmol, 1.0 equiv.), the coupling partner (0.033 mmol, 3.0 equiv.) and oleate-capped CdSe QDs in hexanes (0.132 μmol, 0.012 equiv.), and the solvent was removed *in vacuo.* The vial was then transferred to a N_2 glove box, a magnetic stir bar was added, and the contents were dissolved in 1 mL dry THF. (*Note*: exposure to peroxide-contaminated THF causes QD degradation, so THF for use with QDs should be

regularly tested and stored in a glovebox.) The vial was sealed with a Teflon-lined cap and stirred under 16.5 W white-light LED irradiation for 48 h. Regular fans were employed to maintain the room temperature. After illumination, 14 mL of MeOH was added to the reaction mixture and the resulting QD precipitate was collected by centrifugation. The supernatant was removed by pipette and concentrated under reduced pressure, and the products were purified by reverse phase preparative HPLC (Phenomenex Polar RP 150 × 21.20 mm; 4 μm eluted with a gradient of 30-80 % MeCN:water with 0.1 % formic acid over 50 min, then 10 min at 100 % MeCN. The flow rate was 10 mL/min.) unless otherwise noted. The yields reported in **Figure 2** represent the isolated yield of the major diastereomeric cycloadducts.

QD system: syn-4,4'-(3-benzoylcyclobutane-1,2-diyl)dibenzoic acid (Figure 2, **10**)

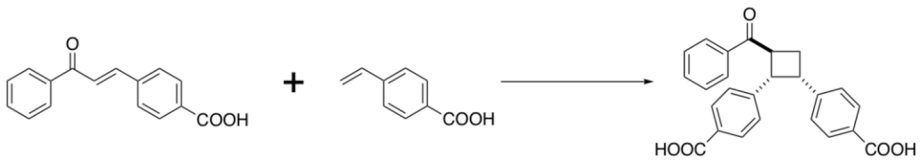

Prepared according to general procedure using 2.8 mg (0.011 mmol, 1.0 equiv.) (*E*)-4-(3-oxo-3-phenylprop-1-en-1-yl)benzoic acid **1** (the sensitized molecule), 4.93 mg (0.033 mmol, 3.0 equiv.) 4-vinylbenzoic acid **3** (the coupling partner) and 0.27 mL 501 μM (0.132 μmol, 0.012 equiv.) 1.4 nm oleate-capped CdSe QDs in hexanes yielding major product *syn*-4,4'-(3-benzoylcyclobutane-1,2-diyl)dibenzoic acid (4.09 mg, 92%) **10** as a white powder.

***syn* Diastereomer** (**10**, *major product*):

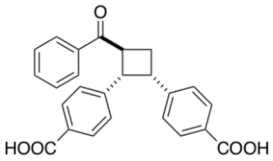

^{1}H NMR (600 MHz, DMSO-d_6): δ = 8.04 – 7.99 (m, 2H), 7.70 – 7.60 (m, 5H), 7.54 (t, *J* = 7.6 Hz, 2H), 7.25 (d, *J* = 7.9 Hz, 2H), 7.12 (d, *J* = 8.0 Hz, 2H), 4.76 (dd, *J* = 8.7, 8.7 Hz, 1H), 4.44 (dd, *J* = 9.1, 9.1 Hz, 1H), 4.04 (dt, *J* = 9.5, 5.0 Hz, 1H), 2.83 (dt, *J* = 11.0, 5.0 Hz, 1H), 2.68 (dt, *J* = 11.8, 8.6 Hz, 1H).

^{13}C NMR (126 MHz, DMSO-d_6): δ = 199.7, 167.7, 167.7, 164.7, 145.1, 143.9, 135.0, 133.4, 128.8, 128.7, 128.6, 128.5 (2C), 128.1, 127.7, 45.2, 43.2, 41.2, 27.6.

HRMS (ESI$^-$) (*m/z*): $[M-H]^-$ calculated for $C_{25}H_{19}O_5$, 399.1232; found, 399.1236.

Important NOE-contacts

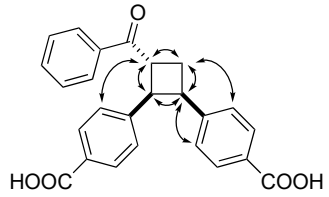

QD system: syn-4,4'-(3-acetylcyclobutane-1,2-diyl)dibenzoic acid (Figure 2, **12**)

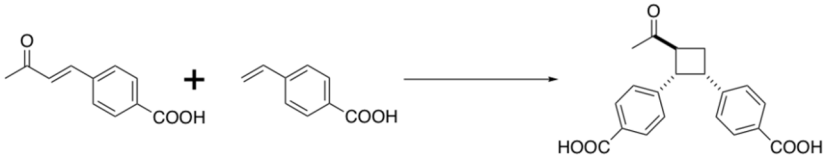

Prepared according to general procedure using 2.11 mg (0.011 mmol, 1.0 equiv.) (*E*)-4-(3-oxobut-1-en-1-yl)benzoic acid **2** (the sensitized molecule), 4.93 mg (0.033 mmol, 3.0 equiv.) 4-vinylbenzoic acid **3** (the coupling partner) and 0.67 mL 200 μM (0.132 μmol, 0.012 equiv.) 1.2 nm oleate-capped CdSe QDs in hexanes yielding major product *syn*-4,4'-(3-acetylcyclobutane-1,2-diyl)dibenzoic acid (3.30 mg, 88%) **12** as a white powder.

***syn* Diastereomer** (**12**, *major product*):

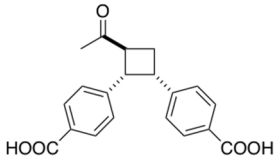

^{1}H NMR (600 MHz, acetone-d_6): δ = 7.74 (d, *J* = 8.1 Hz, 2H), 7.72 (d, *J* = 8.1 Hz, 2H), 7.21 (d, *J* = 8.1 Hz, 2H), 7.14 (d, *J* = 8.1 Hz, 2H), 4.34 (dd, *J* = 9.4, 9.4 Hz, 1H), 4.06 – 4.00 (m, 2H), 2.75 – 2.70 (m, 1H), 2.67 – 2.63 (m, 1H), 2.12 (s, 3H).

^{1}H NMR (600 MHz, DMSO-d_6): δ = 7.63 (d, *J* = 7.9 Hz, 2H), 7.61 (d, *J* = 7.9 Hz, 2H), 7.11 (d, *J* = 7.9 Hz, 2H), 7.04 (d, *J* = 7.9 Hz, 2H), 4.20 (t, *J* = 9.5 Hz, 1H), 3.99 (q, *J* = 9.1 Hz, 1H), 3.89 (td, *J* = 9.4, 4.2 Hz, 1H), 2.65 – 2.59 (m, 1H), 2.55 – 2.50 (m, overlapping with solvent), 2.10 (s, 3H).

^{13}C NMR (126 MHz, DMSO-d_6): δ = 208.25, 167.16, 167.16, 145.94 (2C), 144.66 (2C), 128.82, 128.73, 128.20, 127.85, 46.79, 45.66, 40.90, 27.57, 25.59.

HRMS (ESI$^-$) (*m/z*): $[M-H]^-$ calculated for $C_{20}H_{17}O_5$, 337.1076; found, 337.1080.

Important NOE-contacts

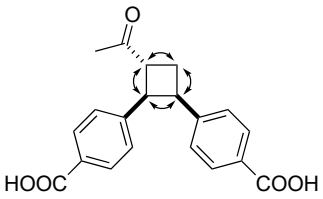

H-4. Diastereoselective Hetero [2+2] Photocycloaddition using $Ir(ppy)_3$ or $Ru(bpy)_3(PF_6)_2$ as Photocatalysts

General Procedure for Homo [2+2] Photocycloaddition with 16.5 W High Output LED using $Ir(ppy)_3$ or $Ru(bpy)_3(PF_6)_2$ as Photocatalysts:

For $Ir(ppy)_3$: A 4 mL vial was charged with the sensitized molecule (1.0 equiv.) and the coupling partner (3.0 equiv.). The vial was then transferred to a N_2 glove box, a magnetic stir bar was added, and the contents were dissolved in 1 mL of a saturated $Ir(ppy)_3$ solution in THF (0.14 mg $Ir(ppy)_3$, 0.208 μmol, 0.0189 equiv.). The vial was sealed with a Teflon-lined cap, removed from the glovebox, and stirred under 16.5 W white-light LED irradiation for 48 h. Axial fans were employed to maintain the room temperature. After illumination, the crude products were purified by reverse phase preparative HPLC (Phenomenex Polar RP 150 × 21.20 mm; 4 µm eluted with a gradient of 30-80 % MeCN:water with 0.1 % formic acid over 50 min, then 10 min at 100 % MeCN. The flow rate was 10 mL/min.) unless otherwise noted. The NMR yields reported in **Figure 2** represent the total yield of both the major and the minor diastereomeric cycloadducts.

For $Ru(bpy)_3(PF_6)_2$: A 4 mL vial was charged with the sensitized molecule (1.0 equiv.), the coupling partner (3.0 equiv.) and $Ru(bpy)_3(PF_6)_2$ (0.47 mg, 0.55 μmol, 0.05 equiv.) in MeCN and the solvent was removed *in vacuo*. The vial was then transferred to a N_2 glove box, a magnetic stir bar was added, and the contents were dissolved in 1 mL 9:1 THF:MeCN solution. The vial was sealed with a Teflon-lined cap, removed from the glovebox, and stirred under 16.5 W white-light LED irradiation for 48 h. Axial fans were employed to keep the sample at room temperature. The NMR yields reported in **Figure 2** represent the total yield of both the major and the minor diastereomeric cycloadducts.

$Ir(ppy)_3$ and $Ru(bpy)_3(PF_6)_2$ systems: anti-4,4'-(3-benzoylcyclobutane-1,2-diyl)dibenzoic acid (Figure 2, **11**)

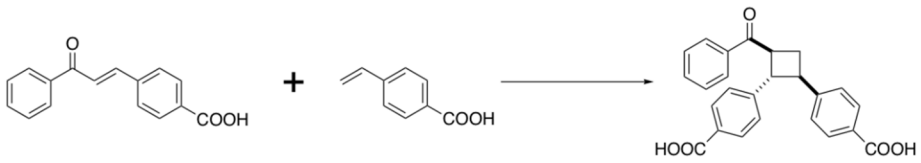

The Ir(ppy)$_3$ system: Prepared according to the general procedure using 2.8 mg (0.011 mmol, 1.0 equiv.) (*E*)-4-(3-oxo-3-phenylprop-1-en-1-yl)benzoic acid **1** (the sensitized molecule) and 4.93 mg (0.033 mmol, 3.0 equiv.) 4-vinylbenzoic acid **3** (the coupling partner), yielding a 5:2 mixture of the major product *anti*-4,4'-(3-benzoylcyclobutane-1,2-diyl)dibenzoic acid **11** and minor product the *syn*-diastereomer **10** as white powders (3.5 mg, 78%).

The Ru(bpy)$_3$(PF$_6$)$_2$ system: Prepared according to the general procedure using 2.8 mg (0.011 mmol, 1.0 equiv.) (*E*)-4-(3-oxo-3-phenylprop-1-en-1-yl)benzoic acid **1** (the sensitized molecule) and 4.93 mg (0.033 mmol, 3.0 equiv.) 4-vinylbenzoic acid **3** (the coupling partner). The yields were obtained by ^{1}H NMR spectroscopic analysis of the crude reaction mixture relative to 3,4,5-trichloropyridine internal standard.

***anti* Diastereomer** (**11**, *major product*) and ***syn* Diastereomer** (**10**, *minor product*) as a mixture:

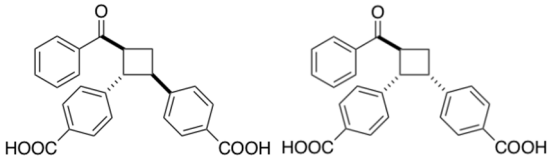

^{1}H NMR (600 MHz, DMSO-*d*$_6$): δ = 8.05 – 8.00 (m, 0.8H), 7.94 – 7.90 (m, 2H), 7.88 (dd, *J* = 8.3, 2.3 Hz, 4H), 7.69 (d, *J* = 8.0 Hz, 0.8H), 7.67 – 7.60 (m, 2.2H), 7.56 – 7.52 (m, 0.8H), 7.51 – 7.46 (m, 2H), 7.43 (d, *J* = 8.1 Hz, 2H), 7.36 (d, *J* = 8.1 Hz, 2H), 7.28 (d, *J* = 8.0 Hz, 0.8H), 7.14 (d, *J* = 8.1 Hz, 0.8H), 4.77 (q, *J* = 8.6 Hz, 0.4H), 4.47 (t, *J* = 9.1 Hz, 0.4H), 4.36 (q, *J* = 9.3 Hz, 1H), 4.05 (td, *J* = 9.4, 5.0 Hz, 0.4H), 3.92 (t, *J* = 9.7 Hz, 1H), 3.85 – 3.79 (m, 1H), 2.87 – 2.79 (m, 1.4H), 2.68 (dt, *J* = 11.8, 8.6 Hz, 0.4H), 2.27 (q, *J* = 10.0 Hz, 1H).

^{13}C NMR (126 MHz, DMSO-*d*$_6$): 199.80, 199.42, 167.42 (4C), 163.92 (2C), 147.95, 146.81, 145.87, 144.64, 135.26, 135.02, 133.58, 133.54, 129.83, 129.67, 129.64, 128.92, 128.88, 128.81, 128.54 (2C), 128.41 (2C), 128.36, 128.01, 127.30, 126.88, 48.91, 45.17, 44.97, 43.21, 42.52, 41.27, 30.69, 27.71.

HRMS (ESI$^-$) (m/z): $[M-H]^-$ calculated for $C_{25}H_{19}O_5$, 399.1232; found, 399.1231.

See section **H-3** for the characterization information of **10**.

Ir(ppy)$_3$ and Ru(bpy)$_3$(PF$_6$)$_2$: anti-4,4'-(3-acetylcyclobutane-1,2-diyl)dibenzoic acid (Figure 2, **13**)

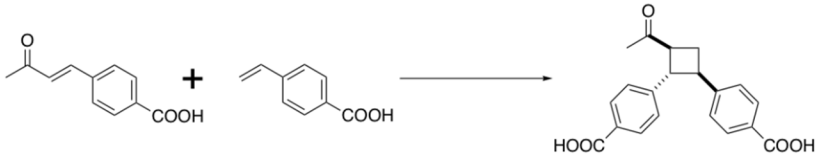

The Ir(ppy)$_3$ system: Prepared according to the general procedure using 2.11 mg (0.011 mmol, 1.0 equiv.) (*E*)-4-(3-oxobut-1-en-1-yl)benzoic acid **2** (the sensitized molecule) and 4.93 mg (0.033 mmol, 3.0 equiv.) 4-vinylbenzoic acid **3** (the coupling partner), yielding a 2:1 mixture of the major product *anti*-4,4'-(3-acetylcyclobutane-1,2-diyl)dibenzoic acid **13** and minor product the *syn*-diastereomer **12** with substrate **3** as white powders (3 mg, containing coupling products 2.6 mg, 70%).

The Ru(bpy)$_3$(PF$_6$)$_2$ system: Prepared according to the general procedure using 2.11 mg (0.011 mmol, 1.0 equiv.) (*E*)-4-(3-oxobut-1-en-1-yl)benzoic acid **2** (the sensitized molecule) and 4.93 mg (0.033 mmol, 3.0 equiv.) 4-vinylbenzoic acid **3** (the coupling partner). The yield of cycloadducts was too small to detect.

anti **Diastereomer** (**13**, *major product*) and ***syn*** **Diastereomer** (**12**, *minor product*) with **substrate 3** as a mixture:

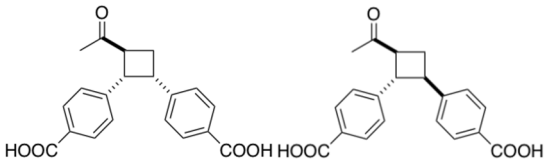

^{1}H NMR (600 MHz, DMSO-d_6): δ = 7.89 (d, *J* = 8.3 Hz, 2H), 7.87 (d, *J* = 8.3 Hz, 2H), 7.66 (d, *J* = 8.3 Hz, 1H), 7.64 (d, *J* = 8.3 Hz, 1H), 7.44 (d, *J* = 8.1 Hz, 2H), 7.32 (d, *J* = 8.1 Hz, 2H), 7.16 (d, *J* = 8.1 Hz, 1H), 7.09 (d, *J* = 8.0 Hz, 1H), 4.24 (t, *J* = 9.5 Hz, 0.5H), 4.01 (q, *J* = 9.1 Hz, 0.5H), 3.92 (td, *J* = 9.3, 4.3 Hz, 0.5H), 3.69 (t, *J* = 9.6 Hz, 1H), 3.64 (q, *J* = 9.4 Hz, 1H), 3.47 (q, *J* = 9.3 Hz, 1H), 2.66 – 2.52 (m, 2H), 2.18 (q, *J* = 10.0 Hz, 1H), 2.11 (s, 1.5H), 2.03 (s, 3H).

with **substrate 3** δ = 7.90 (d, *J* = 8.2 Hz, 1H), 7.57 (d, *J* = 8.2 Hz, 1H), 6.80 (dd, *J* = 17.7, 10.9 Hz, 0.5H), 5.96 (d, *J* = 17.7 Hz, 0.5H), 5.39 (d, *J* = 11.0 Hz, 0.5H).

^{13}C NMR (126 MHz, DMSO-d_6): δ = 208.21, 207.84, 167.33 (2C), 167.30 (2C), 147.74 (2C), 146.59 (2C), 145.63 (2C), 144.36 (2C), 129.53, 129.50, 128.78, 128.68, 128.09, 127.75, 127.12, 126.73, 49.41, 48.61, 46.82, 45.68, 42.11, 40.88, 28.31, 27.72, 27.55, 25.57.
with **substrate 3** δ = 167.26, 140.84, 135.93, 129.60, 126.09, 116.67.

HRMS (ESI$^-$) (*m/z*): [M-H]$^-$ calculated for $C_{20}H_{17}O_5$, 337.1076; found, 337.1081, 295.0975 ($C_{18}H_{15}O_4$, substrate **3**).

See section **H-3** for the characterization information of **12**.

I. Procedure for Control of Homo- vs. Heterocoupling with QD Size (Figure 3)

I-1. Photoluminescence Measurements

The photoluminescence (PL) spectra were measured using a right-angle geometry and a 2 mm/1cm dual-pathlength cuvette. The 420 nm excitation beam was applied along the 1 cm path of the cuvette, and the excitation slit width was 3 nm. The sample emission was collected along the 2 mm path with a slit width of 3 nm. PL spectra were corrected for the absorption of the solution in the 450–700 nm region.

I-2. General Procedure for control of homo- vs. hetero- [2+2] photocycloaddition with different-size CdSe QDs, Ir(ppy)$_3$ or Ru(bpy)$_3$(PF$_6$)$_2$ as photocatalysts:

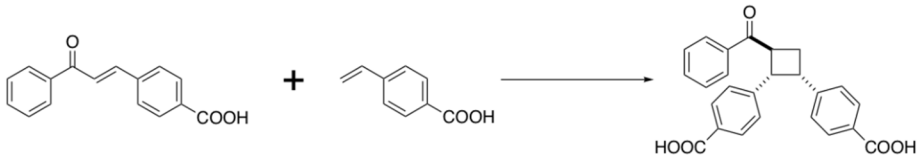

Prepared according to procedure **G-3** using 2.8 mg (0.011 mmol, 1.0 equiv.) (*E*)-4-(3-oxo-3-phenylprop-1-en-1-yl)benzoic acid **1** (the sensitized molecule), 4.93 mg (0.033 mmol, 3.0 equiv.) 4-vinylbenzoic acid **3** (the coupling partner). The photosensitizers are 1.4 nm oleate-capped CdSe QDs, 1.0 nm oleate-capped CdSe QDs, Ir(ppy)$_3$ or Ru(bpy)$_3$(PF$_6$)$_2$ with the same loadings in **H-3** and **H-4**.

See section **H** for the characterization information of **4**, **5**, **8**, **9**, **10** and **11**.

J. Procedure for Regioselective Hetero [2+2] Photocycloadditions (Figure 4)

J-1. General Procedure for Regioselective hetero [2+2] Photocycloadditions using CdSe QDs as Photocatalysts

See section **H-3** for the general procedure.

QD system: syn-4,4'-(3-acetyl-4-benzoylcyclobutane-1,2-diyl)dibenzoic acid (Figure 4, **16**)

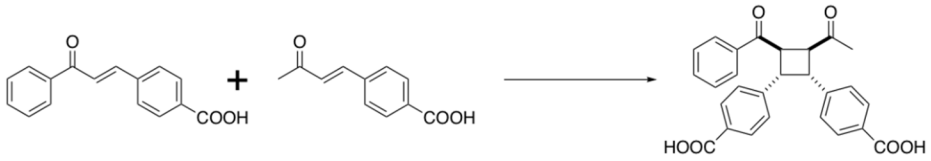

Prepared according to the general procedure using 2.8 mg (0.011 mmol, 1.0 equiv.) (*E*)-4-(3-oxo-3-phenylprop-1-en-1-yl)benzoic acid **1** (the sensitized molecule), 6.33 mg (0.033 mmol, 3.0 equiv.) (*E*)-4-(3-oxobut-1-en-1-yl)benzoic acid (the coupling partner) **2** and 0.27 mL 501 μM (0.132 μmol, 0.012 equiv.) 1.4 nm oleate-capped CdSe QDs in hexanes. The crude products were purified by reverse phase preparative HPLC (Agilent C18 250 × 21.20 mm; 10 µm eluted with a gradient of 30-60 % MeCN:water with 0.1 % formic acid over 40 min, then 20 min at 100 % MeCN. The flow rate was 10 mL/min.) yielding major product *syn*-4,4'-(3-acetyl-4-benzoylcyclobutane-1,2-diyl)dibenzoic acid (3.7 mg, 75%) **16** as a white powder.

syn **Diastereomer** (**16**, *major product*):

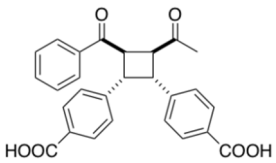

^{1}H NMR (600 MHz, DMSO-*d*$_6$): δ = 7.91 (d, *J* = 7.3 Hz, 2H), 7.70 – 7.65 (m, 4H), 7.63 (t, *J* = 7.4 Hz, 1H), 7.52 (t, *J* = 7.6 Hz, 2H), 7.26 – 7.23 (m, 4H), 5.05 – 4.93 (m, 1H), 4.45 – 4.36 (m, 1H), 4.31 – 4.23 (m, 2H), 2.00 (s, 3H).

^{13}C NMR (126 MHz, DMSO-*d*$_6$): δ = 206.40, 198.34, 167.08 (2C), 167.06, 144.41, 144.09, 135.40, 133.30, 128.86, 128.80, 128.75, 128.65, 128.56, 128.20, 128.05, 50.50, 46.40, 43.81, 43.76, 28.09.

HRMS (ESI$^-$) (*m/z*): [M-H]$^-$ calculated for $C_{27}H_{21}O_6$, 441.1338; found, 441.1341.

Important NOE-contacts

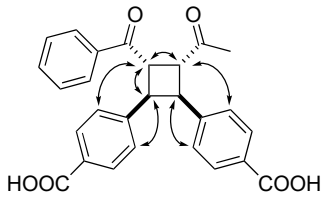

QDs system: syn-4-(3-acetyl-2-(4-carboxyphenyl)-4-phenylcyclobutane-1-carbonyl)benzoic acid (Figure 4, **18**)

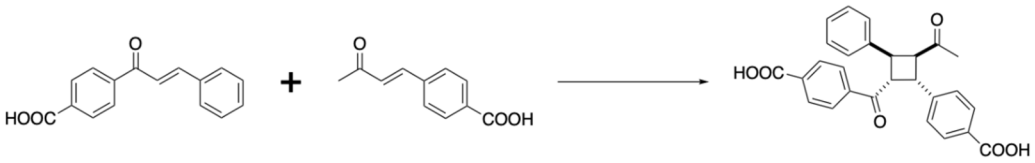

The reaction was conducted on large (0.033 mmol) scale. Prepared according to general procedure using 8.4 mg (0.033 mmol, 1.0 equiv.) (*E*)-4-(1-oxo-3-phenyl-2-propen-1-yl)benzoic acid **14** (the sensitized molecule), 18.99 mg (0.099 mmol, 3.0 equiv.) (*E*)-4-(3-oxobut-1-en-1-yl)benzoic acid (the coupling partner) **2** and 0.81 mL 501 μM (0.396 μmol, 0.036 equiv.) 1.4 nm oleate-capped CdSe QDs in hexanes. The system was stirred under 34W blue LED irradiation for 4 days. The crude products were purified by reverse phase preparative HPLC (Agilent C18 250 × 21.20 mm; 10 μm; eluted with a gradient of 30-60 % MeCN:water with 0.1 % formic acid over 80 min, then 20 min at 100 % MeCN. The flow rate was 10 mL/min.) yielding major product *syn*-4-(3-acetyl-2-(4-carboxyphenyl)-4-phenylcyclobutane-1-carbonyl)benzoic acid (1.5 mg, 10%) **18** as a white powder.

***syn* Diastereomer** (**18**, *major product*):

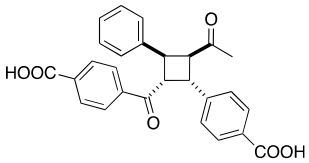

^{1}H NMR (600 MHz, DMSO-*d*$_6$): δ = 7.81 (d, *J* = 7.6 Hz, 2H), 7.74 (d, *J* = 7.6 Hz, 2H), 7.62 (d, *J* = 8.2 Hz, 2H), 7.46 (d, *J* = 7.5 Hz, 2H), 7.36 (t, *J* = 7.6 Hz, 2H), 7.29 – 7.25 (m, 3H), 4.91 (dd, *J* = 10.7, 7.8 Hz, 1H), 4.75 (dd, *J* = 11.2, 7.8 Hz, 1H), 4.70 (dd, *J* = 10.8, 6.5 Hz, 1H), 4.16 (dd, *J* = 11.2, 6.4 Hz, 1H), 1.63 (s, 3H).

^{13}C NMR (126 MHz, DMSO-*d*$_6$): δ = 206.40, 198.07, 166.95, 166.54, 163.03, 139.17, 138.95, 134.34, 129.23, 128.92, 128.85, 128.42, 128.28, 128.23, 128.09, 127.08, 53.51, 48.98, 41.15, 40.46, 29.61.

HRMS (ESI$^-$) (*m/z*): [M-H]$^-$ calculated for $C_{20}H_{17}O_5$, 441.1338; found, 441.1329.

Important NOE-contacts

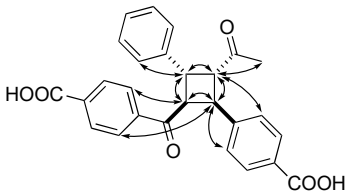

Important HMBC-contacts

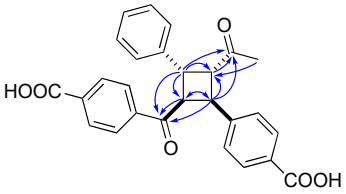

***anti* Diastereomer** (**S1**, *minor product*):

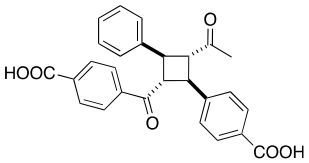

^{1}H NMR (600 MHz, DMSO-d_6): δ = 7.91 (d, *J* = 8.2 Hz, 2H), 7.70 (d, *J* = 7.3 Hz, 2H), 7.60 – 7.54 (m, 4H), 7.46 (d, *J* = 7.4 Hz, 2H), 7.37 (t, *J* = 7.6 Hz, 2H), 7.29 (t, *J* = 7.3 Hz, 1H), 4.39 (t, *J* = 9.2 Hz, 1H), 3.87 (t, *J* = 9.4 Hz, 1H), 3.78 – 3.66 (m, 2H), 1.91 (s, 3H).

^{13}C NMR (126 MHz, DMSO-d_6): δ = 206.66, 198.22, 167.23, 167.18 (2C), 163.43, 163.39, 140.70, 129.53, 128.93, 128.90, 128.58, 128.25, 127.76, 127.72, 127.17, 55.17, 51.69, 42.77, 41.20, 40.02, 39.85, 39.69, 39.52, 39.35, 39.19, 39.02, 28.08.

HRMS (ESI$^-$) (*m/z*): $[M-H]^-$ calculated for $C_{20}H_{17}O_5$, 441.1338; found, 441.1328.

Important NOE-contacts

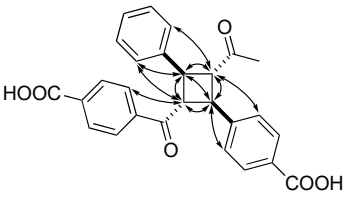

Important HMBC-contacts

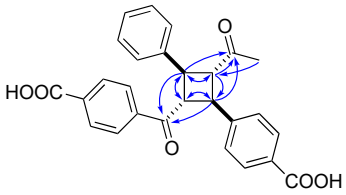

QD system: anti- 4-(2-acetyl-3-benzoyl-4-phenylcyclobutyl)benzoic acid (Figure 4, control study, **20**)

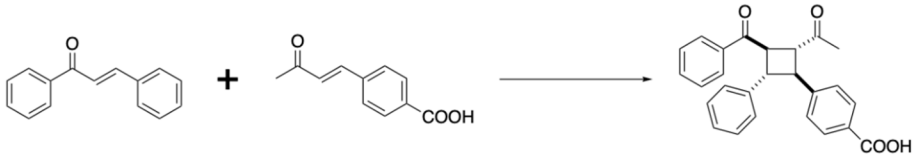

Prepared according to general procedure using 2.3 mg (0.011 mmol, 1.0 equiv.) chalcone **15** (the sensitized molecule), 6.33 mg (0.033 mmol, 3.0 equiv.) (*E*)-4-(3-oxobut-1-en-1-yl)benzoic acid (the coupling partner) **2** and 0.27 mL 501 μM (0.132 μmol, 0.012 equiv.) 1.4 nm oleate-capped CdSe QDs in hexanes. The crude product mixture was concentrated under reduced pressure. The yield reported is obtained by ^{1}H NMR spectroscopic analysis of the crude reaction mixture relative to 3,4,5-trichloropyridine internal standard. The NMR yields represent the total yield of both the major **20** and the minor **S3** diastereomeric cycloadducts.

See section **J-2** for the characterization information of **20** and **S3**.

J-2. Diastereoselective Hetero [2+2] Photocycloaddition using Ir(ppy)$_3$ as a Photocatalyst

See section **H-4** for the general procedure.

Ir(ppy)$_3$ system: anti-4,4'-(3-acetyl-4-benzoylcyclobutane-1,2-diyl)dibenzoic acid (Figure 4, **16**)

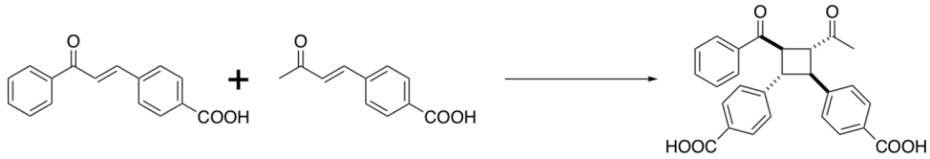

The Ir(ppy)$_3$ system: Prepared according to the general procedure using 2.8 mg (0.011 mmol, 1.0 equiv.) (*E*)-4-(3-oxo-3-phenylprop-1-en-1-yl)benzoic acid **1** (the sensitized molecule), 6.33 mg (0.033 mmol, 3.0 equiv.) (*E*)-4-(3-oxobut-1-en-1-yl)benzoic acid (the coupling partner) **2**. The crude products were purified by reverse phase preparative HPLC (Agilent C18 250 × 21.20 mm; 10 µm eluted with a gradient of 30-60 % MeCN:water with 0.1 % formic acid over 40 min, then 20 min at 100 % MeCN. The flow rate was 10 mL/min.) yielding major product *anti*-4,4'-(3-acetyl-4-benzoylcyclobutane-1,2-diyl)dibenzoic acid (2.3 mg, 47%) **16** and minor product the *syn*-diastereomer (0.6 mg, 14%) **17**, both as white powders.

***anti* Diastereomer** (**17**, *major product*):

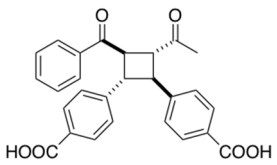

^{1}H NMR (600 MHz, DMSO-d_6): δ = 7.90 (d, *J* = 7.5 Hz, 2H), 7.86 (d, *J* = 7.5 Hz, 2H), 7.81 (d, *J* = 7.8 Hz, 2H), 7.59 (t, *J* = 7.3 Hz, 1H), 7.42 (t, *J* = 6.7 Hz, 4H), 7.38 (d, *J* = 7.5 Hz, 2H), 4.52 (t, *J* = 8.2 Hz, 1H), 3.89 – 3.80 (m, 2H), 3.69 (t, *J* = 8.8 Hz, 1H), 2.02 (s, 3H).

^{13}C NMR (126 MHz, DMSO-d_6): δ = 206.48, 198.13, 167.44, 167.44, 164.16, 145.67, 145.04, 135.27, 133.73, 129.65, 129.64, 128.68 (2C), 128.53, 127.46, 127.15, 50.51, 47.27, 46.63, 45.86, 28.02.

HRMS (ESI$^-$) (*m/z*): [M-H]$^-$ calculated for $C_{27}H_{21}O_6$, 441.1338; found, 441.1342.

Important NOE-contacts

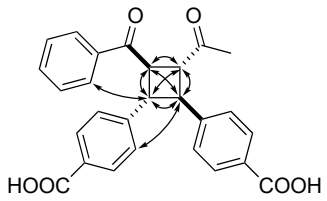

See section **J-1** for the characterization information of **16**.

Ir(ppy)$_3$ system: anti-4-(2-acetyl-3-(4-carboxybenzoyl)-4-phenylcyclobutyl)benzoic acid (Figure 2, **19**)

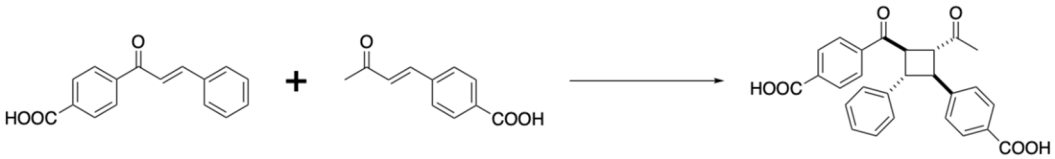

The Ir(ppy)$_3$ system: Prepared according to general procedure using 2.8 mg (0.011 mmol, 1.0 equiv.) (*E*)-4-(1-oxo-3-phenyl-2-propen-1-yl)benzoic acid **14** (the sensitized molecule), 6.33 mg (0.033 mmol, 3.0 equiv.) (*E*)-4-(3-oxobut-1-en-1-yl)benzoic acid (the coupling partner) **2**. The system was stirred under 34W blue LED irradiation for 4 days. The crude products were purified by reverse phase preparative HPLC (Agilent C18 250 × 21.20 mm; 10 μm; eluted with a gradient of 30-60 % MeCN:water with 0.1 % formic acid over 80 min, then 20 min at 100 % MeCN. The flow rate was 10 mL/min.) yielding major product *anti*-4-(2-acetyl-3-(4-carboxybenzoyl)-4-phenylcyclobutyl)benzoic acid (2.6 mg, 53%) **19** and minor product the *syn*-diastereomer (0.6 mg, 13%) **S2**, both as white powders.

***anti* Diastereomer** (**19**, *major product*):

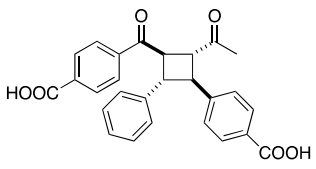

^{1}H NMR (600 MHz, DMSO-d_6): δ = 7.89 (dd, *J* = 14.2, 8.4 Hz, 4H), 7.84 (dd, *J* = 8.3, 2.5 Hz, 2H), 7.46 (d, *J* = 8.4 Hz, 2H), 7.34 – 7.28 (m, 4H), 7.26 (t, *J* = 6.8 Hz, 1H), 4.49 (t, *J* = 8.9 Hz, 1H), 3.88 – 3.79 (m, 2H), 3.63 (t, *J* = 9.4 Hz, 1H), 2.02 (s, 3H).

^{13}C NMR (126 MHz, DMSO-d_6): δ = 206.5, 198.1, 167.1, 166.8, 166.7, 163.5, 163.3, 146.2, 140.5, 129.6, 129.2, 128.7, 128.5, 127.4, 127.3 (2C), 50.4, 47.6, 47.4, 45.8, 28.0.

HRMS (ESI$^-$) (*m/z*): [M-H]$^-$ calculated for $C_{27}H_{21}O_6$, 441.1338; found, 441.1343.

Important NOE-contacts

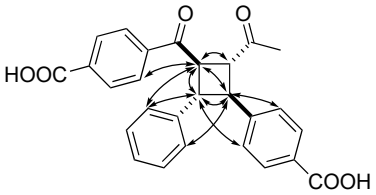

Important HMBC-contacts

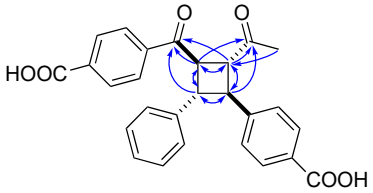

***syn* Diastereomer** (**S2**, *minor product*):

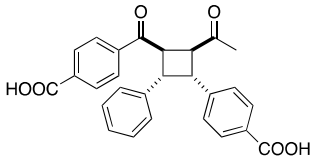

^{1}H NMR (600 MHz, DMSO-d_6): δ = 7.87 (d, *J* = 8.0 Hz, 2H), 7.79 (d, *J* = 8.2 Hz, 2H), 7.56 (d, *J* = 7.7 Hz, 2H), 7.10 (d, *J* = 6.7 Hz, 4H), 7.00 (dd, *J* = 16.4, 7.3 Hz, 3H), 4.86 (dd, *J* = 9.7, 6.1 Hz, 1H), 4.29 (dd, *J* = 9.5, 7.0 Hz, 1H), 4.12 (td, *J* = 10.0, 6.7 Hz, 2H), 1.98 (s, 3H).

^{13}C NMR (126 MHz, DMSO-d_6): δ = 206.67, 198.56, 168.78, 168.27, 165.62 (2C), 139.05, 135.60, 129.04, 128.52, 128.05, 127.77, 127.38, 127.29, 126.10, 50.69, 46.95, 43.99, 43.66, 28.19.

HRMS (ESI$^-$) (*m/z*): [M-H]$^-$ calculated for $C_{27}H_{21}O_6$, 441.1338; found, 441.1337.

Important NOE-contacts

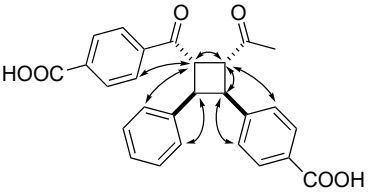

Important HMBC-contacts

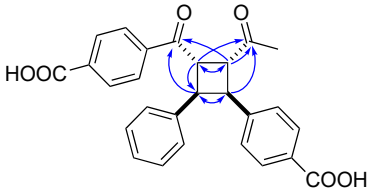

Ir system: anti-4-(2-acetyl-3-benzoyl-4-phenylcyclobutyl)benzoic acid (Figure 4, control study, **20**)

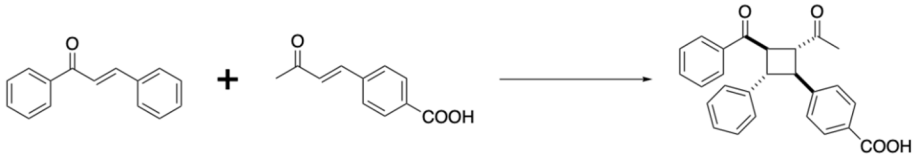

Prepared according to general procedure using 2.3 mg (0.011 mmol, 1.0 equiv.) chalcone **15** (the sensitized molecule), 6.33 mg (0.033 mmol, 3.0 equiv.) (*E*)-4-(3-oxobut-1-en-1-yl)benzoic acid (the coupling partner) **2**. The crude products were purified by reverse phase preparative HPLC (Agilent C18 250 × 21.20 mm; 10 µm; eluted with a gradient of 35-60 % MeCN:water with 0.1 % formic acid over 80 min, then 20 min at 100 % MeCN. The flow rate was 10 mL/min.) yielding major product *anti*-4-(2-acetyl-3-benzoyl-4-phenylcyclobutyl)benzoic acid (2.1 mg, 43%) **20** and minor product the *syn*-diastereomer (0.6 mg, 12%) **S3**, both as white powders.

***anti* Diastereomer** (**20**, *major product*):

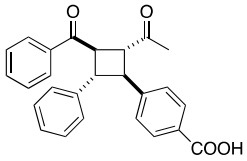

^{1}H NMR (600 MHz, DMSO-d_6): δ = 7.93 – 7.89 (m, 2H), 7.80 (d, *J* = 7.6 Hz, 2H), 7.60 (t, *J* = 7.4 Hz, 1H), 7.47 – 7.44 (m, 2H), 7.41 (t, *J* = 7.8 Hz, 2H), 7.33 – 7.30 (m, 4H), 7.27 – 7.25 (m, 1H), 4.48 (t, *J* = 8.4 Hz, 1H), 3.88 – 3.78 (m, 2H), 3.63 (t, *J* = 9.0 Hz, 1H), 2.02 (s, 3H).

^{13}C NMR (126 MHz, DMSO-d_6): δ = 206.53, 198.26, 167.14, 140.68, 135.34, 133.65, 129.62 (2C), 128.63, 128.62, 128.49, 127.34, 127.20, 127.16 (2C), 50.47, 47.59, 46.92, 45.91, 28.00.

HRMS (ESI$^-$) (*m/z*): $[M-H]^-$ calculated for $C_{26}H_{21}O_4$, 397.1440; found, 397.1445.

Important NOE-contacts

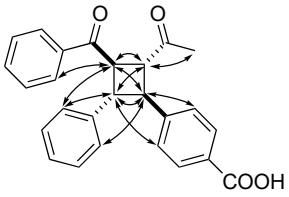

***syn* Diastereomer** (**S3**, *minor product*): 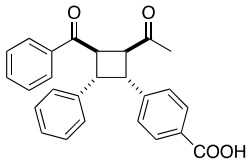

^{1}H NMR (600 MHz, DMSO-d_6): δ = 7.90 (d, *J* = 7.8 Hz, 2H), 7.63 (t, *J* = 7.5 Hz, 3H), 7.51 (t, *J* = 7.7 Hz, 2H), 7.17 (d, *J* = 8.0 Hz, 2H), 7.15 – 7.07 (m, 4H), 7.07 – 6.99 (m, 1H), 4.91 (dd, *J* = 9.4, 6.7 Hz, 1H), 4.37 – 4.32 (m, 1H), 4.25 – 4.21 (m, 1H), 4.14 (dd, *J* = 10.3, 6.6 Hz, 1H), 2.00 (s, 3H).

^{13}C NMR (126 MHz, DMSO-d_6): δ = 206.67, 198.55, 165.64, 139.07, 139.05, 135.52, 129.02, 128.98, 128.50 (2C), 128.05, 127.76, 127.27 (2C), 126.08, 50.70, 46.95, 44.00, 43.65, 28.20.

HRMS (ESI$^-$) (*m/z*): $[M-H]^-$ calculated for $C_{26}H_{21}O_4$, 397.1440; found, 397.1437.

Important NOE-contacts

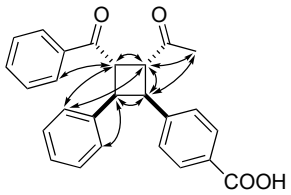

K. X-Ray Crystallographic Data for 4

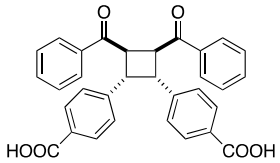

Single crystals of **4** were prepared by vapor diffusion of hexanes into MeOH at room temperature. A suitable crystal was selected and mounted in inert oil and transferred to the cold gas stream of a prospector diffractometer. The crystal was kept at 100 K during data collection. Using Olex2[42], the structure was solved with the ShelXT[43] structure solution program using Intrinsic Phasing and refined with the XL[44] refinement package using Least Squares minimisation.

Crystal Data for $C_{32}H_{24}O_6$ (M =504.51) (**Figure S4** and **Tables S5-S9**): orthorhombic, space group Pbca (no. 61), a = 14.6934(15) Å, b = 11.1245(12) Å, c = 36.222(3) Å, V = 5920.7(10) Å^3, Z = 8, T = 100 K, μ(CuKα) = 0.637 mm^{-1}, $Dcalc$ = 1.132 g/mm^3, 46142 reflections measured (7.748 ≤ 2Θ ≤ 135.366), 5278 unique (R_{int} = 0.0585, R_{sigma} = 0.0327) which were used in all calculations. The final R_1 was 0.0455 (I > 2σ(I)) and wR_2 was 0.1256 (all data).

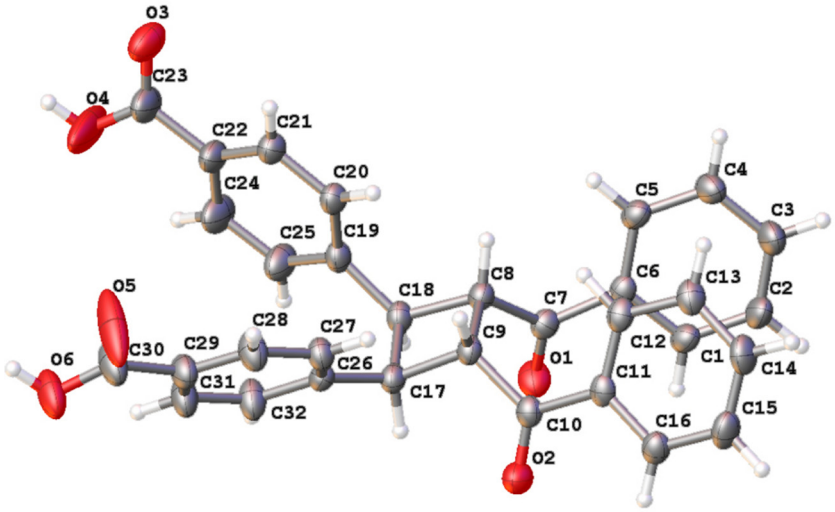

Figure S4. A molecular drawing of **4** shown with 50% probability ellipsoids.

Table S5. Crystal Data and Structure Refinement for **4**

Identification code	**4**
Empirical formula	$C_{32}H_{24}O_6$
Formula weight	504.51
Temperature / K	100
Crystal system	orthorhombic
Space group	Pbca
a / Å, b / Å, c / Å	14.6934(15), 11.1245(12), 36.222(3)
α/°, β/°, γ/°	90, 90, 90
Volume / Å^3	5920.7(10)
Z	8
ρ_{calc} / mg mm^{-3}	1.132
μ / mm^{-1}	0.637
F(000)	2112
Crystal size / mm^3	0.742 × 0.06 × 0.06
2Θ range for data collection	7.748 to 135.366°
Index ranges	$-17 \leq h \leq 16$, $-10 \leq k \leq 13$, $-42 \leq l \leq 42$
Reflections collected	46142
Independent reflections	5278[R(int) = 0.0585]
Data/restraints/parameters	5278/0/343
Goodness-of-fit on F^2	1.030
Final R indexes [I>2σ (I)]	R_1 = 0.0455, wR_2 = 0.1173
Final R indexes [all data]	R_1 = 0.0591, wR_2 = 0.1256
Largest diff. peak/hole / e Å^{-3}	0.178/-0.298

Table S6. Fractional Atomic Coordinates ($\times 10^4$) and Equivalent Isotropic Displacement Parameters ($Å^2 \times 10^3$) for **4**. U_{eq} is defined as 1/3 of of the trace of the orthogonalised U_{IJ} tensor.

Atom	*x*	*y*	*z*	U(eq)
O1	5861.8(9)	8045.1(11)	7103.5(3)	42.0(3)
O2	8107.8(9)	7852.6(12)	7084.7(3)	42.0(3)
O3	4804.6(11)	1853.3(13)	5510.7(4)	56.0(4)
O4	4749(2)	3426.5(17)	5132.9(5)	118.6(10)
O5	9359.3(19)	3071.6(18)	5386.1(4)	108.6(9)
O6	8990.2(12)	4523.1(14)	4999.0(3)	60.7(4)
C1	5837.6(12)	7610.1(16)	7864.9(5)	34.6(4)
C2	5730.8(14)	7372.3(18)	8236.0(5)	44.1(5)
C3	5442.2(14)	6255.0(18)	8350.6(5)	45.9(5)
C4	5252.0(13)	5370.8(17)	8094.1(5)	40.6(4)
C5	5377.7(11)	5590.0(16)	7720.8(5)	33.3(4)
C6	5681.0(10)	6713.7(15)	7604.1(4)	28.3(4)
C7	5889.7(11)	7006.9(16)	7212.0(4)	30.7(4)
C8	6237.8(11)	6030.6(15)	6960.1(4)	30.1(4)
C9	7318.1(11)	6057.5(15)	6926.2(4)	28.5(4)
C10	7846.1(11)	6866.1(15)	7188.2(4)	29.8(4)
C11	8021.5(10)	6455.6(15)	7573.6(4)	28.4(4)
C12	7679.4(11)	5378.5(16)	7709.1(4)	32.0(4)
C13	7820.9(13)	5061.5(17)	8074.8(5)	37.5(4)
C14	8325.1(13)	5799.0(19)	8303.7(5)	42.5(5)
C15	8681.5(13)	6861.0(19)	8169.6(5)	42.4(5)
C16	8526.7(11)	7196.0(17)	7806.7(5)	34.4(4)
C17	7226.8(11)	6514.6(15)	6525.6(4)	30.6(4)
C18	6159.9(12)	6331.0(16)	6542.6(4)	31.8(4)
C19	5779.8(11)	5408.0(16)	6283.3(4)	32.7(4)
C20	5916.8(11)	4183.7(16)	6327.3(4)	33.2(4)
C21	5619.5(12)	3375.3(17)	6060.8(5)	37.1(4)
C22	5197.7(14)	3790.8(18)	5741.5(5)	43.9(5)
C23	4902.2(17)	2940(2)	5451.8(5)	56.1(6)
C24	5050.2(17)	5015(2)	5697.9(5)	56.4(6)
C25	5325.8(15)	5805.0(19)	5967.4(5)	47.9(5)
C26	7736.5(11)	5892.9(15)	6221.2(4)	30.8(4)
C27	8309.4(12)	4929.2(16)	6281.2(5)	34.5(4)
C28	8729.5(14)	4358.8(18)	5988.4(5)	43.4(5)
C29	8584.8(13)	4732.7(17)	5628.9(5)	40.3(4)
C30	9014.8(17)	4053(2)	5325.3(5)	53.9(6)
C31	8025.3(15)	5710.3(18)	5565.4(5)	46.9(5)
C32	7604.8(15)	6278.3(18)	5857.9(5)	44.8(5)

Table S7. Anisotropic Displacement Parameters ($Å^2 \times 10^3$) for **4**. The Anisotropic displacement factor exponent takes the form: $-2\pi^2[h^2a^{*2}U_{11}+2hka^*b^*U_{12}+\ldots]$.

Atom	U_{11}	U_{22}	U_{33}	U_{23}	U_{13}	U_{12}
O1	58.3(8)	31.5(7)	36.3(7)	0.5(6)	2.3(6)	7.0(6)
O2	55.1(8)	39.9(8)	31.0(6)	0.9(5)	-3.2(6)	-10.1(6)
O3	77.3(10)	45.9(9)	44.7(8)	-2.9(7)	-22.6(7)	-8.2(8)
O4	245(3)	70.1(13)	40.4(9)	7.8(9)	-58.7(13)	-60.7(16)
O5	211(3)	81.7(13)	33.1(8)	9.1(8)	33.8(11)	85.6(16)
O6	98.1(12)	54.3(9)	29.7(7)	1.2(6)	20.4(7)	17.0(8)
C1	36.1(9)	32.2(9)	35.3(9)	-7.6(7)	6.5(7)	-4.5(7)
C2	53.6(11)	45.6(11)	33.1(9)	-14.1(8)	9.9(8)	-11.4(9)
C3	57.4(12)	48.7(12)	31.5(9)	-4.3(8)	14.4(8)	-8.1(9)
C4	48.1(11)	36.4(10)	37.3(10)	-3.5(8)	12.9(8)	-6.1(8)
C5	33.3(9)	31.3(9)	35.2(9)	-7.5(7)	4.6(7)	-2.7(7)
C6	24.6(8)	32.2(9)	28.1(8)	-5.7(7)	1.6(6)	2.4(7)
C7	29.8(8)	31.8(10)	30.4(8)	-2.3(7)	-2.4(7)	1.3(7)
C8	35.6(9)	29.3(9)	25.2(8)	-2.9(7)	0.2(6)	-1.2(7)
C9	33.9(9)	28.4(9)	23.2(8)	-2.6(6)	0.5(6)	2.3(7)
C10	30.1(8)	33.0(9)	26.2(8)	7-2.4(7)	2.1(6)	3.3(7)
C11	24.6(8)	35.6(9)	25.1(8)	-3.8(7)	2.3(6)	6.2(7)
C12	32.9(9)	34.3(9)	28.7(8)	-4.8(7)	-0.9(7)	7.4(7)
C13	43.8(10)	39.2(10)	29.6(9)	0.6(7)	0.7(7)	6.7(8)
C14	48.1(11)	54.1(12)	25.3(8)	1.7(8)	-4.6(8)	5.3(9)
C15	38.6(10)	58.1(13)	30.6(9)	-7.7(9)	-5.9(8)	-1.5(9)
C16	29.9(8)	42.9(10)	30.5(9)	-4.4(8)	1.3(7)	-0.8(8)
C17	38.3(9)	29.5(9)	24.1(8)	-0.8(7)	-1.0(7)	-0.9(7)
C18	37.4(9)	33.6(10)	24.4(8)	-0.6(7)	-0.8(7)	2.5(7)
C19	35.1(9)	39.6(10)	23.4(8)	-0.1(7)	-1.2(6)	-0.9(8)
C20	35.4(9)	37.6(10)	26.5(8)	-0.4(7)	-3.9(7)	-1.5(8)
C21	42.5(10)	39.3(10)	29.4(9)	-1.0(7)	-3.6(7)	-4.7(8)
C22	59.4(12)	44.2(12)	28.1(9)	-0.3(8)	-9.7(8)	-13.5(9)
C23	83.7(16)	54.5(14)	30.2(10)	3.1(9)	-16.9(10)	-18.2(12)
C24	80.8(16)	53.1(14)	35.3(11)	6.0(9)	-25.7(10)	-9.7(11)
C25	67.3(13)	40.9(11)	35.6(10)	1.9(8)	-16.4(9)	-1.6(10)
C26	37.9(9)	29.3(9)	25.3(8)	-3.9(7)	1.8(7)	-5.6(7)
C27	41.2(10)	36.4(10)	25.9(8)	0.6(7)	2.2(7)	2.3(8)
C28	55.2(12)	43.1(11)	31.7(9)	0.9(8)	8.0(8)	13.3(9)
C29	53.1(11)	38.0(10)	29.7(9)	-3.7(8)	9.9(8)	0.7(9)
C30	82.3(16)	47.4(13)	32.0(10)	2.3(9)	18.5(10)	12.9(11)
C31	69.0(13)	46.4(12)	25.4(9)	0.8(8)	5.9(8)	9.9(10)
C32	63.6(12)	43.5(11)	27.4(9)	0.6(8)	3.2(8)	12.3(10)

Table S8. Bond Lengths for **4**.

Atom	Atom	Length/Å	Atom	Atom	Length/Å
O1	C7	1.221(2)	C12	C13	1.387(2)
O2	C10	1.222(2)	C13	C14	1.382(3)
O3	C23	1.236(3)	C14	C15	1.381(3)
O4	C23	1.295(3)	C15	C16	1.385(2)
O5	C30	1.224(3)	C17	C18	1.582(2)
O6	C30	1.293(2)	C17	C26	1.502(2)
C1	C2	1.379(2)	C18	C19	1.500(2)
C1	C6	1.393(2)	C19	C20	1.386(3)
C2	C3	1.377(3)	C19	C25	1.396(2)
C3	C4	1.382(3)	C20	C21	1.390(2)
C4	C5	1.386(2)	C21	C22	1.391(3)
C5	C6	1.393(2)	C22	C23	1.478(3)
C6	C7	1.489(2)	C22	C24	1.388(3)
C7	C8	1.508(2)	C24	C25	1.375(3)
C8	C9	1.592(2)	C26	C27	1.380(2)
C8	C18	1.553(2)	C26	C32	1.397(2)
C9	C10	1.520(2)	C27	C28	1.381(2)
C9	C17	1.543(2)	C28	C29	1.383(3)
C10	C11	1.491(2)	C29	C30	1.476(3)
C11	C12	1.389(2)	C29	C31	1.383(3)
C11	C16	1.394(2)	C31	C32	1.380(3)

Table S9. Bond Angles for **4**.

Atom	Atom	Atom	Angle/°	Atom	Atom	Atom	Angle/°
C2	C1	C6	120.33(17)	C26	C17	C18	117.60(13)
C3	C2	C1	120.13(17)	C8	C18	C17	89.58(12)
C2	C3	C4	120.14(17)	C19	C18	C8	119.35(14)
C3	C4	C5	120.24(17)	C19	C18	C17	115.66(14)
C4	C5	C6	119.78(16)	C20	C19	C18	123.15(15)
C1	C6	C5	119.31(15)	C20	C19	C25	118.33(16)
C1	C6	C7	117.13(15)	C25	C19	C18	118.34(16)
C5	C6	C7	123.51(15)	C19	C20	C21	120.68(16)
O1	C7	C6	120.50(15)	C20	C21	C22	120.17(18)
O1	C7	C8	119.86(15)	C21	C22	C23	120.53(19)
C6	C7	C8	119.29(15)	C24	C22	C21	119.36(17)
C7	C8	C9	111.79(13)	C24	C22	C23	120.11(17)
C7	C8	C18	114.16(14)	O3	C23	O4	122.87(19)
C18	C8	C9	89.69(12)	O3	C23	C22	122.54(18)
C10	C9	C8	118.15(13)	O4	C23	C22	114.59(19)

C10	C9	C17	115.86(14)	C25	C24	C22	120.04(18)
C17	C9	C8	89.54(12)	C24	C25	C19	121.36(19)
O2	C10	C9	120.03(14)	C27	C26	C17	123.12(15)
O2	C10	C11	120.53(15)	C27	C26	C32	118.10(16)
C11	C10	C9	119.43(15)	C32	C26	C17	118.75(16)
C12	C11	C10	122.17(15)	C26	C27	C28	120.56(16)
C12	C11	C16	119.25(15)	C27	C28	C29	121.05(18)
C16	C11	C10	118.57(16)	C28	C29	C30	118.77(18)
C13	C12	C11	120.18(16)	C31	C29	C28	118.99(16)
C14	C13	C12	120.18(18)	C31	C29	C30	122.22(17)
C15	C14	C13	120.03(17)	O5	C30	O6	122.46(18)
C14	C15	C16	120.12(17)	O5	C30	C29	120.00(18)
C15	C16	C11	120.22(17)	O6	C30	C29	117.53(18)
C9	C17	C18	90.40(12)	C32	C31	C29	119.92(17)
C26	C17	C9	119.68(14)	C31	C32	C26	121.37(18)

L. HPLC Chromatograms

Note that detection for these chromatograms is by mass spectrometry, and so the quantification of each species is less precise than by NMR. All reported selectivities were measured by NMR.

Figure 2: Homocoupling of **1**

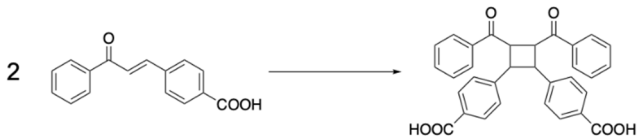

Gradient 48-100 % MeCN:water with 0.1 % formic acid over 4 min, 0.3 mL/min.

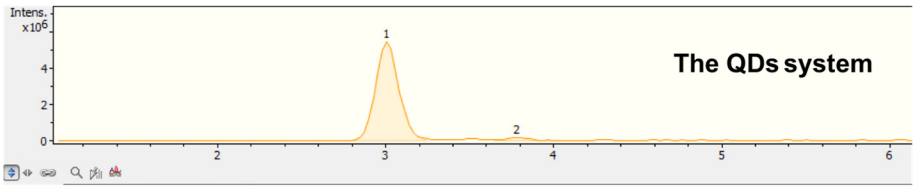

Peak #	RT (min)	Area	Area %	Structure
1	3.0	52855568	100	syn
2	3.8	1418041	2.68	anti

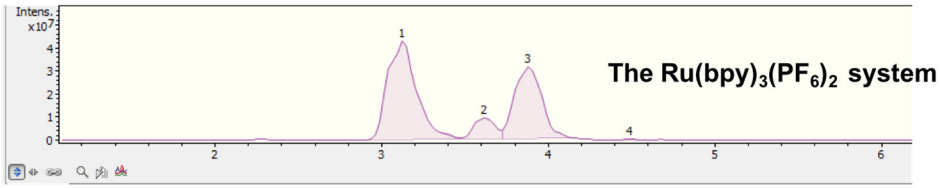

Peak #	RT (min)	Area	Area %	Structure
1	3.1	513148640	100	syn + unknown
2	3.6	79946664	15.58	unknown
3	3.9	352282336	68.65	anti
4	4.5	31451988	6.13	unknown

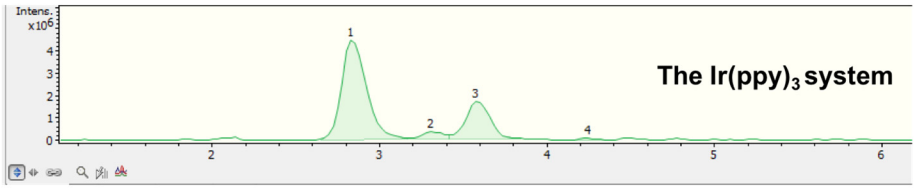

Peak #	RT (min)	Area	Area %	Structure
1	2.8	47094860	100	syn
2	3.3	3232780	6.86	unknown
3	3.6	17365546	36.87	anti
4	4.2	491942	1.04	unknown

Figure 2: Homocoupling of **2**

Gradient 30-100 % MeCN:water with 0.1 % formic acid over 4 min, 0.3 mL/min.

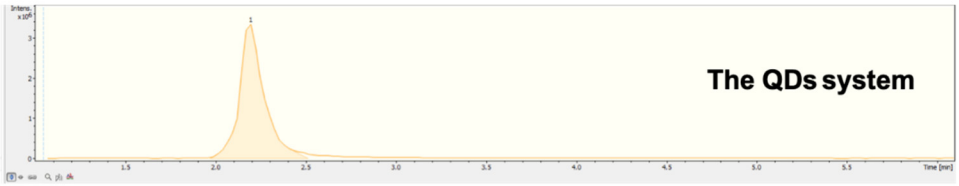

Peak #	RT (min)	Area	Area %	Structure
1	2.1	263496944	100	syn

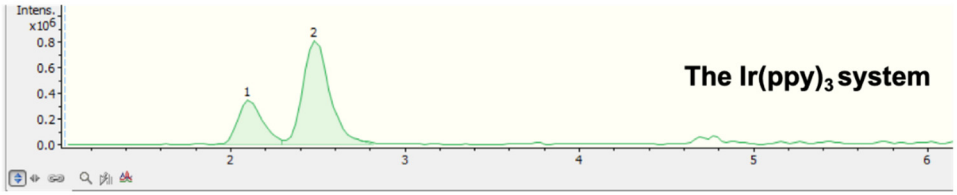

Peak #	RT (min)	Area	Area %	Structure
1	2.0	56952160	100	anti
2	2.2	24985024	43.87	syn

Figure 2: Homocoupling of **3**

Gradient 48-100 % MeCN:water with 0.1 % formic acid over 4 min, 0.3 mL/min.

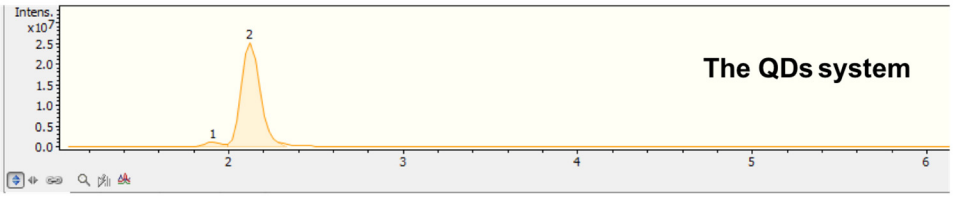

Peak #	RT (min)	Area	Area %	Structure
1	1.9	6736022	3.61	anti
2	2.1	186733040	100	syn

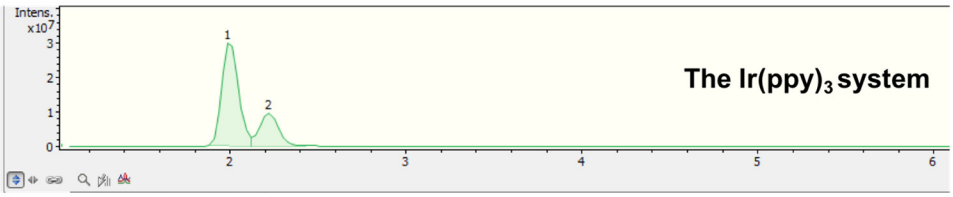

Peak #	RT (min)	Area	Area %	Structure
1	2.0	56952160	100	anti
2	2.2	24985024	43.87	syn

Figure 2: Heterocoupling of **1** and **3**

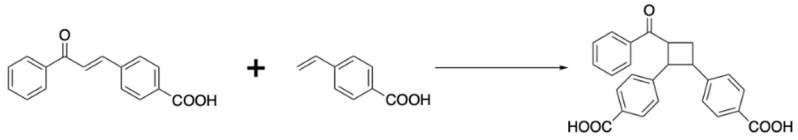

Gradient 48-100 % MeCN:water with 0.1 % formic acid over 4 min, 0.3 mL/min.

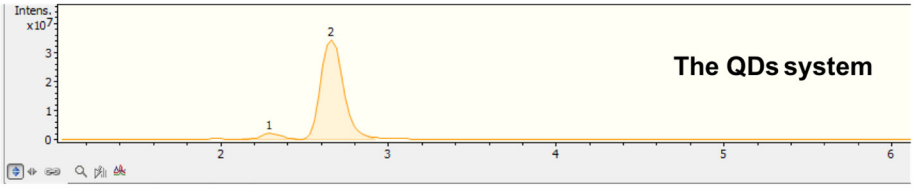

Peak #	RT (min)	Area	Area %	Structure
1	2.3	18245754	5.66	anti
2	2.6	322349152	100	syn

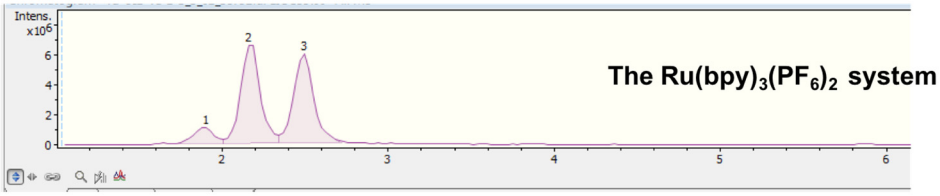

Peak #	RT (min)	Area	Area %	Structure
1	3.1	513148640	100	syn + unknown
2	3.6	79946664	15.58	unknown
3	3.9	352282336	68.65	anti

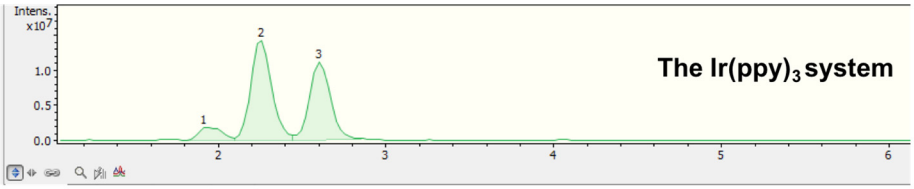

Peak #	RT (min)	Area	Area %	Structure
1	1.9	1803978	14.49	unknown
2	2.3	124730400	100	anti
3	2.6	96781456	77.59	syn

Figure 2: Heterocoupling of **2** and **3**

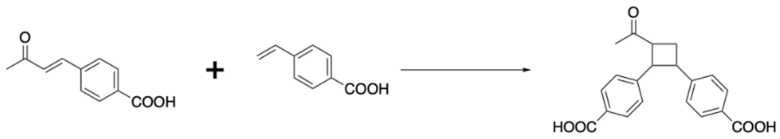

Gradient 40-100 % MeCN:water with 0.1 % formic acid over 4 min, 0.3 mL/min.

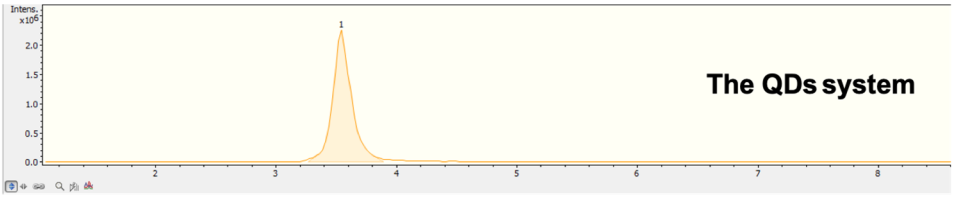

Peak #	RT (min)	Area	Area %	Structure
1	3.5	24455142	100	syn

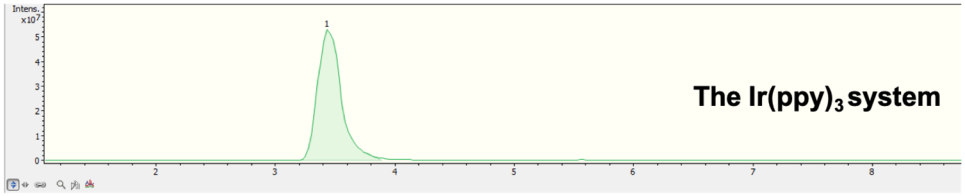

Peak #	RT (min)	Area	Area %	Structure
3	3.4	731186816	100	anti + syn

Figure 4: Heterocoupling of **1** and **2**

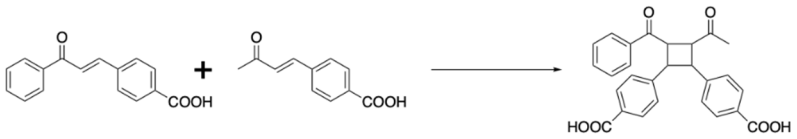

Gradient 40-100 % MeCN:water with 0.1 % formic acid over 4 min, 0.3 mL/min.

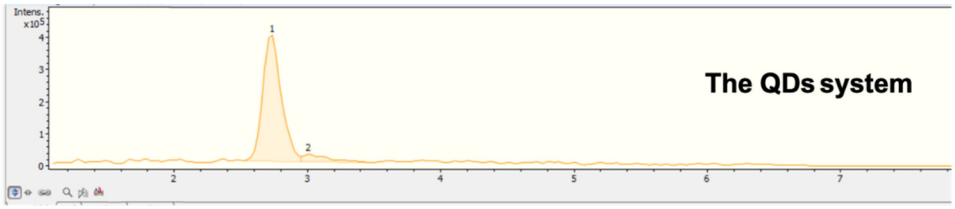

Peak #	RT (min)	Area	Area %	Structure
1	2.7	3776612	100	syn
2	3.0	290672	7.70	anti

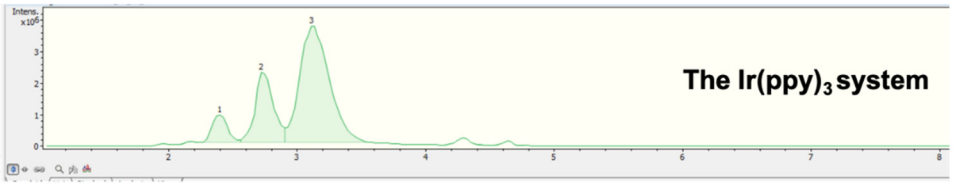

Peak #	RT (min)	Area	Area %	Structure
1	2.4	7274536	12.10	unknown
2	2.7	22166038	36.86	syn
3	3.1	60129640	100	anti

Figure 4: Heterocoupling of **14** and **2**

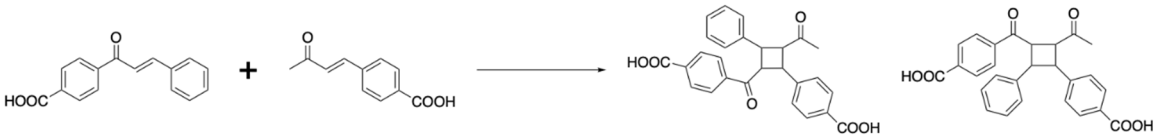

Gradient 40-100 % MeCN:water with 0.1 % formic acid over 4 min, 0.3 mL/min.

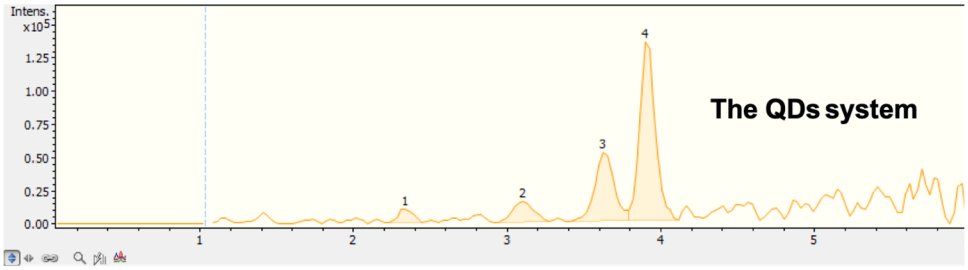

Peak #	RT (min)	Area	Area %	Structure
1	2.3	68586	7.14	syn-HH
2	3.1	148189	15.43	anti-HH
3	3.6	450016	46.85	anti-HT
4	3.9	960571	100	syn-HT

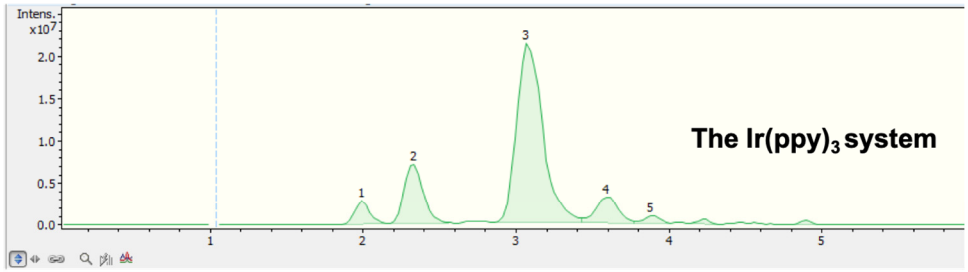

Peak #	RT (min)	Area	Area %	Structure
1	2.0	18945366	7.42	unknown
2	2.3	61388628	24.04	syn-HH
3	3.1	255328384	100	anti-HH
4	3.6	31634470	12.39	anti-HT
5	3.9	6365005	1.13	syn-HH

Figure 4: Heterocoupling of **15** and **2** (control experiment)

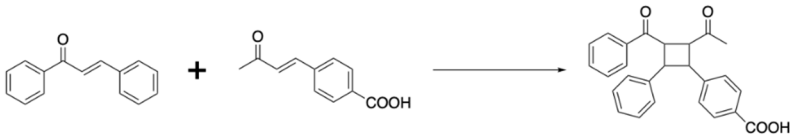

Gradient 48-100 % MeCN:water with 0.1 % formic acid over 4 min, 0.3 mL/min.

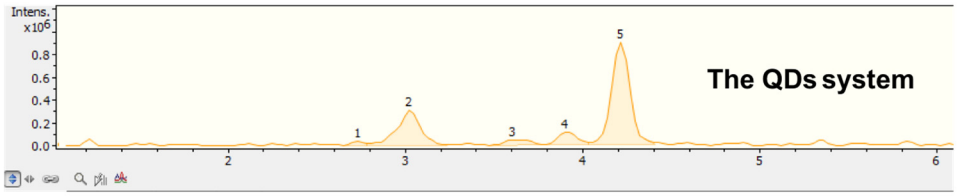

Peak #	RT (min)	Area	Area %	Structure
1	2.7	171556	2.58	unknown
2	3.0	2821396	42.48	unknown
3	3.4	79583	1.20	unknown
4	3.6	534043	8.04	unknown
5	3.9	881759	13.28	unknown
6	4.2	6641102	100	anti

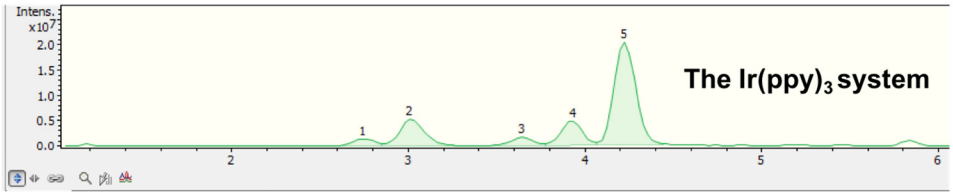

Peak #	RT (min)	Area	Area %	Structure
1	2.7	11195180	6.30	unknown
2	3.0	51572132	29.01	unknown
3	3.6	1402184	7.88	unknown
4	3.9	41099164	23.12	unknown
5	4.2	177779104	100	anti

Figure 2: Heterocoupling of **2** and styrene (control study)

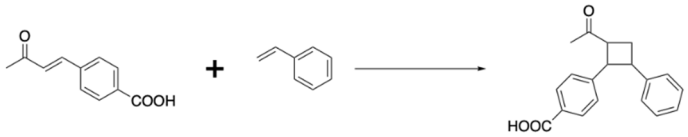

Gradient 48-100 % MeCN:water with 0.1 % formic acid over 4 min, 0.3 mL/min.

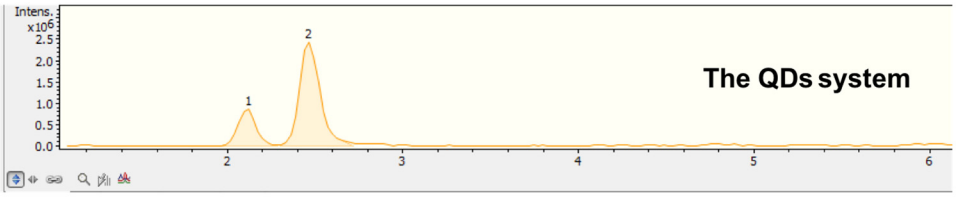

Peak #	RT (min)	Area	Area %	Structure
1	2.1	108020512	30.12	anti
2	2.4	358591648	100	syn

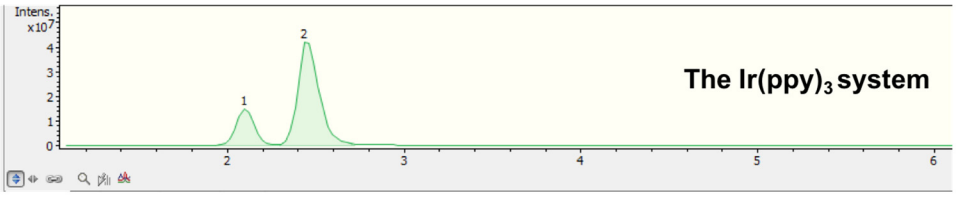

Peak #	RT (min)	Area	Area %	Structure
1	2.1	6229119	30.96	unknown
2	2.5	20117858	100	anti

M. NMR Spectra

4,4'-(3,4-dibenzoylcyclobutane-1,2-diyl)dibenzoic acid

syn diastereomer **4**

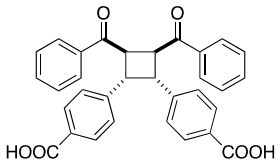

^{1}H NMR (600 MHz, DMSO-d_6)

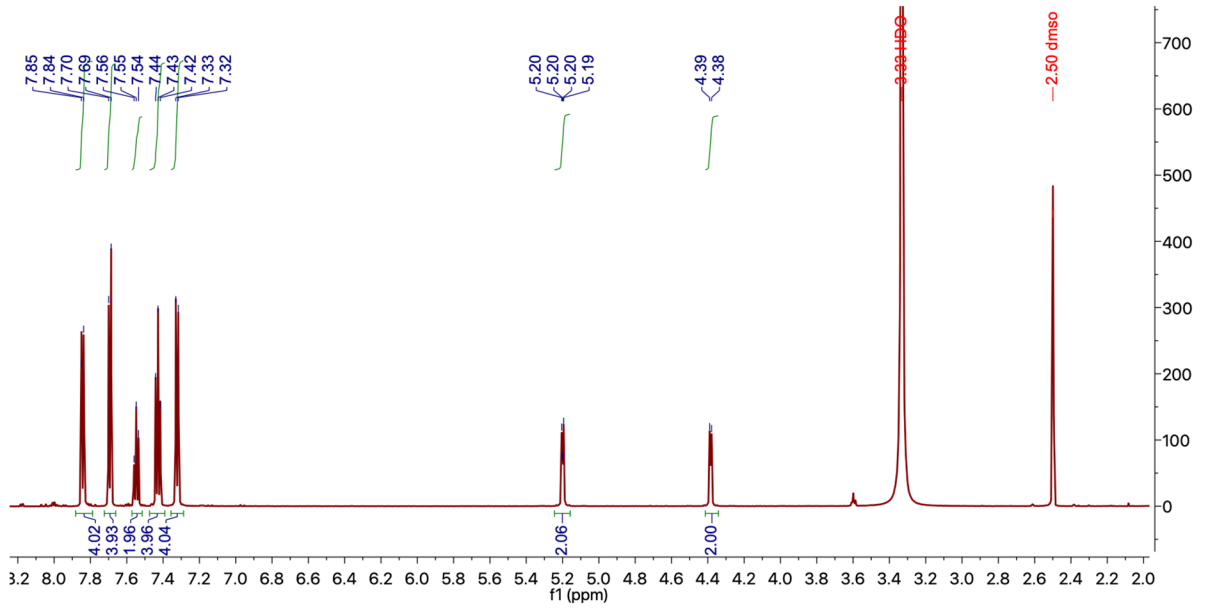

^{13}C NMR (126 MHz, DMSO-d_6)

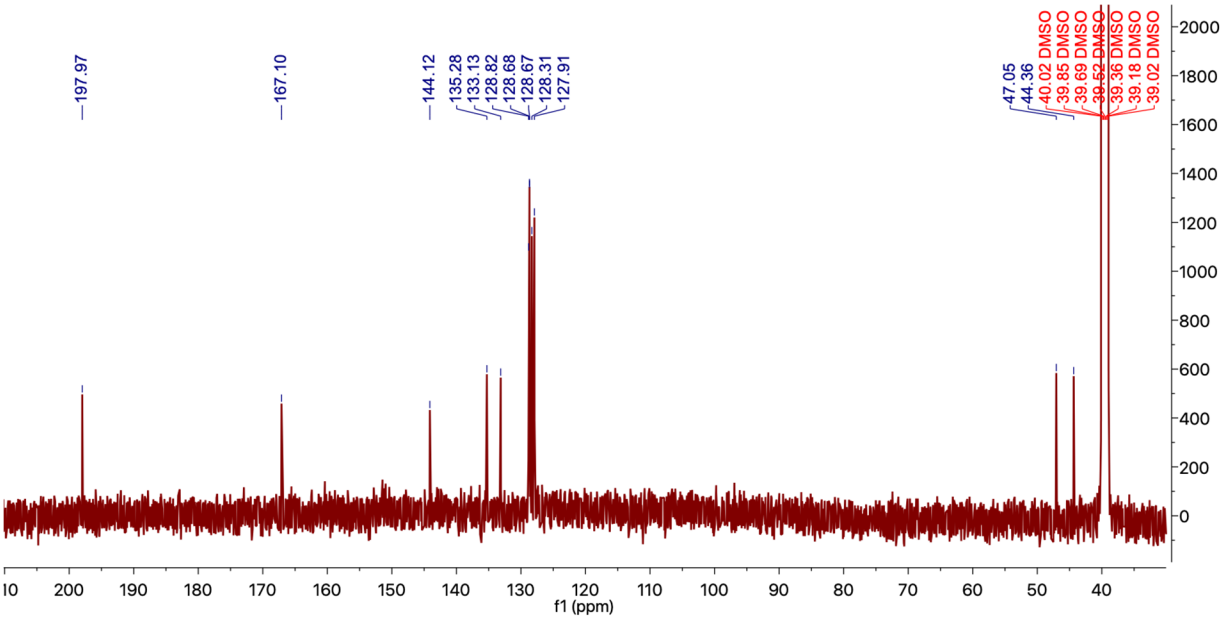

4,4'-(3-acetyl-4-benzoylcyclobutane-1,2-diyl)dibenzoic acid

anti diastereomer **5**

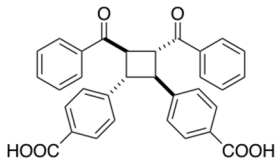

^{1}H NMR (600 MHz, DMSO-d_6)

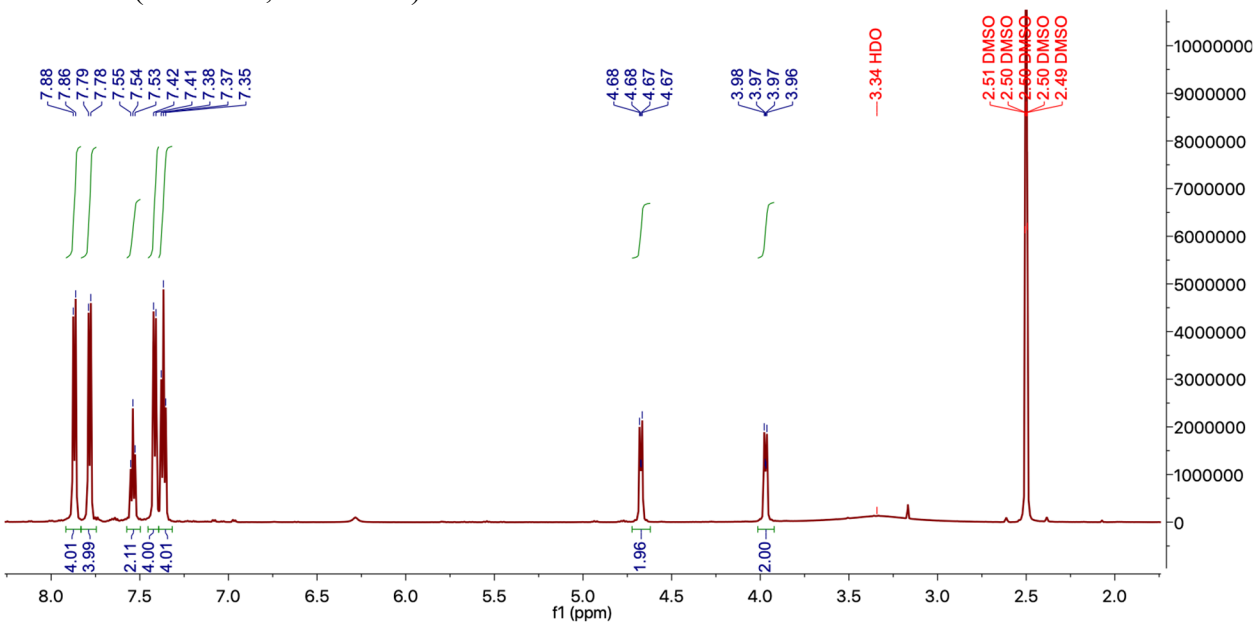

^{13}C NMR (126 MHz, DMSO-d_6)

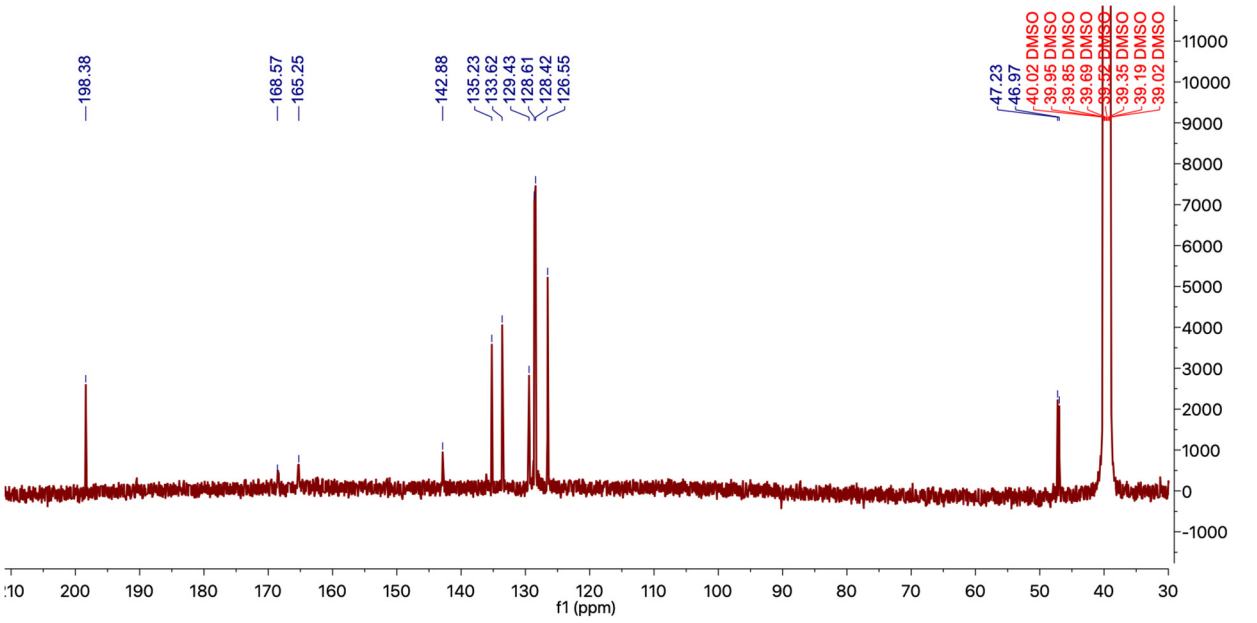

4,4'-(3,4-diacetylcyclobutane-1,2-diyl)dibenzoic acid

syn diastereomer **6**

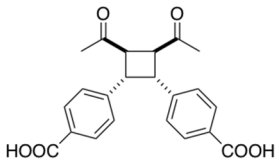

^{1}H NMR (600 MHz, DMSO-d_6)

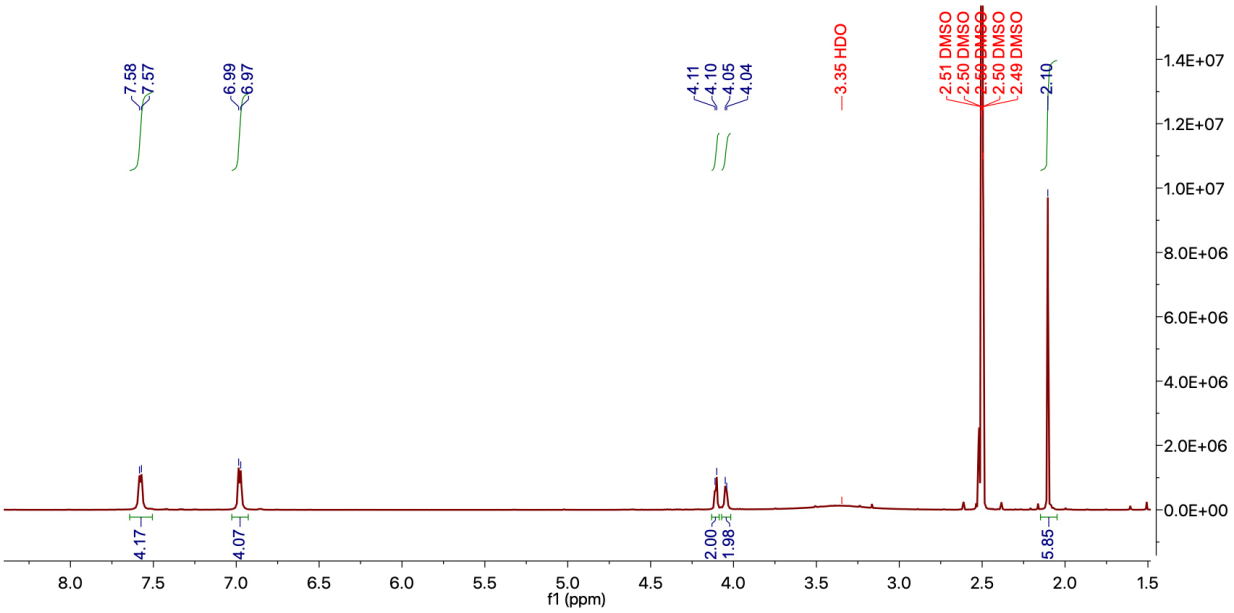

^{13}C NMR (126 MHz, DMSO-d_6)

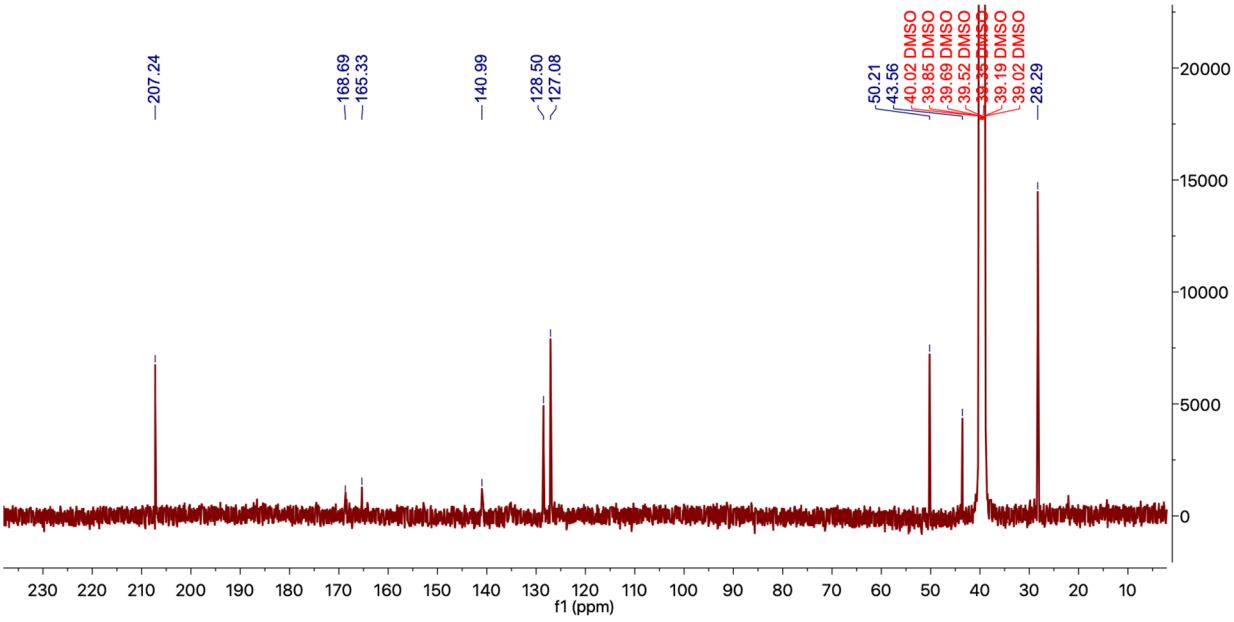

4,4'-(3,4-dibenzoylcyclobutane-1,2-diyl)dibenzoic acid

anti diastereomer **7**

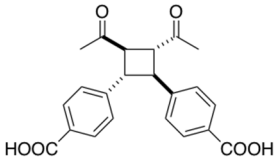

^{1}H NMR (600 MHz, DMSO-d_6)

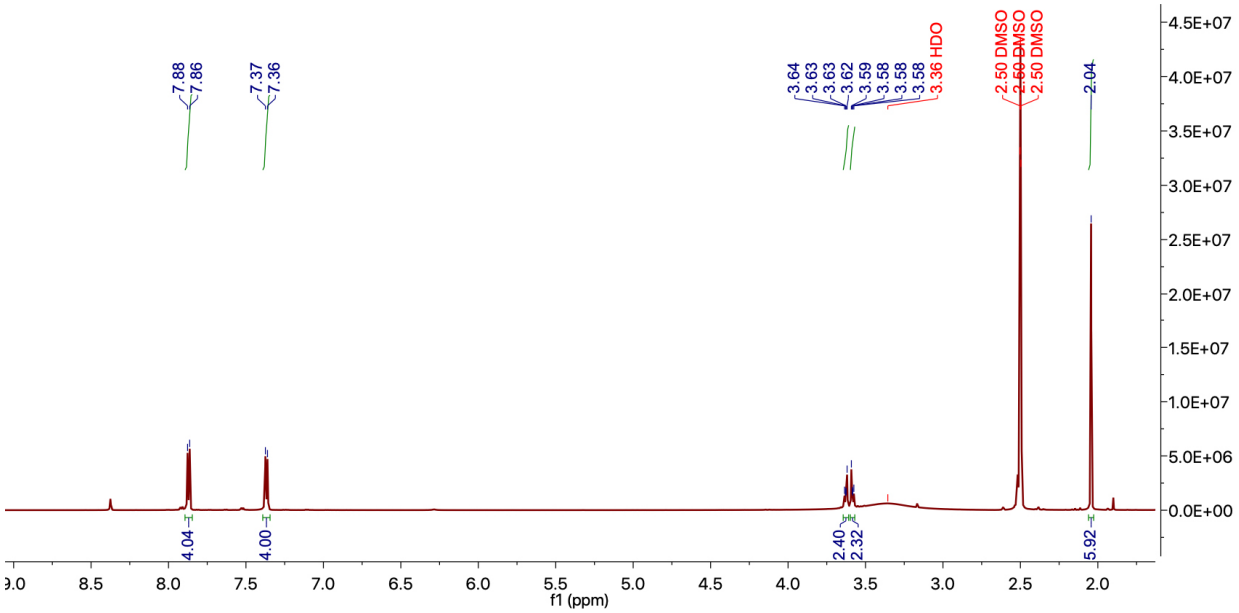

^{13}C NMR (126 MHz, DMSO-d_6)

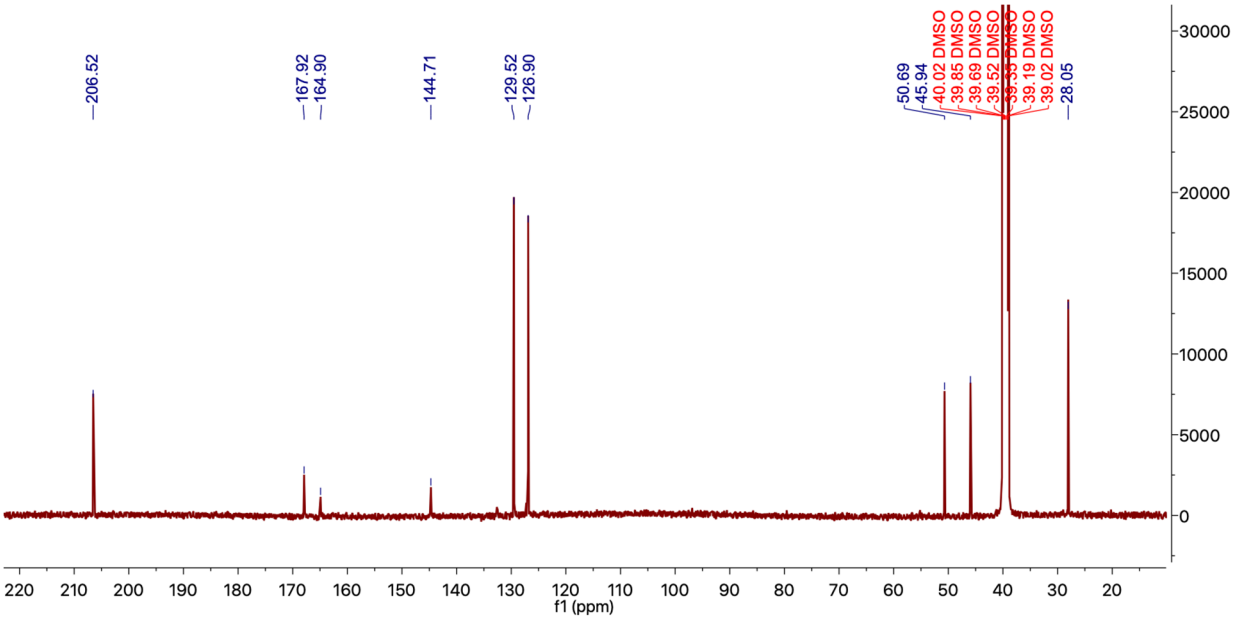

4,4'-(cyclobutane-1,2-diyl)dibenzoic acid

syn diastereomer **8**

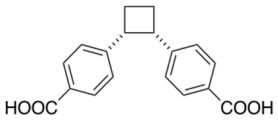

^{1}H NMR (600 MHz, DMSO-d_6)

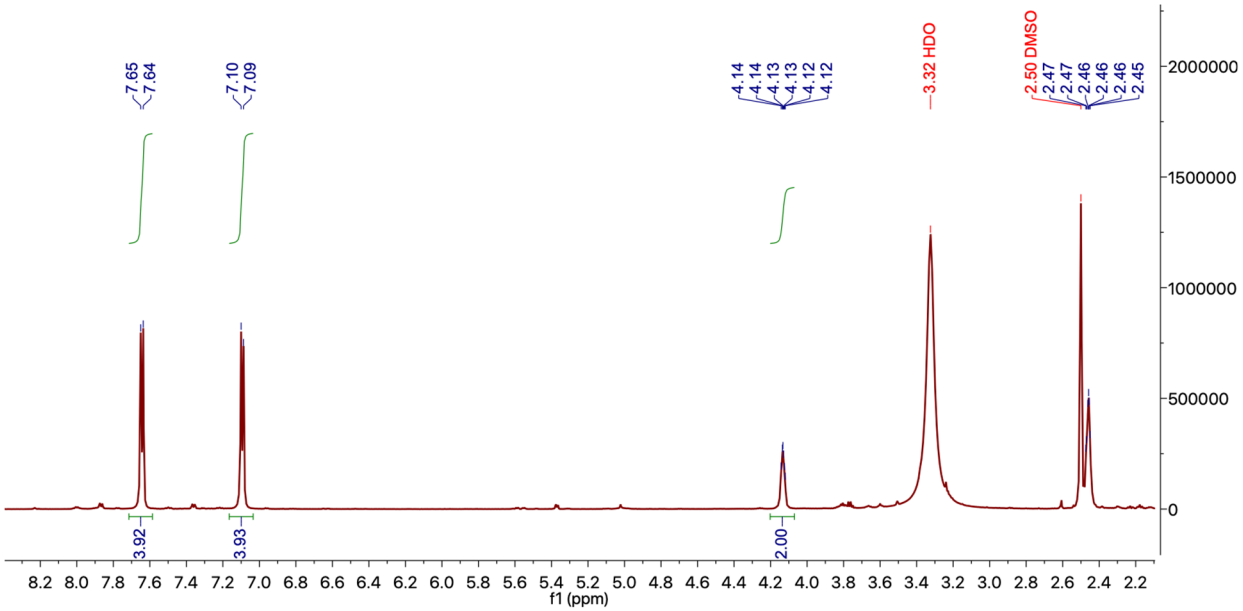

^{13}C NMR (126 MHz, DMSO-d_6)

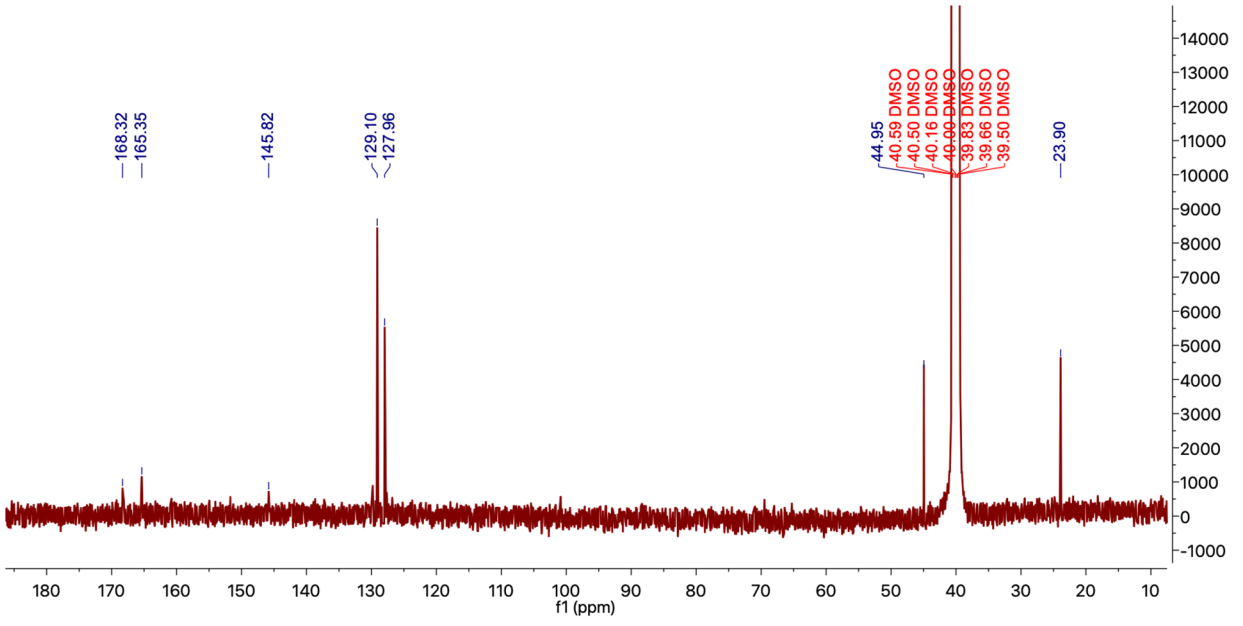

4,4'-(cyclobutane-1,2-diyl)dibenzoic acid

syn and anti diastereomer **9** and **10**

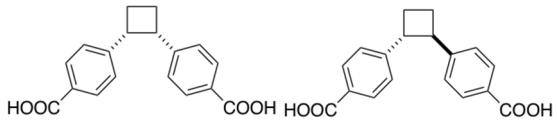

^{1}H NMR (600 MHz, DMSO-d_6)

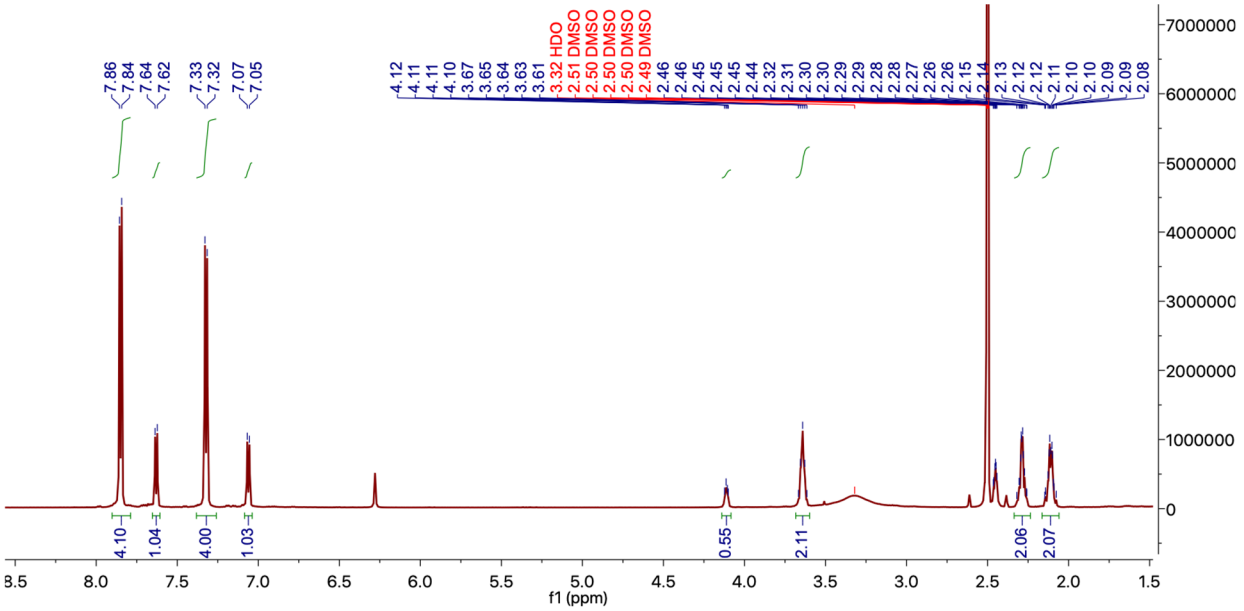

^{13}C NMR (126 MHz, DMSO-d_6)

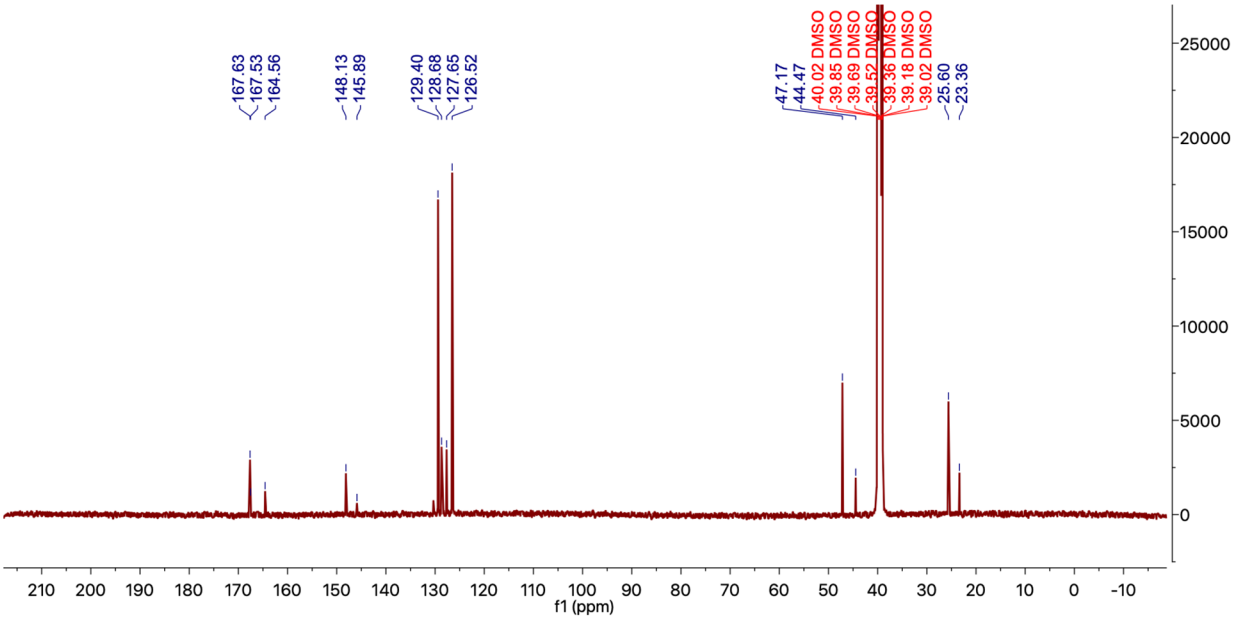

4,4'-(3-benzoylcyclobutane-1,2-diyl)dibenzoic acid

syn diastereomer **11**

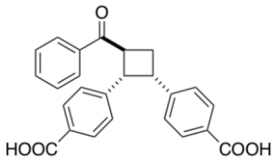

^{1}H NMR (600 MHz, DMSO-d_6)

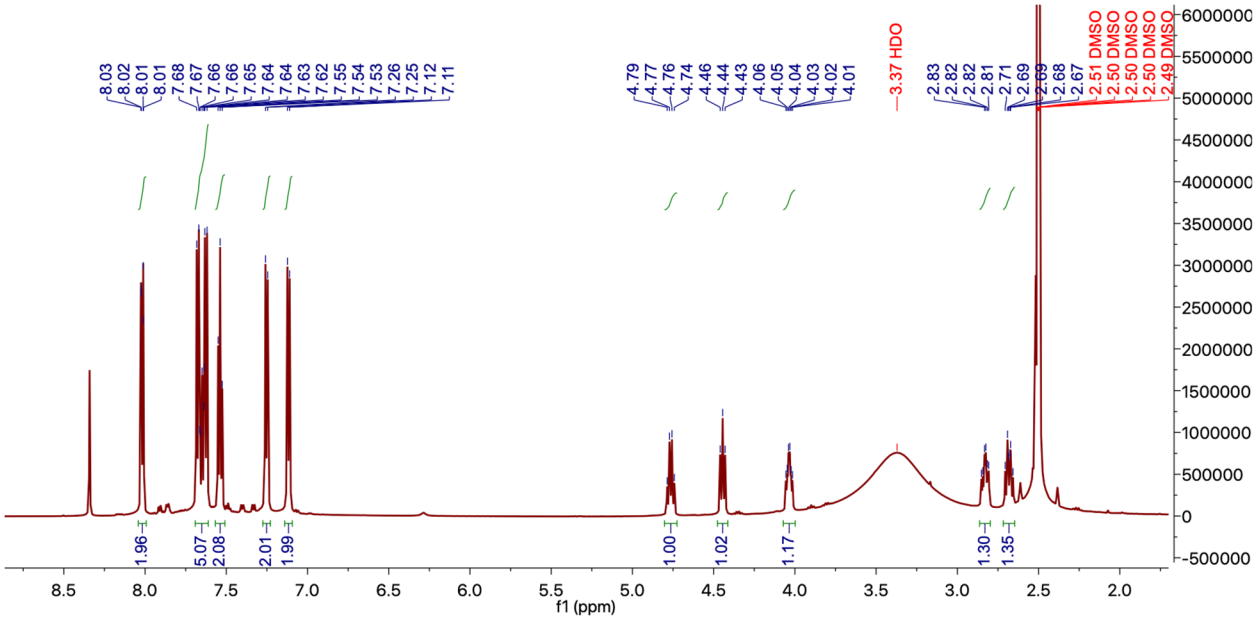

^{13}C NMR (126 MHz, DMSO-d_6)

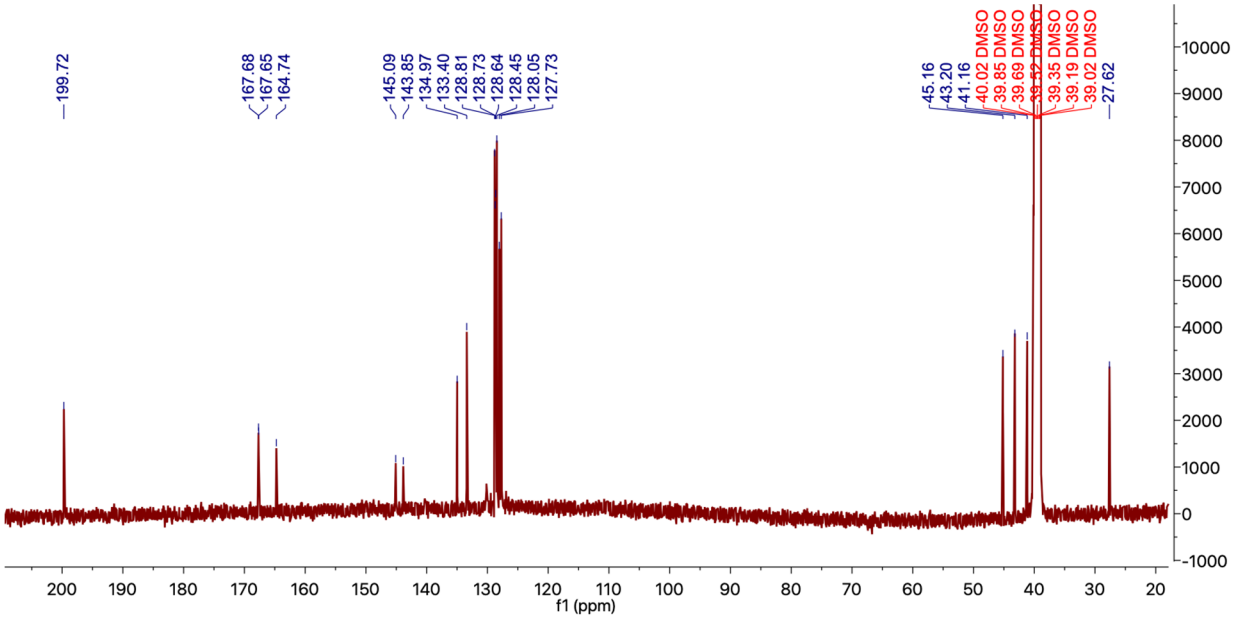

4,4'-(3-benzoylcyclobutane-1,2-diyl)dibenzoic acid

syn and anti diastereomer **11** and **12**

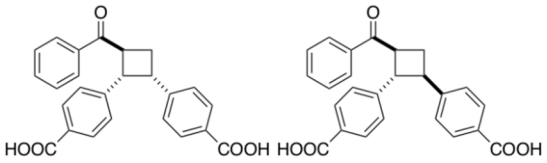

^{1}H NMR (600 MHz, DMSO-d_6)

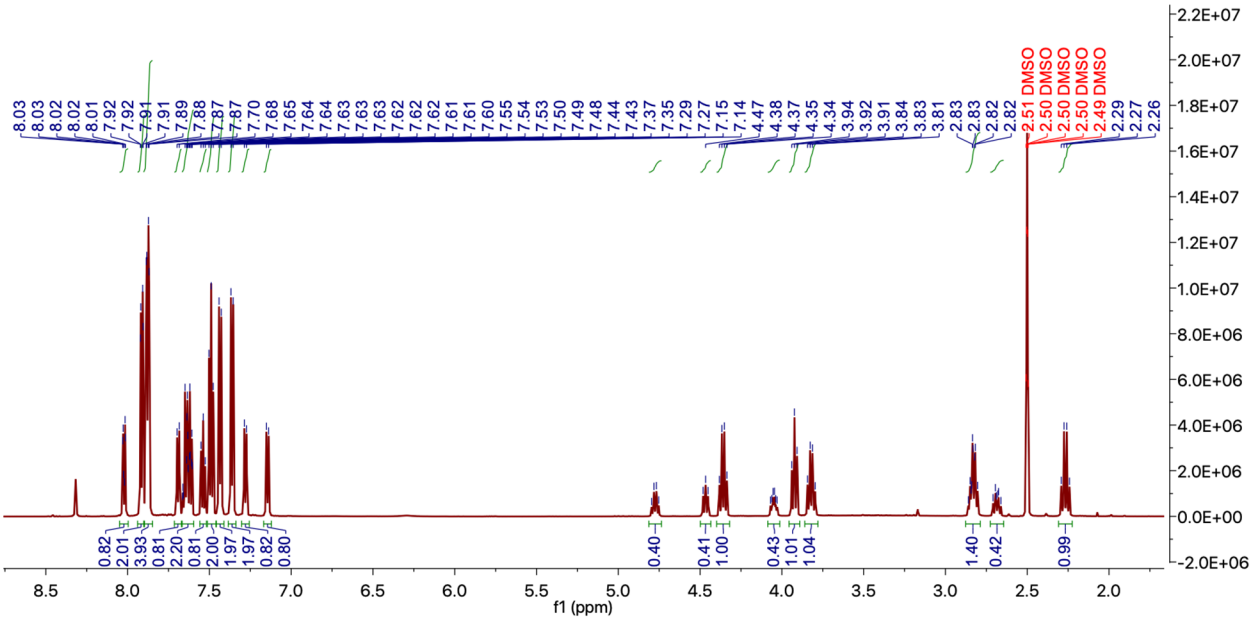

^{13}C NMR (126 MHz, DMSO-d_6)

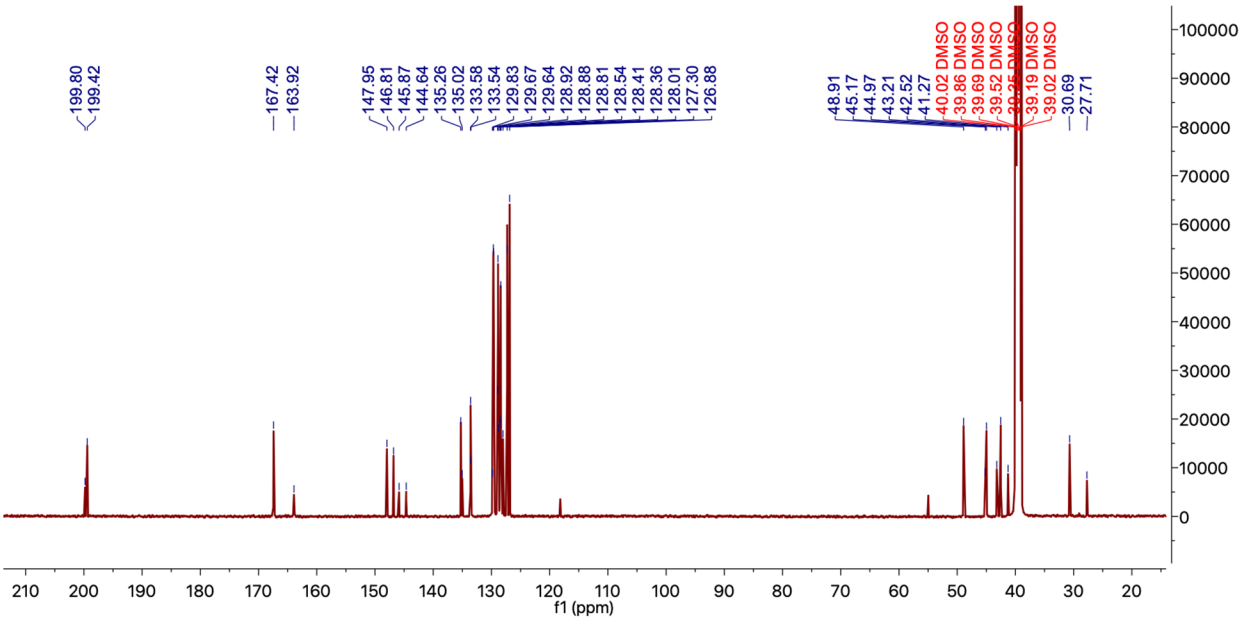

4,4'-(3-acetylcyclobutane-1,2-diyl)dibenzoic acid

syn diastereomer **12**

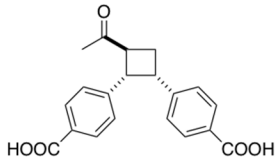

^{1}H NMR (600 MHz, DMSO-d_6)

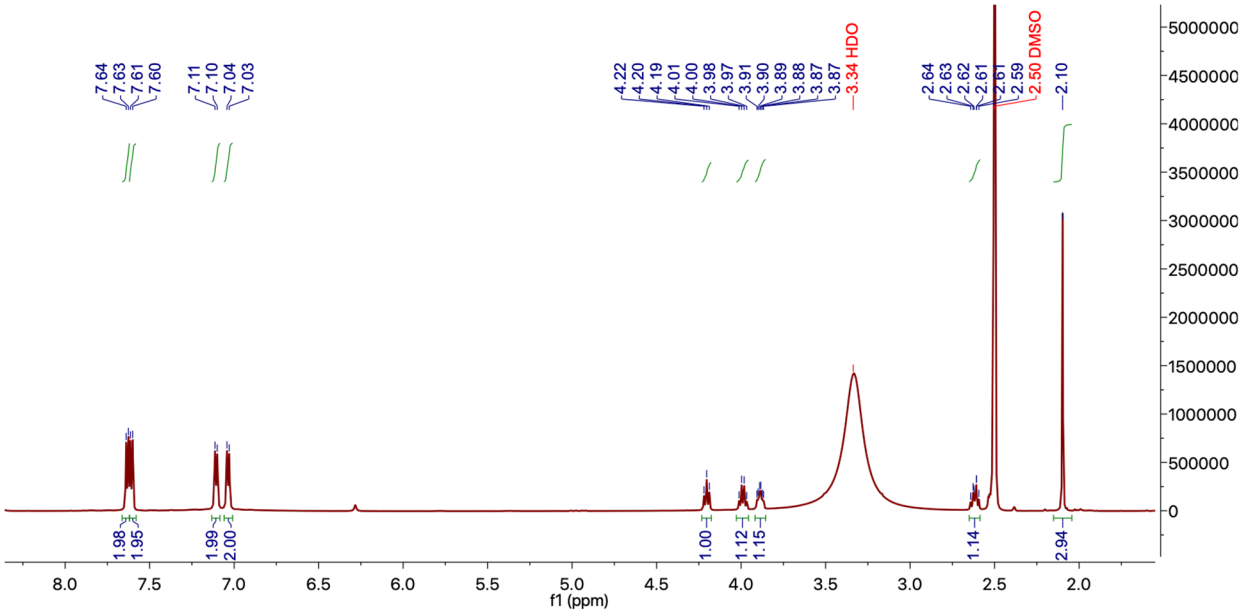

^{13}C NMR (126 MHz, DMSO-d_6)

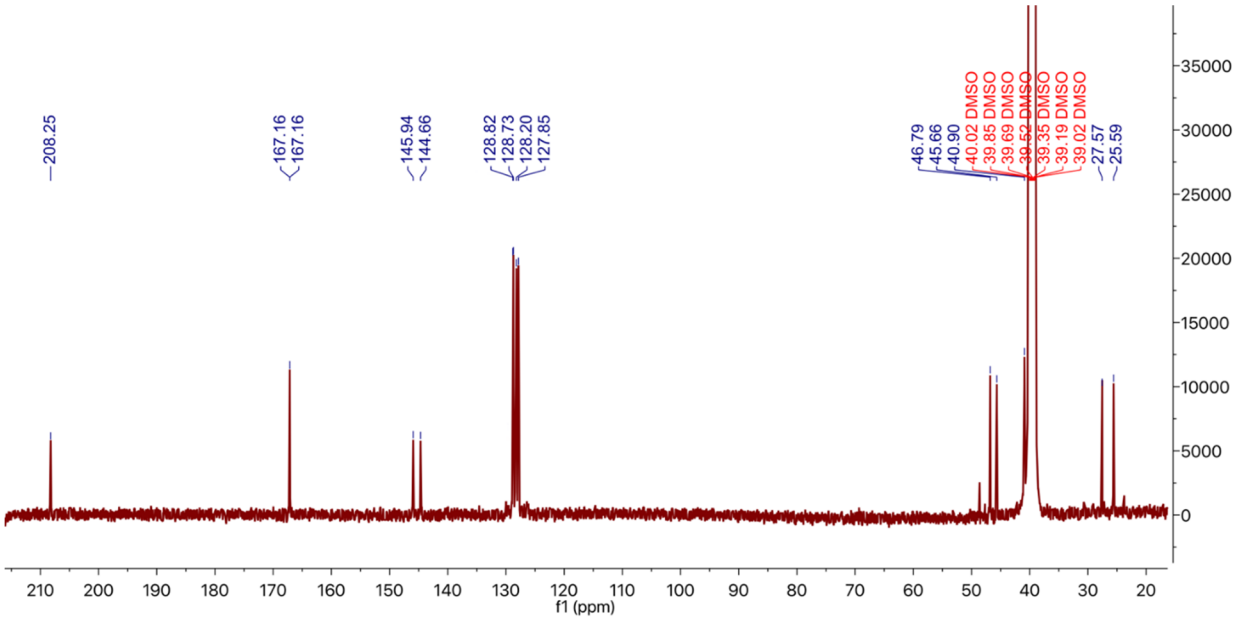

4,4'-(3-acetylcyclobutane-1,2-diyl)dibenzoic acid

anti diastereomer **13**

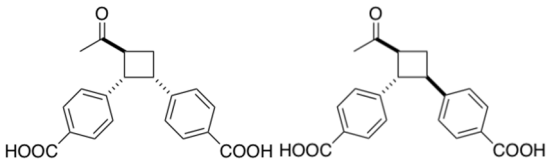

^{1}H NMR (600 MHz, DMSO-d_6) Gray signals correspond to **substrate 3**

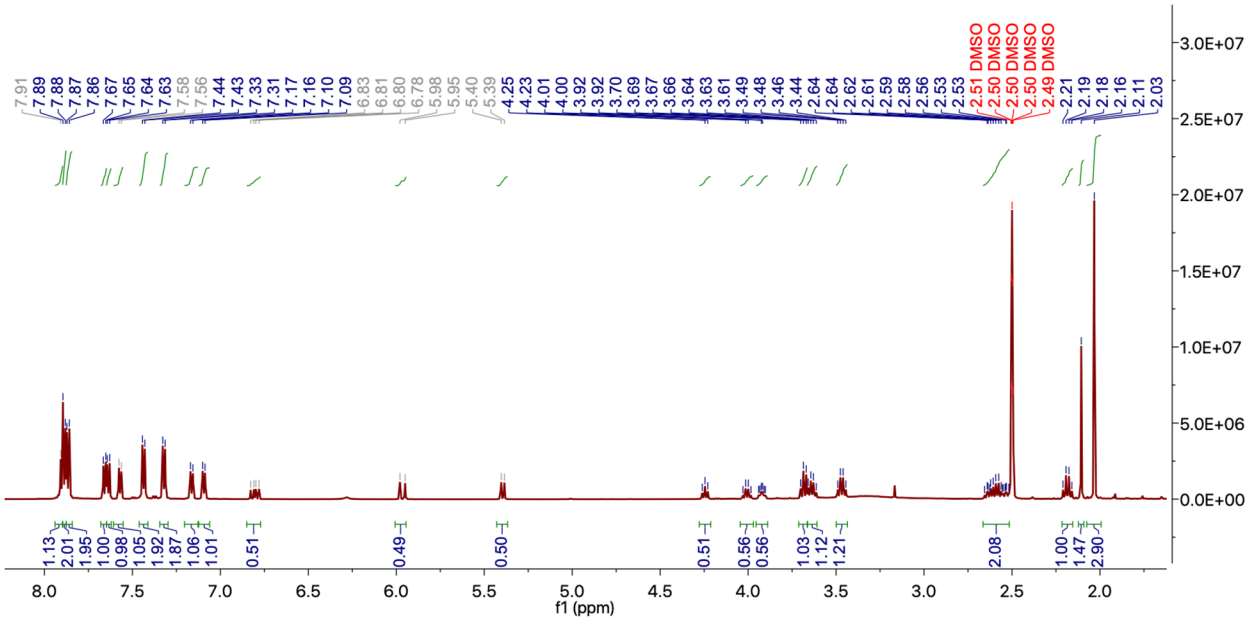

^{13}C NMR (126 MHz, DMSO-d_6) Gray peaks corresponding to the **substrate 3**

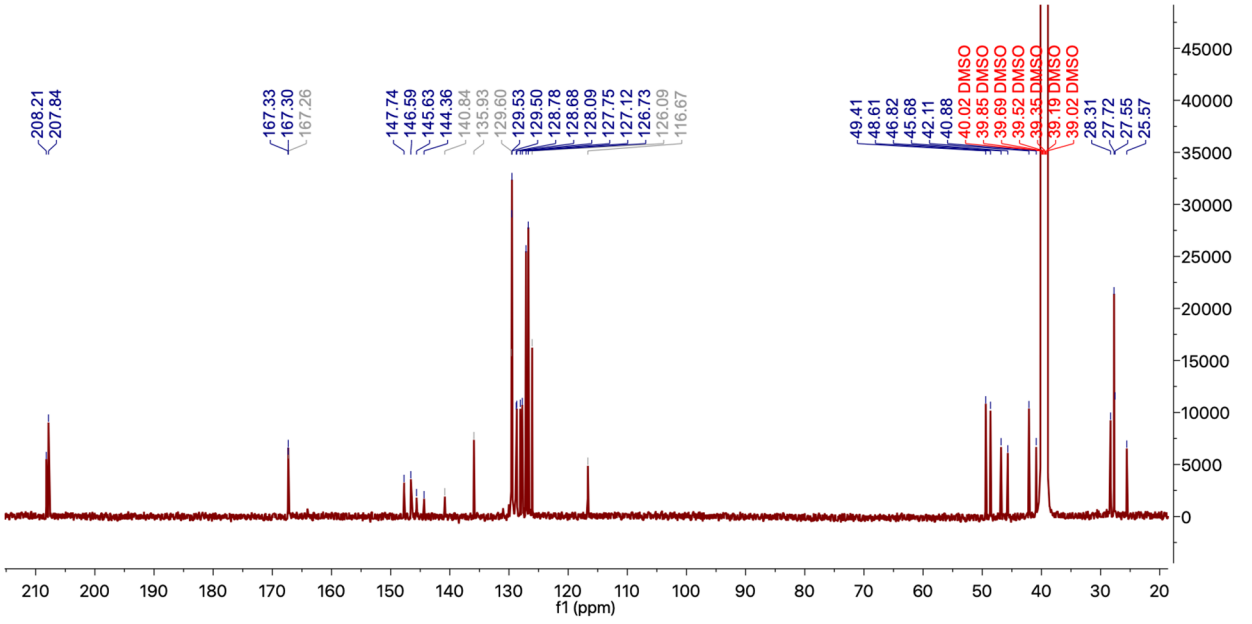

4,4'-(3-acetyl-4-benzoylcyclobutane-1,2-diyl)dibenzoic acid

syn diastereomer **16**

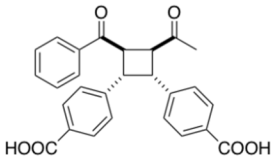

^{1}H NMR (600 MHz, DMSO-d_6)

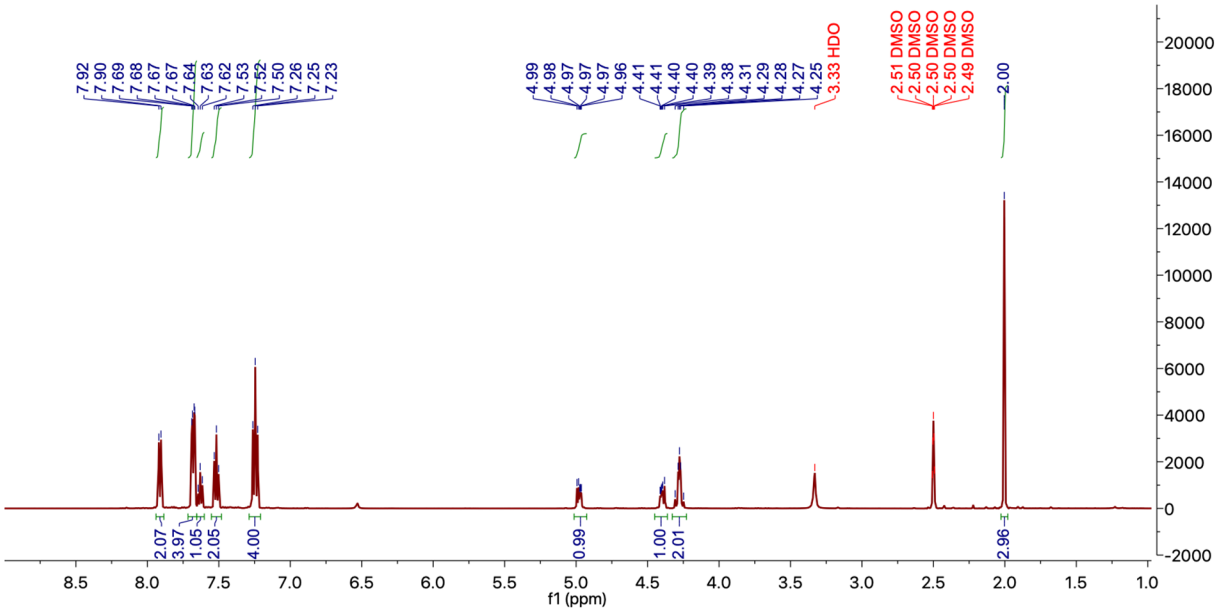

^{13}C NMR (126 MHz, DMSO-d_6)

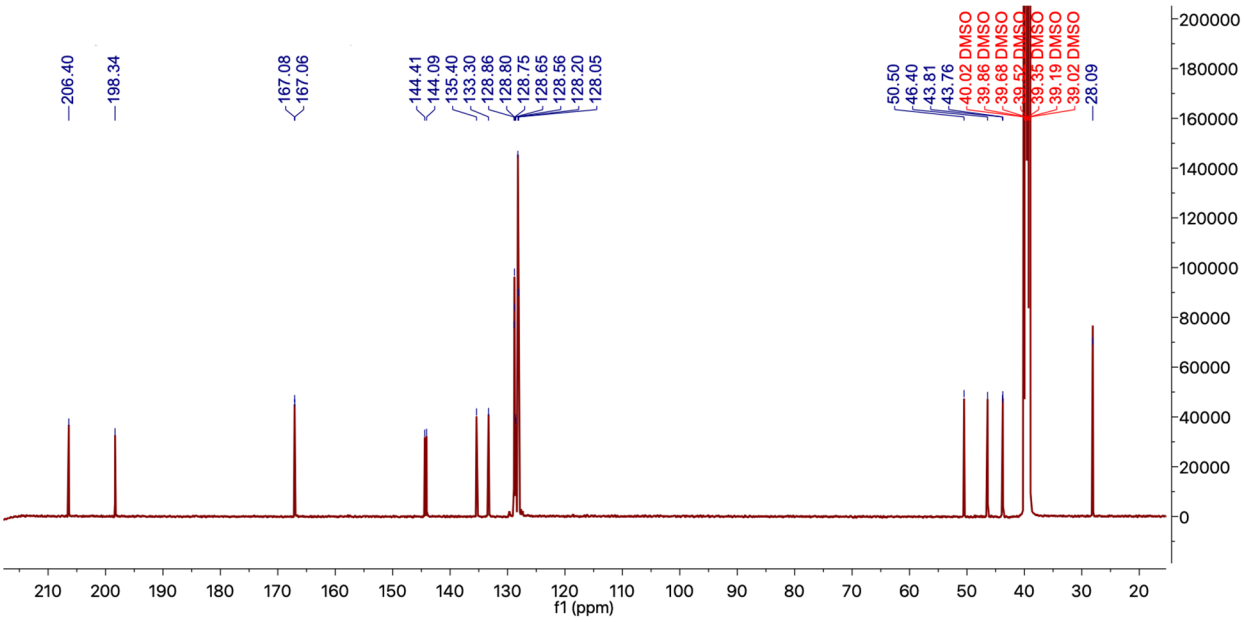

4,4'-(3-acetyl-4-benzoylcyclobutane-1,2-diyl)dibenzoic acid

anti diastereomer **17**

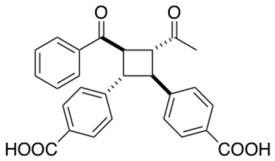

^{1}H NMR (600 MHz, DMSO-d_6)

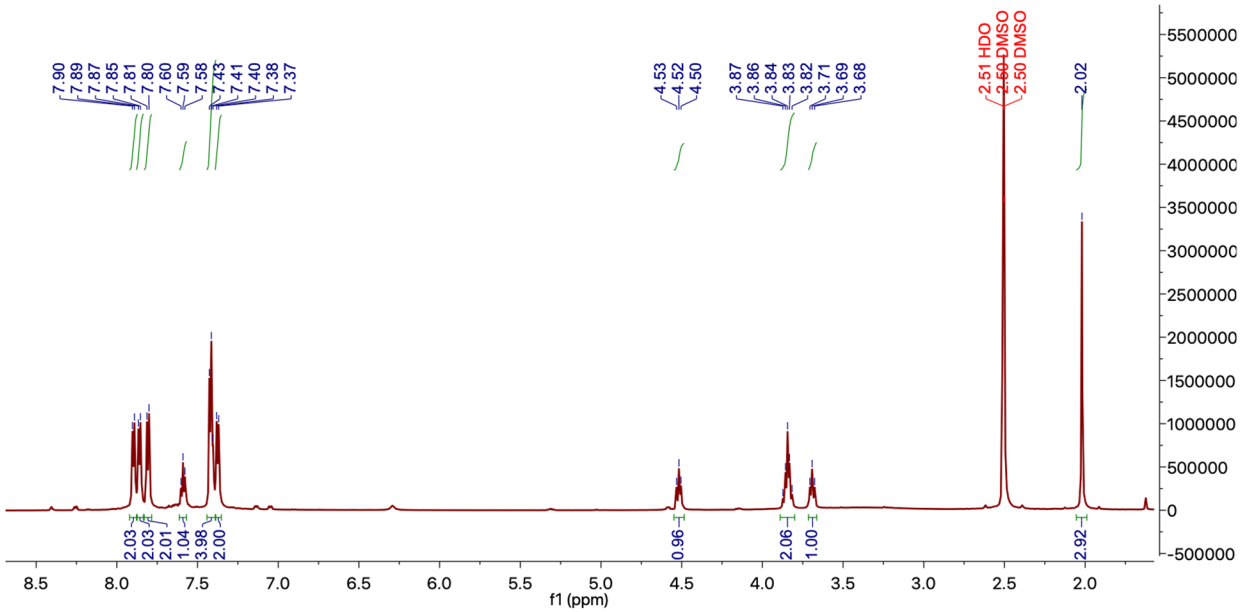

^{13}C NMR (126 MHz, DMSO-d_6)

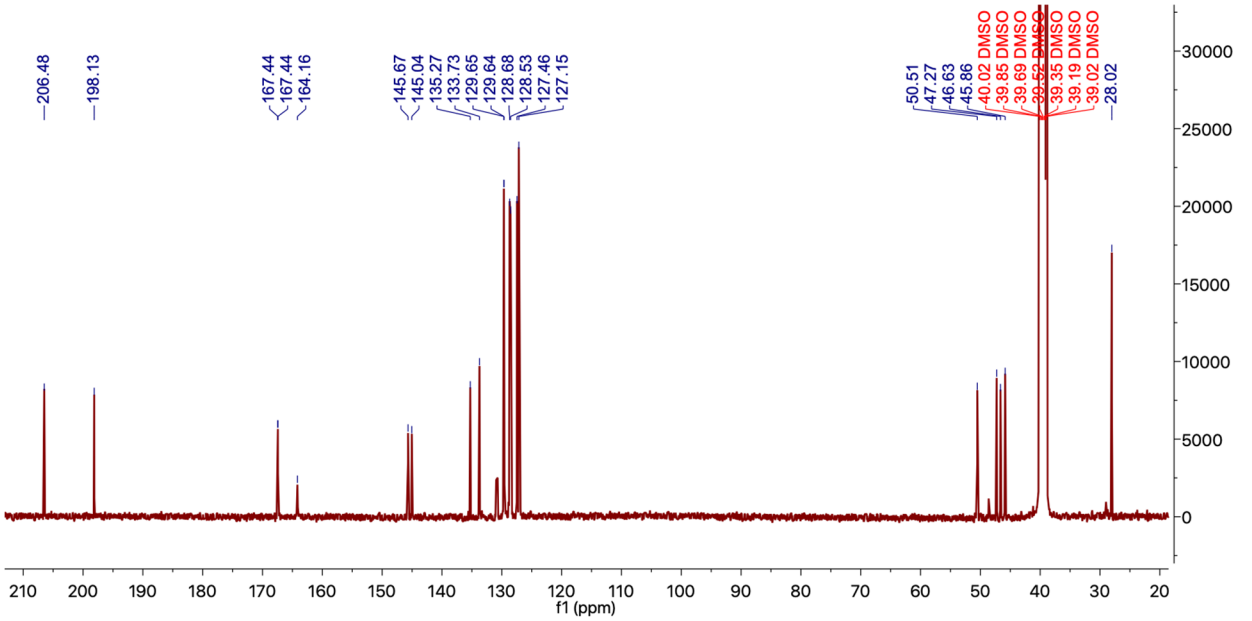

4-(3-acetyl-2-(4-carboxyphenyl)-4-phenylcyclobutane-1-carbonyl)benzoic acid
syn diastereomer **18**

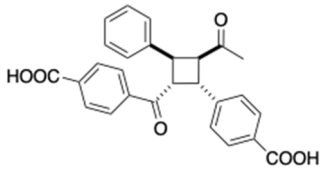

^{1}H NMR (600 MHz, DMSO-d_6)

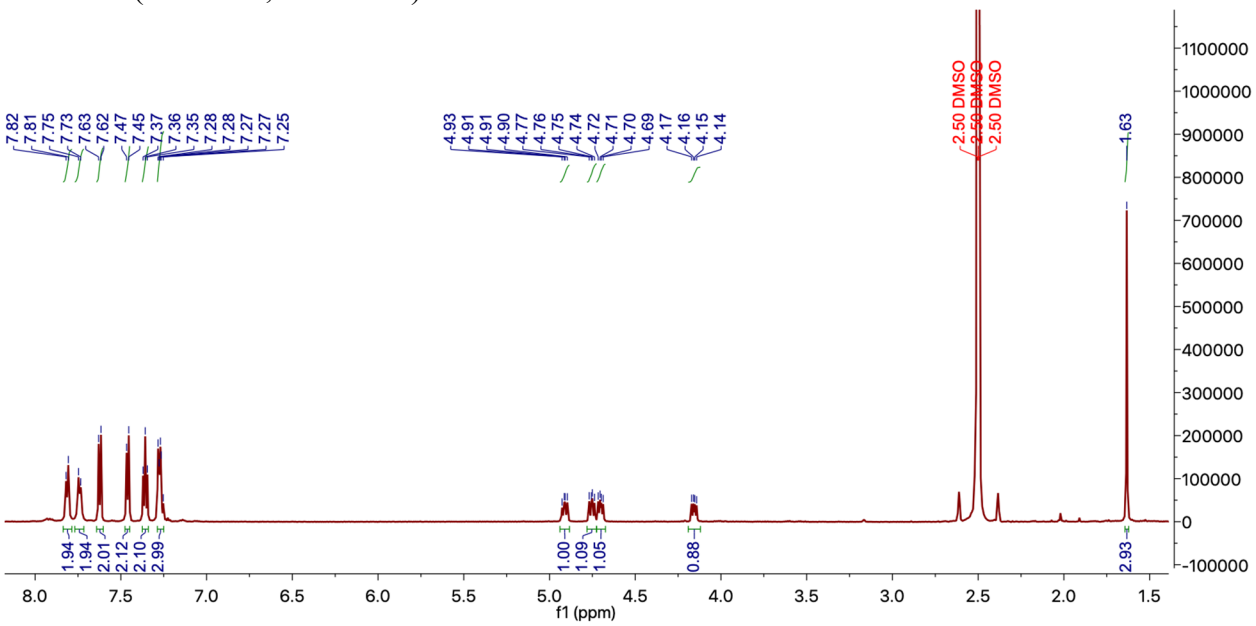

^{13}C NMR (126 MHz, DMSO-d_6)

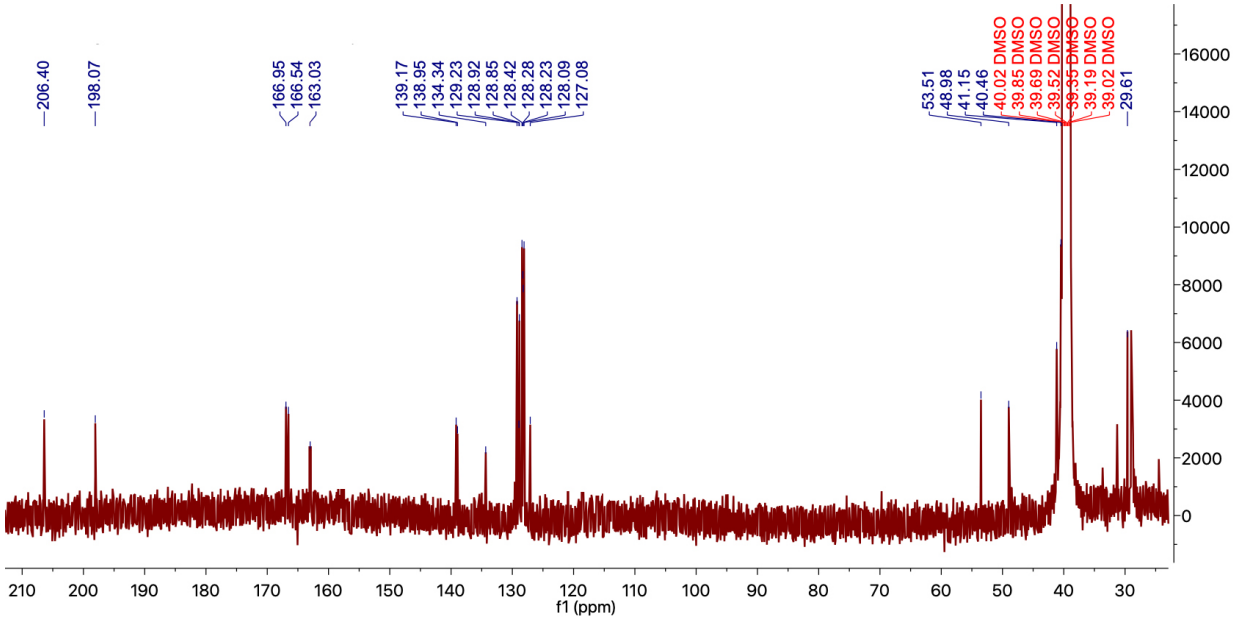

4-(3-acetyl-2-(4-carboxyphenyl)-4-phenylcyclobutane-1-carbonyl)benzoic acid
anti diastereomer **S1**

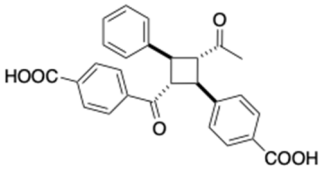

^{1}H NMR (600 MHz, DMSO-d_6)

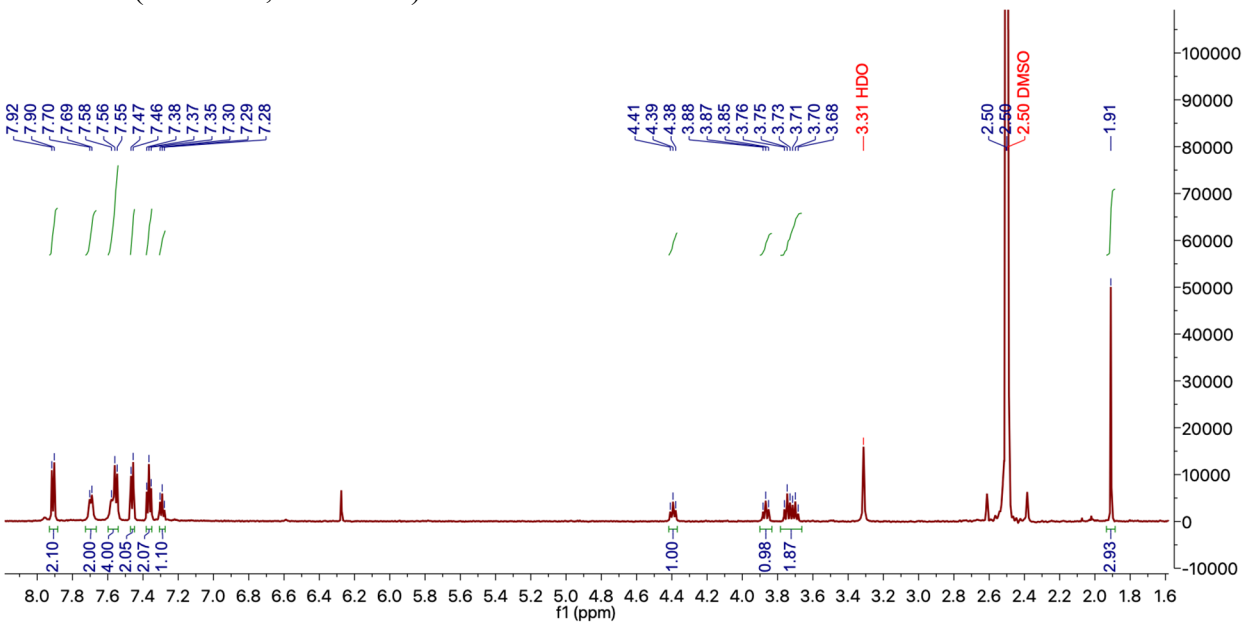

^{13}C NMR (126 MHz, DMSO-d_6)

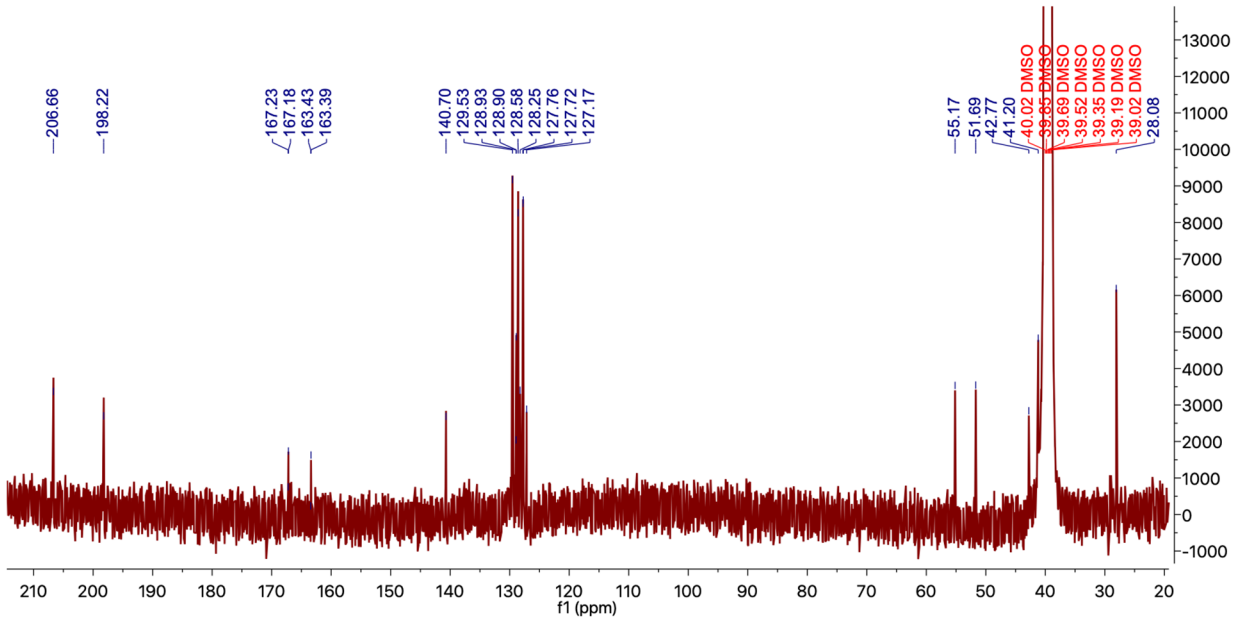

4,4'-(3-acetyl-4-benzoylcyclobutane-1,2-diyl)dibenzoic acid

anti diastereomer **19**

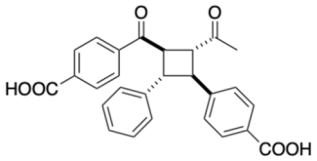

^{1}H NMR (600 MHz, DMSO-d_6)

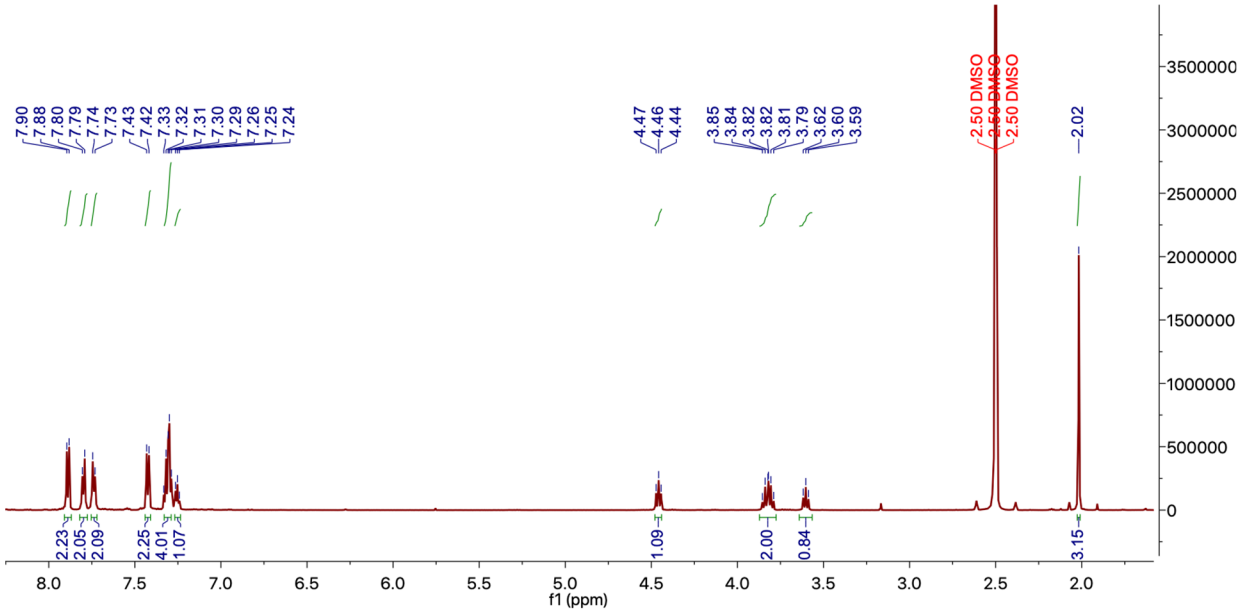

^{13}C NMR (126 MHz, DMSO-d_6)

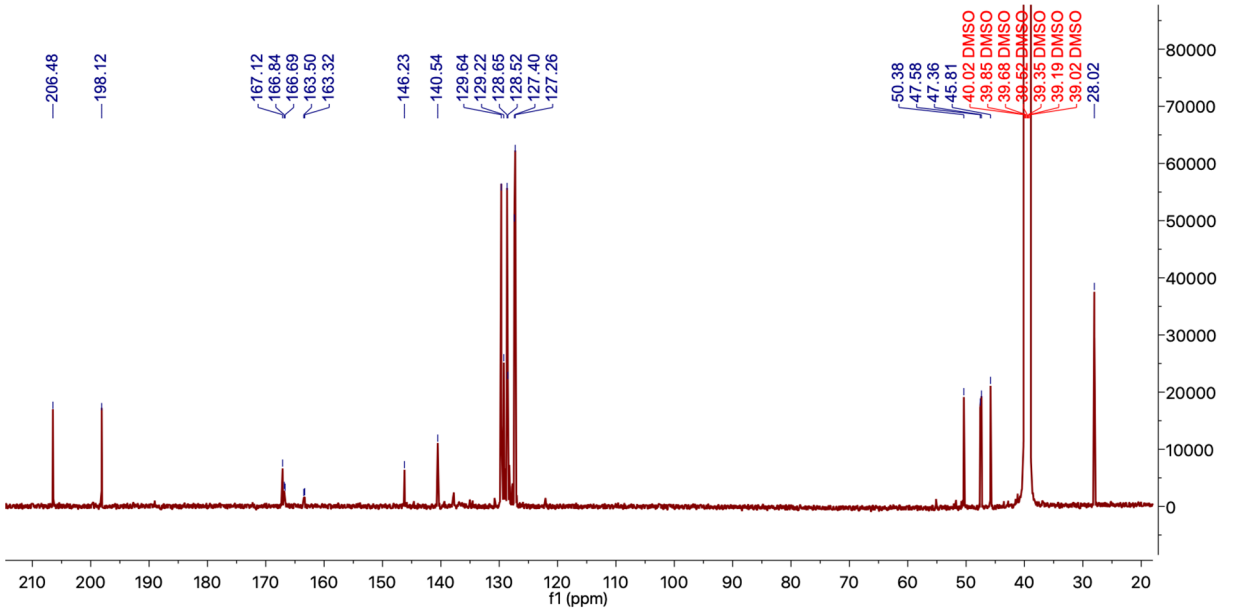

4,4'-(3-acetyl-4-benzoylcyclobutane-1,2-diyl)dibenzoic acid

syn diastereomer **S2**

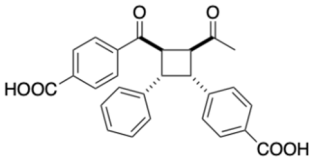

^{1}H NMR (600 MHz, DMSO-d_6)

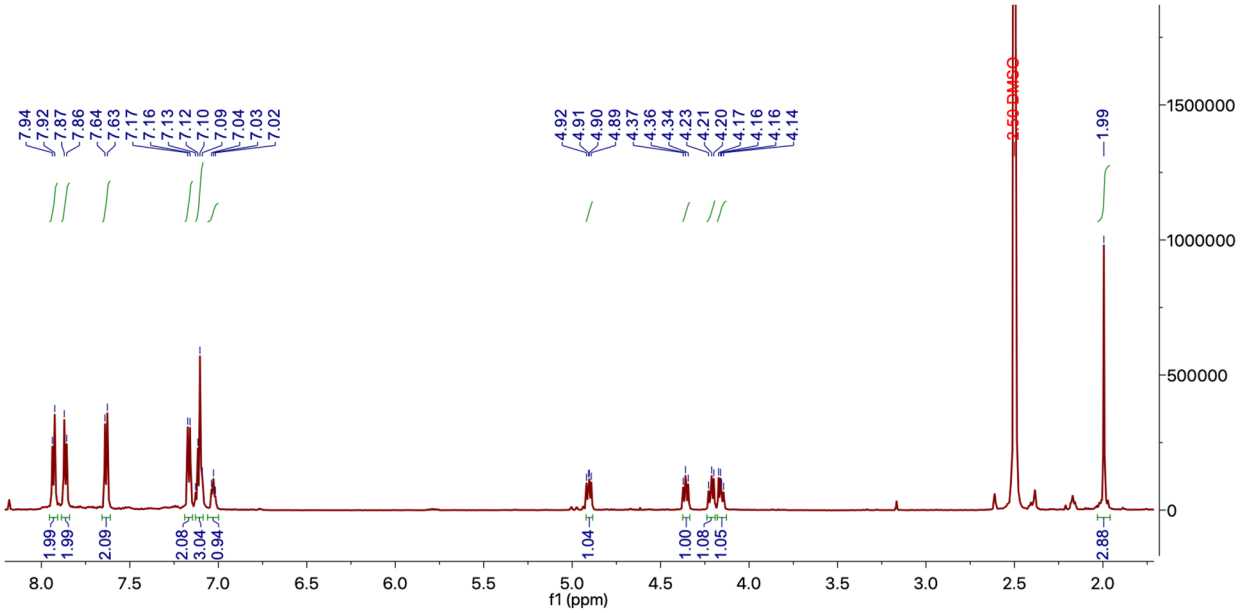

^{13}C NMR (126 MHz, DMSO-d_6)

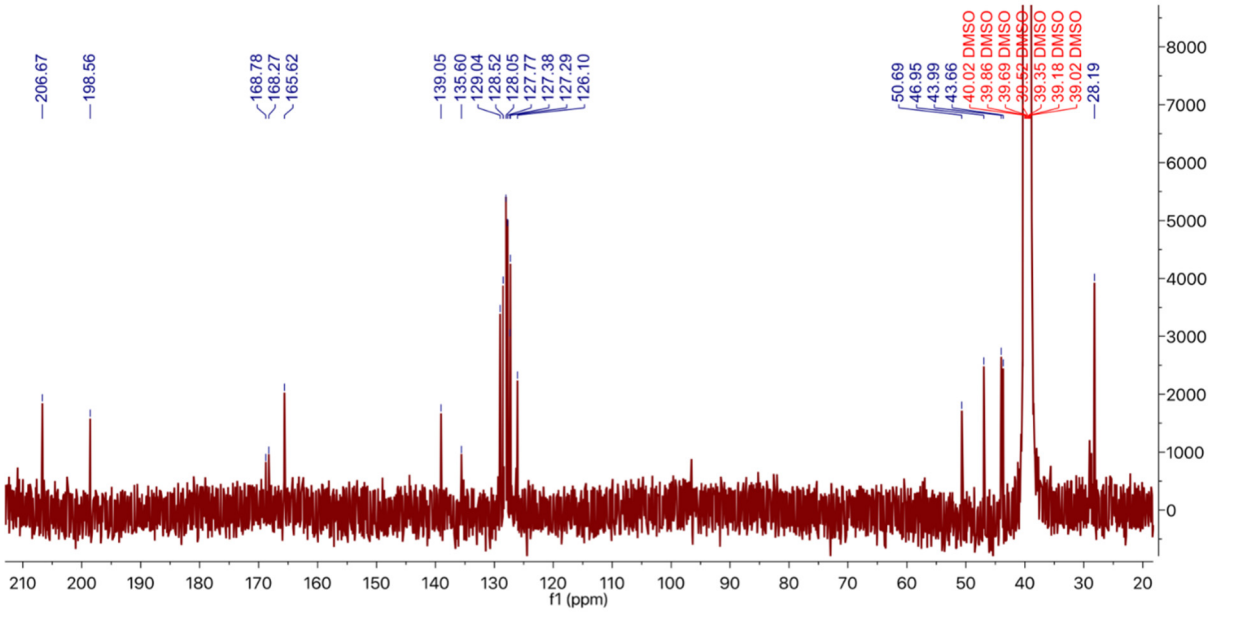

4-(2-acetyl-3-benzoyl-4-phenylcyclobutyl)benzoic acid

anti diastereomer **20**

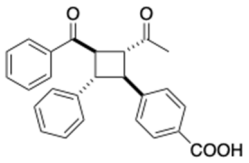

^{1}H NMR (600 MHz, DMSO-d_6)

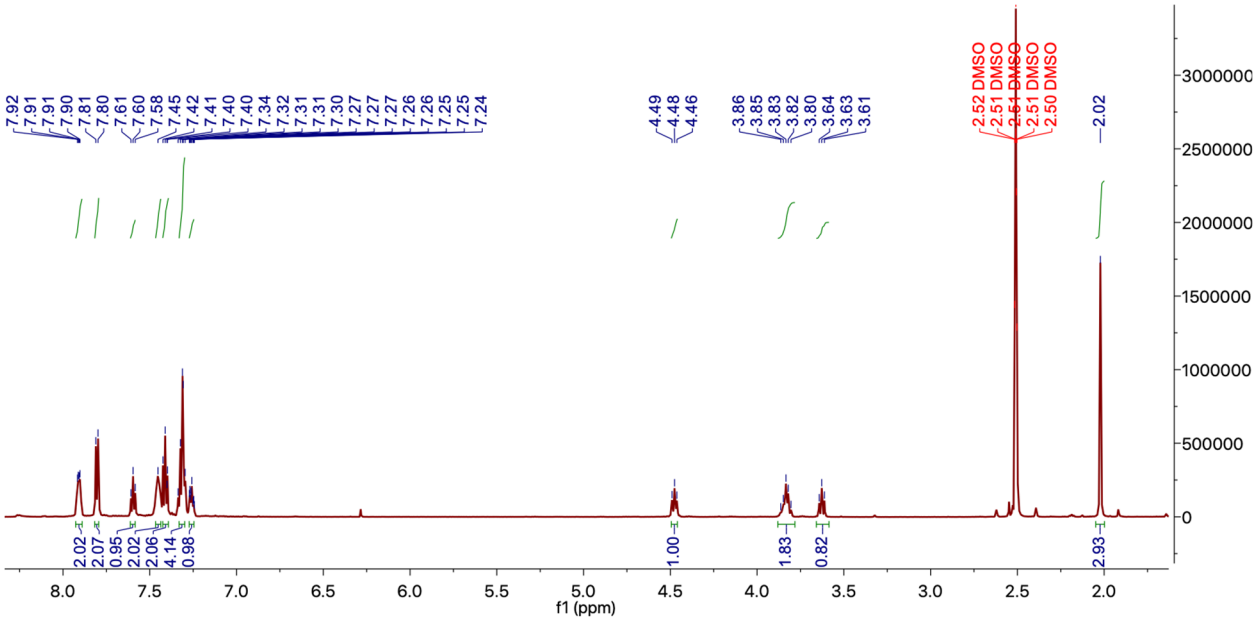

^{13}C NMR (126 MHz, DMSO-d_6)

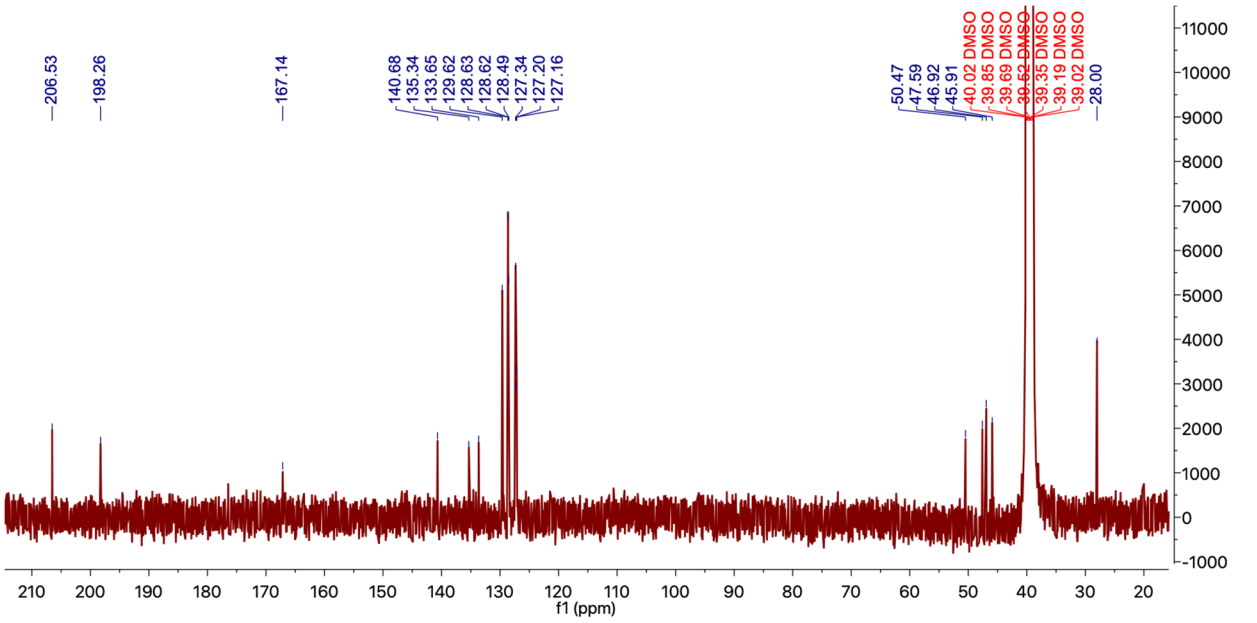

4-(2-acetyl-3-benzoyl-4-phenylcyclobutyl)benzoic acid

syn diastereomer **S3**

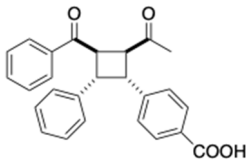

^{1}H NMR (600 MHz, DMSO-d_6)

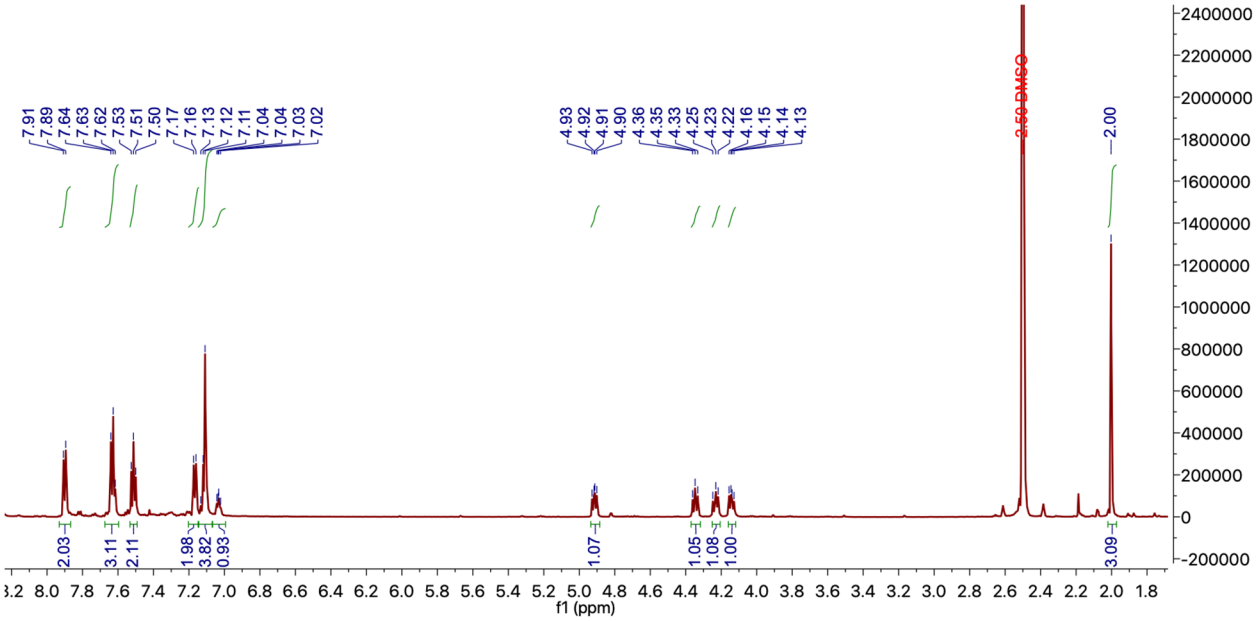

^{13}C NMR (126 MHz, DMSO-d_6)

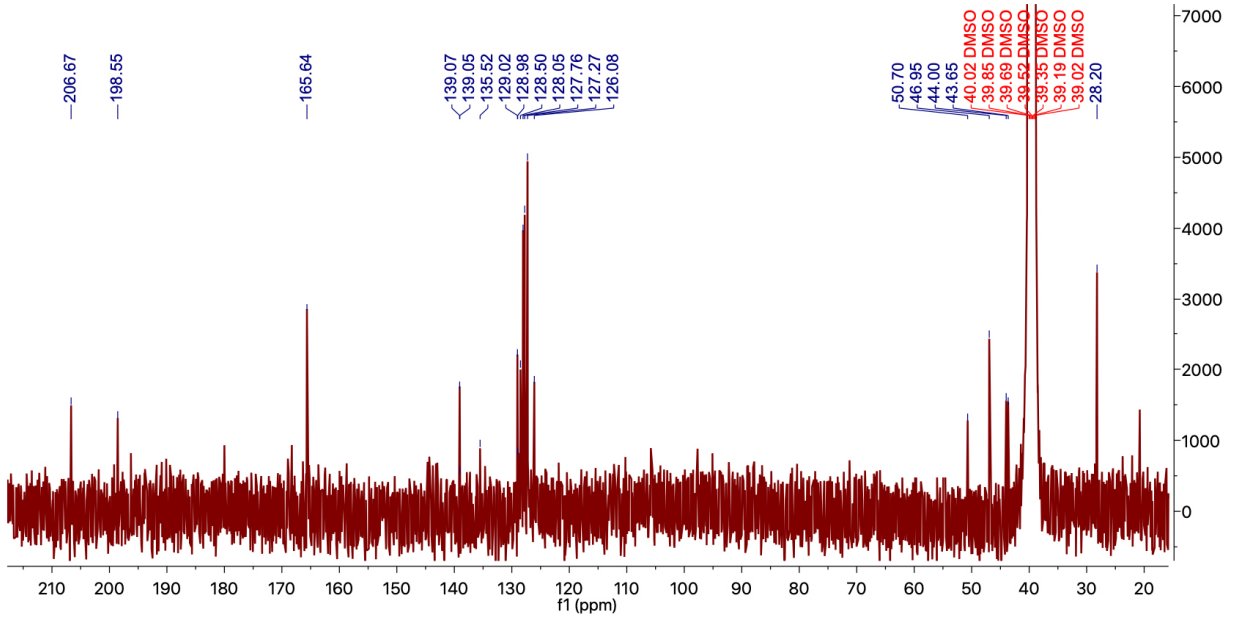

References

29 Pangborn, A. B., Giardello, M. A., Grubbs, R. H., Rosen, R. K. & Timmers, F. J. Safe and Convenient Procedure for Solvent Purification. *Organometallics* **15**, 1518-1520, doi:10.1021/om9503712 (1996).

30 McArthur, E. A., Morris-Cohen, A. J., Knowles, K. E. & Weiss, E. A. Charge Carrier Resolved Relaxation of the First Excitonic State in CdSe Quantum Dots Probed with Near-Infrared Transient Absorption Spectroscopy. *J. Phys. Chem. B* **114**, 14514-14520, doi:10.1021/jp102101f (2010).

31 Burda, C., Link, S., Mohamed, M. & El-Sayed, M. The Relaxation Pathways of CdSe Nanoparticles Monitored with Femtosecond Time-Resolution from the Visible to the IR: Assignment of the Transient Features by Carrier Quenching. *J. Phys. Chem. B* **105**, 12286-12292, doi:10.1021/jp0124589 (2001).

32 Mongin, C., Garakyaraghi, S., Razgoniaeva, N., Zamkov, M. & Castellano, F. N. Direct observation of triplet energy transfer from semiconductor nanocrystals. *Science* **351**, 369-372, doi:10.1126/science.aad6378 (2016).

33 Maturi, M. M. *et al.* Intramolecular [2+ 2] Photocycloaddition of 3-and 4-(But-3-enyl) oxyquinolones: Influence of the Alkene Substitution Pattern, Photophysical Studies, and Enantioselective Catalysis by a Chiral Sensitizer. *Chem. Eur. J* **19**, 7461-7472 (2013).

34 Miller, Z. D., Lee, B. J. & Yoon, T. P. Enantioselective Crossed Photocycloadditions of Styrenic Olefins by Lewis Acid Catalyzed Triplet Sensitization. *Angew. Chem.* **129**, 12053-12057 (2017).

35 Valiev, M. *et al.* NWChem: A comprehensive and scalable open-source solution for large scale molecular simulations. *Comput. Phys. Commun.* **181**, 1477-1489, doi:http://dx.doi.org/10.1016/j.cpc.2010.04.018 (2010).

36 York, D. M. & Karplus, M. A Smooth Solvation Potential Based on the Conductor-Like Screening Model. *J. Phys. Chem. A* **103**, 11060-11079, doi:10.1021/jp992097l (1999).

37 Grimme, S., Antony, J., Ehrlich, S. & Krieg, H. A consistent and accurate ab initio parametrization of density functional dispersion correction (DFT-D) for the 94 elements H-Pu. *J. Chem. Phys.* **132**, 154104, doi:10.1063/1.3382344 (2010).

38 Ullrich, T., Ghobrial, M., Weigand, K. & Marzinzik, A. L. Scope and Applicability of an Expedient Synthesis Leading to Polysubstituted 3‐(Carboxyphenyl)pyrroles. *Synth. Commun.* **37**, 1109-1119, doi:10.1080/00397910701198898 (2007).

39 Chen, F., Zhang, Y., Yu, L. & Zhu, S. Enantioselective NiH/Pmrox‐Catalyzed 1,2‐Reduction of α,β‐Unsaturated Ketones. *Angew. Chem. Int. Ed.* **56**, 2022-2025, doi:10.1002/anie.201610990 (2017).

40 Deck, L. M. *et al.* Activation of anti-oxidant Nrf2 signaling by enone analogues of curcumin. *Eur. J. Med. Chem.* **143**, 854-865 (2018).

41 Flamee, S. *et al.* Fast, High Yield, and High Solid Loading Synthesis of Metal Selenide Nanocrystals. *Chem. Mater.* **25**, 2476-2483, doi:10.1021/cm400799e (2013).

42 Dolomanov, O. V., Bourhis, L. J., Gildea, R. J., Howard, J. A. & Puschmann, H. OLEX2: a complete structure solution, refinement and analysis program. *J. Appl. Crystallogr.* **42**, 339-341 (2009).

43 Sheldrick, G. M. SHELXT–Integrated space-group and crystal-structure determination. *Acta Crystallogr. Sect. A: Found. Adv.* **71**, 3-8 (2015).
44 Sheldrick, G. M. A short history of SHELX. *Acta Crystallogr. Sect. A: Found. Crystallogr.* **64**, 112-122 (2008).